Advances in Microwave Photonic Systems

Jianping Yao

School of Electrical Engineering and Computer Science
Microwave Photonics Research Laboratory
University of Ottawa, CANADA

Université d'Ottawa | University of Ottawa

uOttawa

L'Université canadienne
Canada's university

MWP2021

15-17 November 2020
Pisa, Italy

www.uOttawa.ca

Outline

- Recent research activities in MWP
- Microwave signal generation
- Microwave signal processing
- Radio over fiber based on coherent detection
- Microwave photonics for sensing
- Conclusion

Recent activities in MWP

Integrated MWP

1. Silicon on Insulator (SOI)
- Optoelectronic oscillator (OEO)
- MWP filters
- Programmable signal processors

2. Silicon Nitride
- True time delay (TTD) beamforming
- Optical comb for RF generation

3. InP
- Monolithically integrated microwave photonic systems
- Programmable signal processors

4. InP+SiO+SiN
- Heterogenous integration (system on chip)

MWP systems

1. Microwave signal generation
- Parity time (PT) symmetric OEO
- Fourier domain mode locked OEO
- Photonic integrated OEO

2. Microwave signal processing
- MWP filters（incoherent and coherent MWP filters))
- Photonic integrated MWP filters

3. Radio over fiber (transmission)
- Radio over fiber based on coherent detection

4. MWP for sensing (optical → microwave domain with higher speed and higher resolution)
- MWP sensor based on SS-WTT mapping
- OEO based high resolution sensor

D. Marpaung, J. P. Yao, and J. Capmany, “Integrated microwave photonics,” Nature Photon., vol. 13, no. 1, pp. 80-90, Feb. 2019.

Outline

- Recent research activities in MWP
- Microwave signal generation
- Microwave signal processing
- Radio over fiber based on coherent detection
- Microwave photonics for sensing
- Conclusion

Microwave signal generation

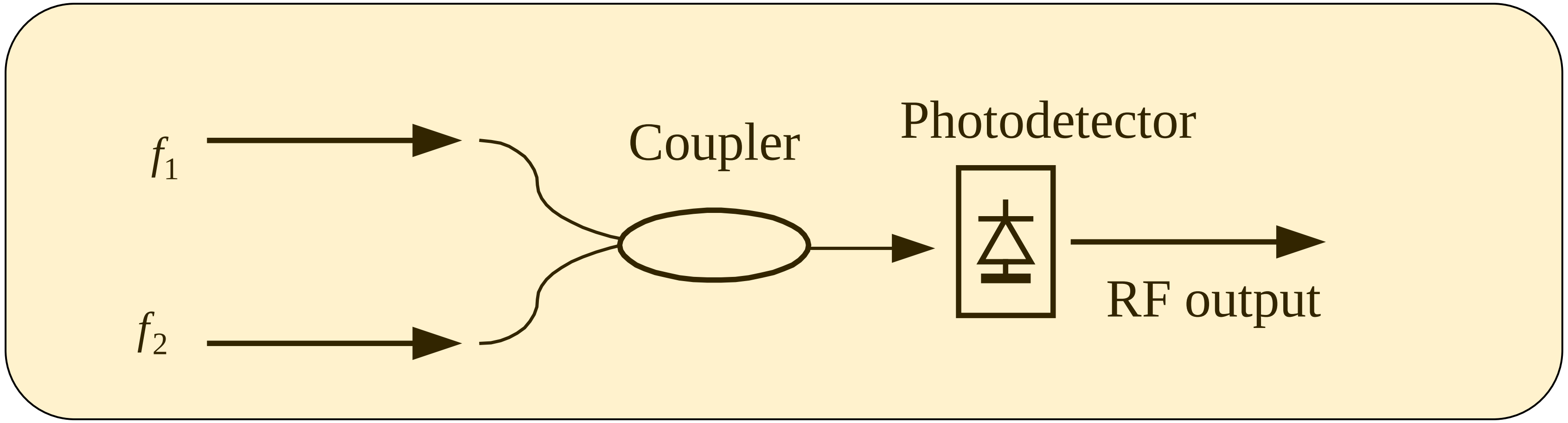

The output of two beat signals applied to a photodetector:

$$I = \Re P = \Re\left[E_1(t) + E_2(t)\right]^2 = \Re P_1 + \Re P_2 + 2\Re\sqrt{P_1 P_2}\cos\left[2\pi\left(f_1 - f_2\right)t + \left(\phi_1 - \phi_2\right)\right]$$

where E1 (t) and E2 (t) are two optical inputs.

$f_{RF} = f_1 - f_2$ is the RF frequency.

At 1550 nm, 0.8 nm→100 GHz

Microwave generation

1. **Dual-frequency laser source**
2. **Phase locked loop**
3. **Injection locking**
4. **External modulation**
5. **Optoelectronic oscillation**

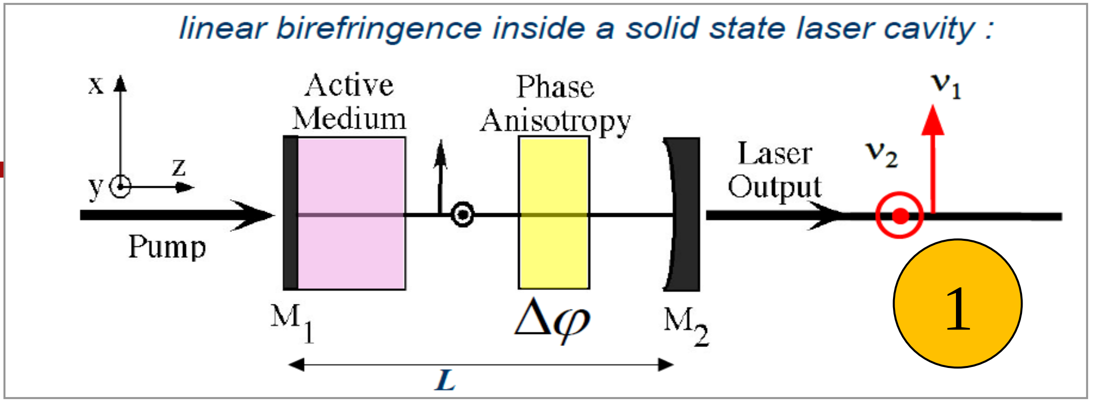

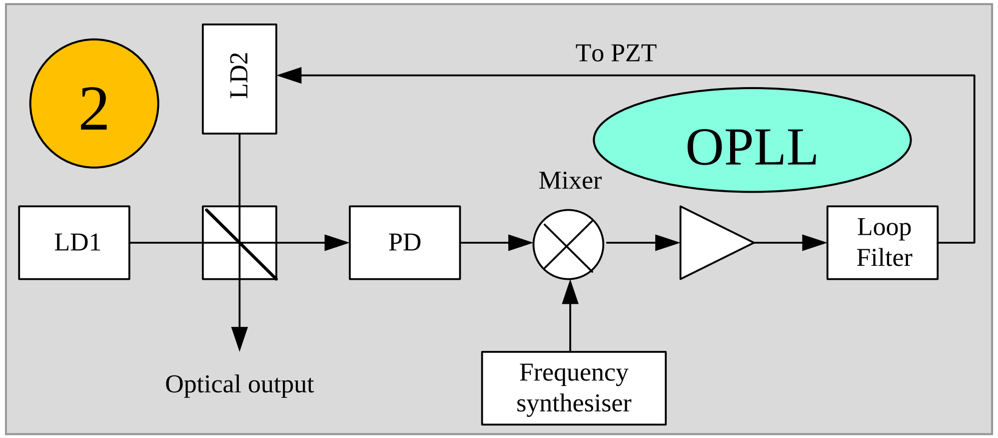

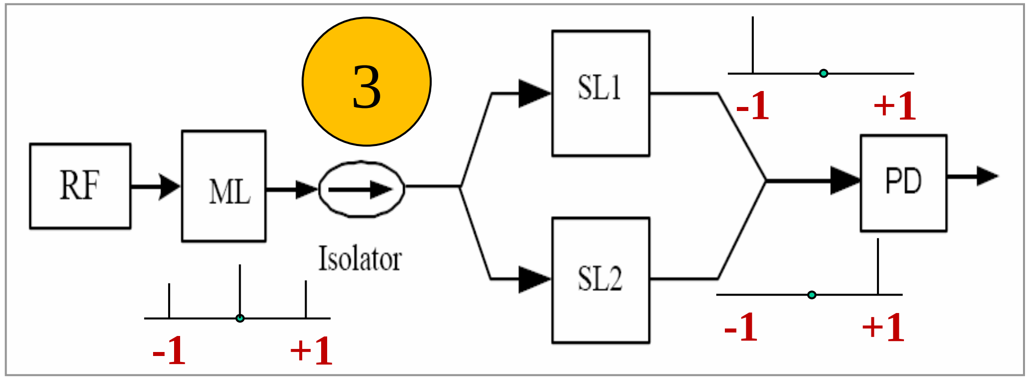

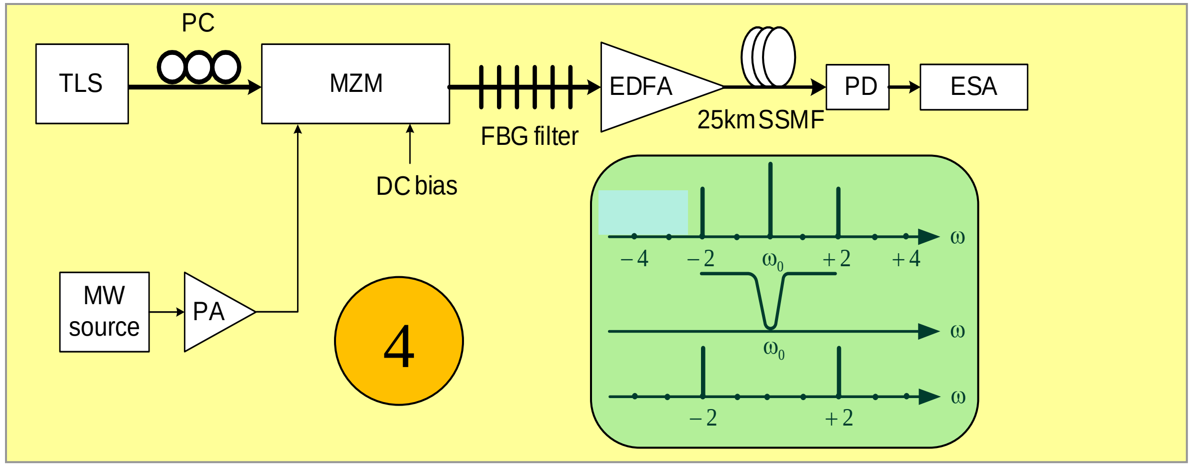

Opto-electronic oscillator (OEO)

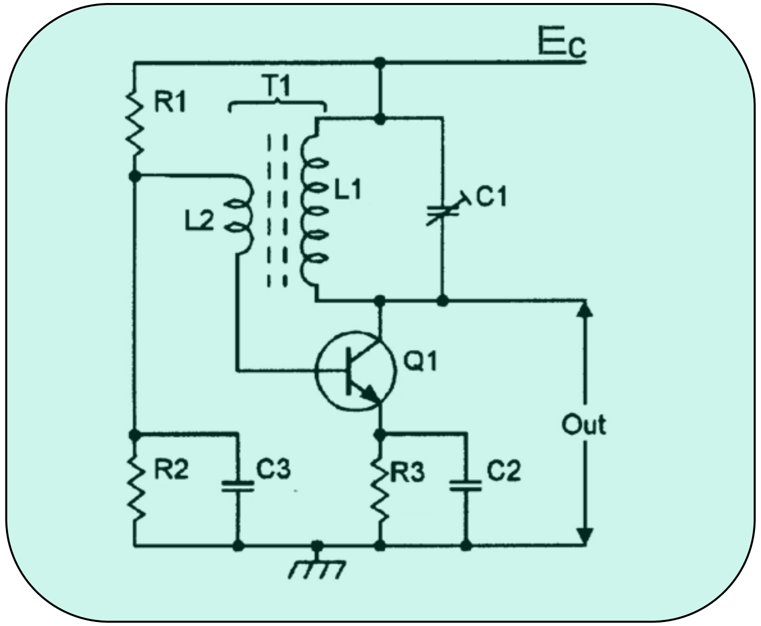

Electronic oscillator

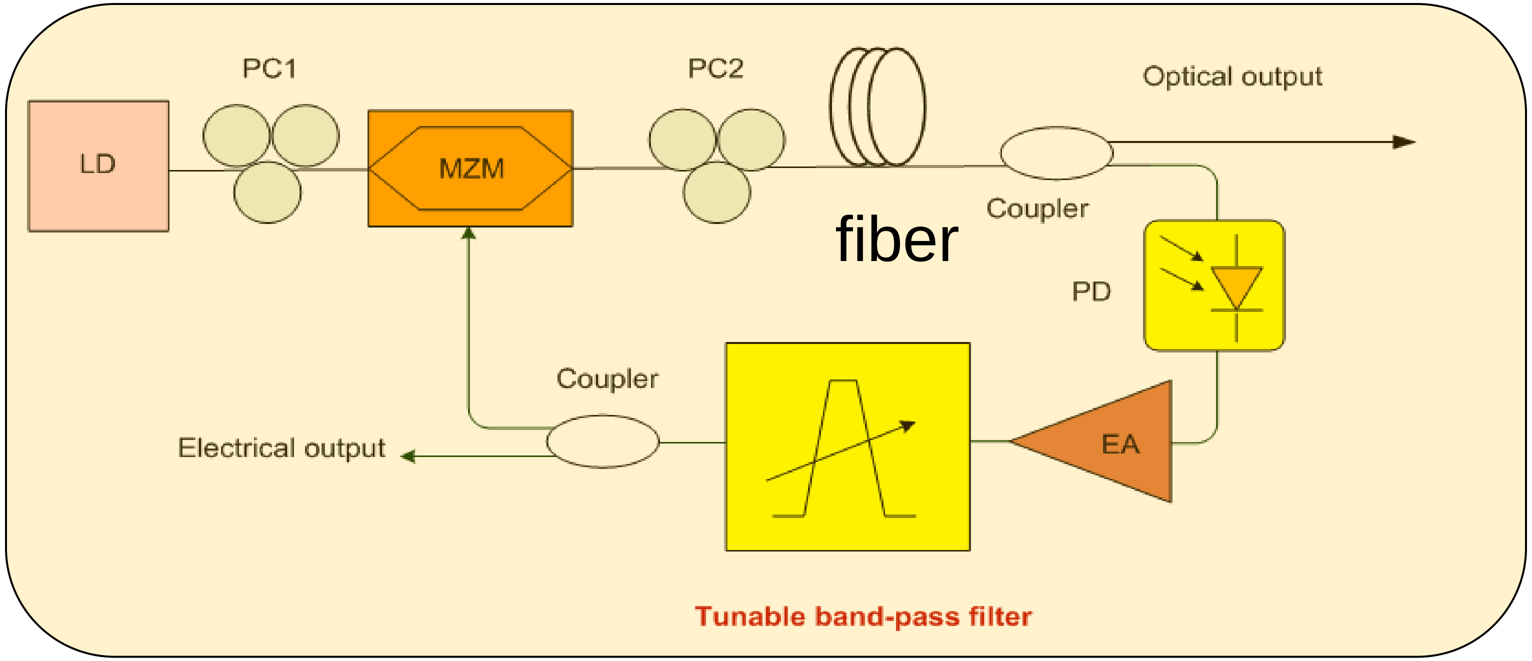

Opto-electronic oscillator

To oscillate: 1) positive feedback, gain>loss, 2) frequency selection mechanism

Long fiber → high Q factor → low phase noise

OEO – Mode Selection

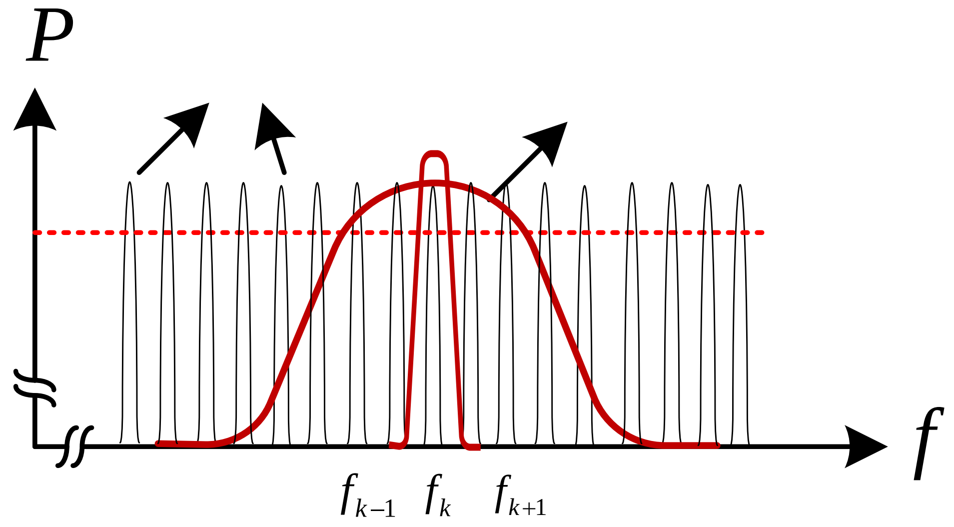

- Longer loop → closely spaced modes → Multi-mode oscillation.
- **Solutions:**

1) Shorter loop length (but higher phase noise)
2) Dual or multiple loops (Vernier effect) to extend the effective FSR, but complicated system
3) **Parity-Time (PT) Symmetry**

Gain difference between main mode and sidemode

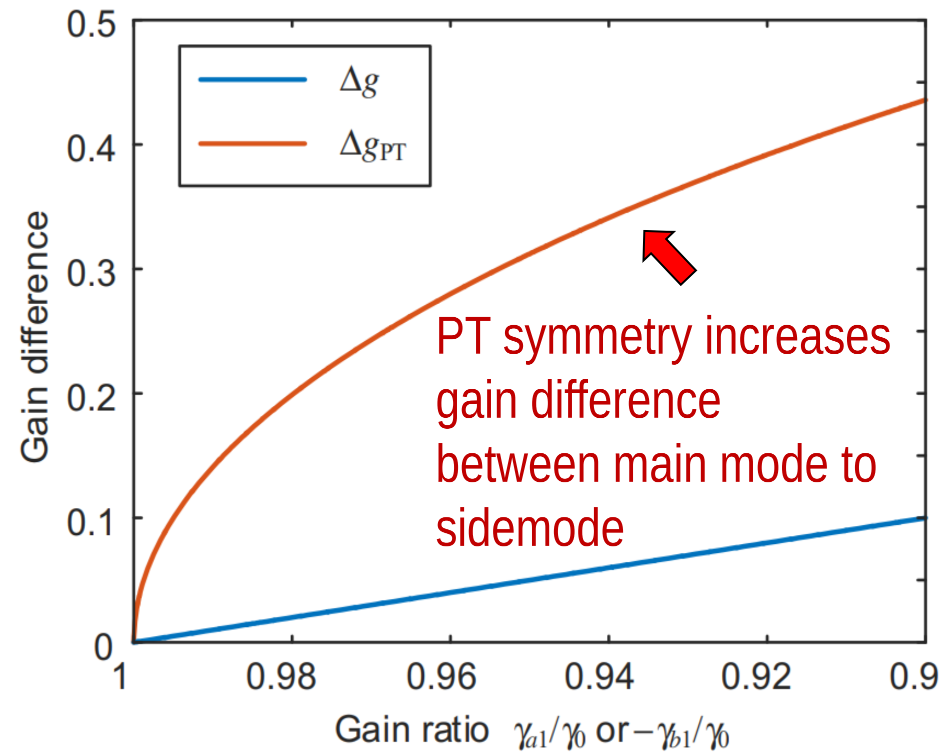

Fig. 2. Gain difference enhancement with PT symmetry. The gain difference between the oscillating mode and the secondary mode within a regular single-loop OEO (blue) and a PT-symmetric OEO (red) is illustrated for comparison.

Parity time symmetry

Coupled mode equations in the two cavities:

$$\frac{da_n}{dt} = -i\omega_n a_n + i\kappa b_n + \gamma_{a_n} a_n \qquad \text{(S1)}$$

$$\frac{db_n}{dt} = -i\omega_n b_n + i\kappa a_n + \gamma_{b_n} b_n \qquad \text{(S2)}$$

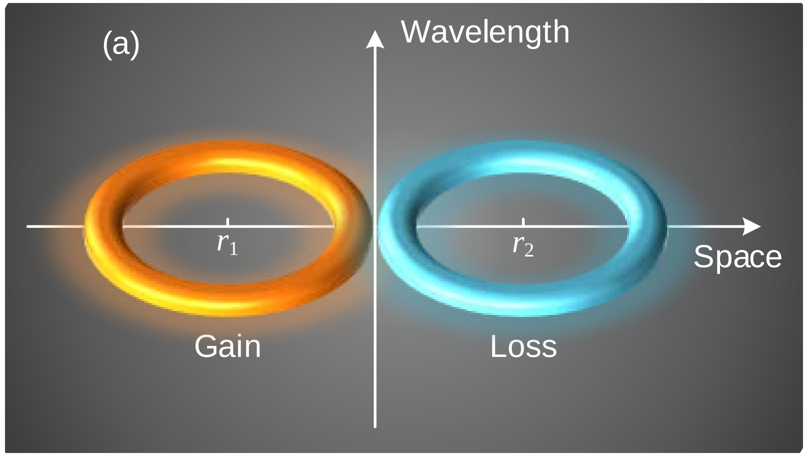

Solving (S1) and (S2), we can get the **eigenfrequencies** of the PT symmetric system:

$$\omega_n^{(1,2)} = \omega_n + i\frac{\gamma_{a_n} + \gamma_{b_n}}{2} \pm \sqrt{\kappa_n^2 - \left(\frac{\gamma_{a_n} - \gamma_{b_n}}{2}\right)^2} \qquad \text{(S3)}$$

When PT symmetry is satisfied, $\gamma_{a_0} = -\gamma_{b_0} = \gamma_0$, (S3) can be written as

$$\omega_0^{(1,2)} = \omega_0 \pm \sqrt{\kappa_0^2 - \gamma_0^2}$$

PT symmetry is broken

$$\omega_0^{(1,2)} = \omega_0 \pm j\delta \Rightarrow e^{j(\omega_0 \pm j\delta)t} = e^{j\omega_0 t} e^{\mp\delta t}$$

growing and **decaying**

Once the gain or loss exceeds the coupling coefficient (γo > κo), there will be a conjugate pair of modes → **growing** (oscillation) and **decaying** (PT symmetry is broken)

SCIENCE ADVANCES | RESEARCH ARTICLE

OPTICS

Parity-time–symmetric optoelectronic oscillator

Jiejun Zhang and Jianping Yao*

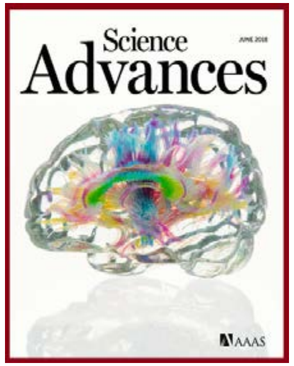

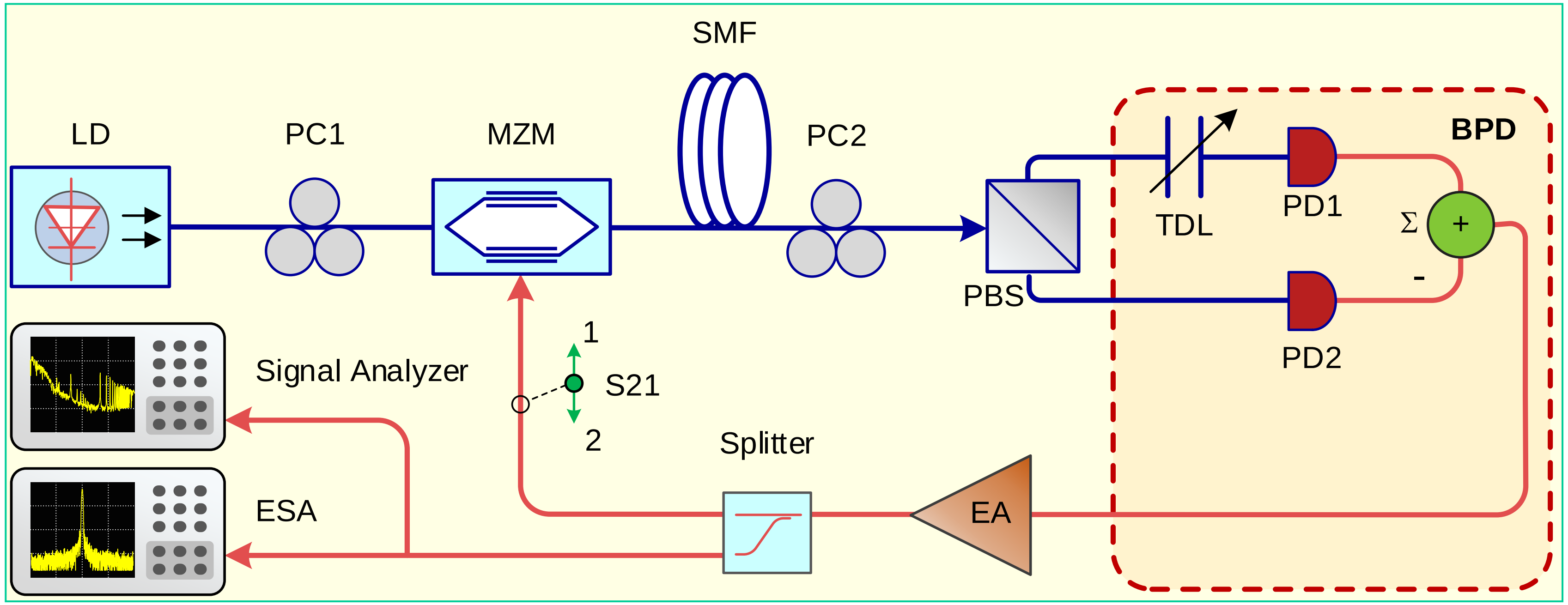

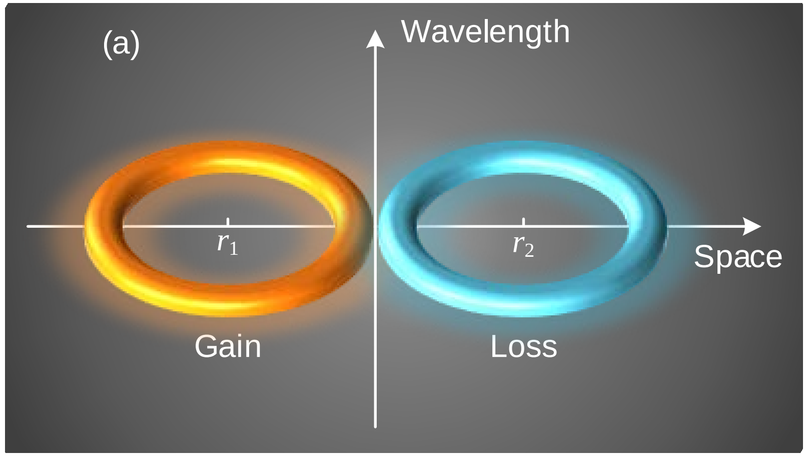

The key importance of the concept is that it enables the implementation of an OEO for single-frequency and ultra-low phase noise microwave generation **without the need of an ultra-narrow optical or microwave filter.**

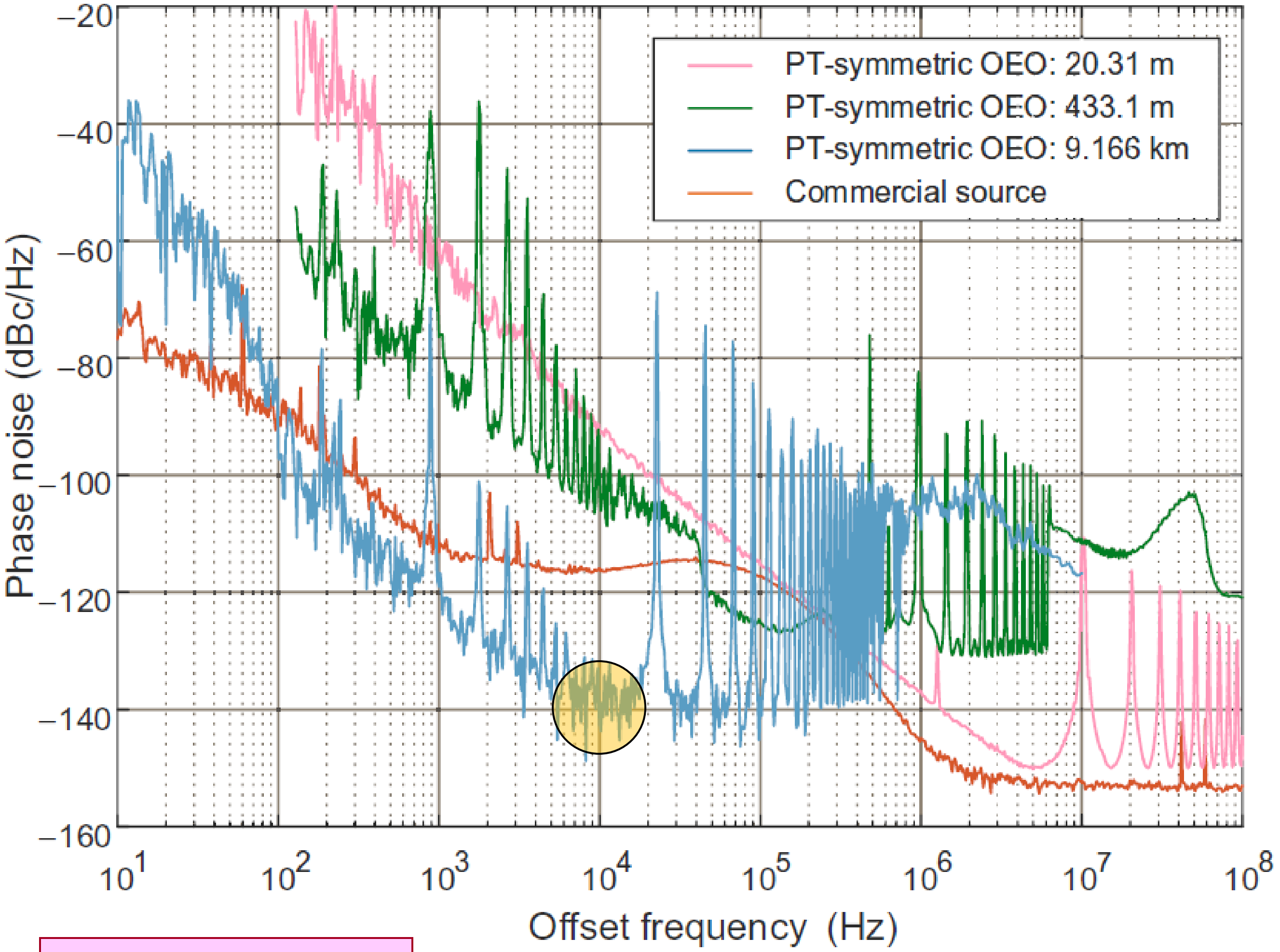

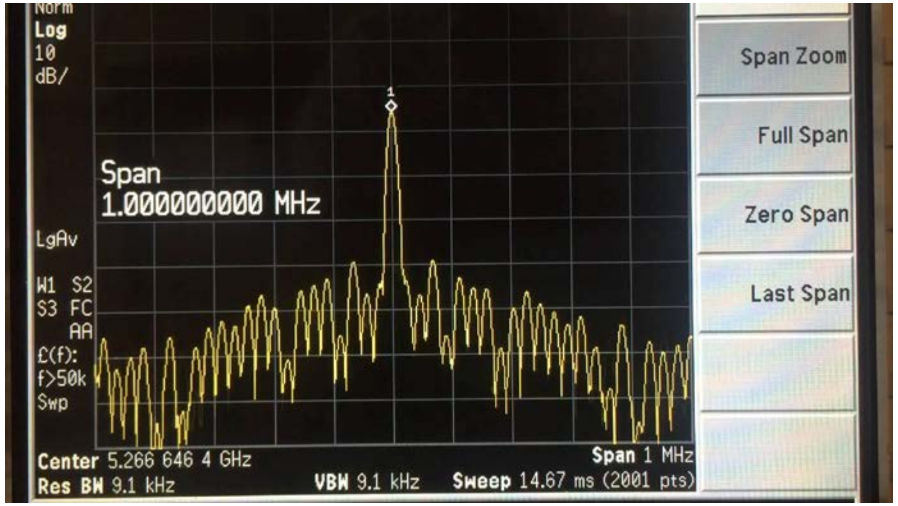

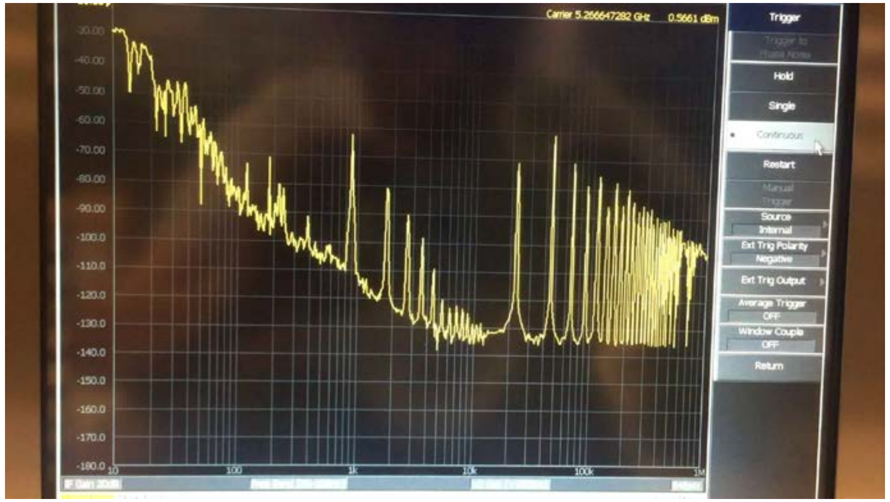

$$\Delta f = \frac{d\phi}{dt}$$

Phase noise measurement

Liu et al. *Light: Science & Applications* (2018)7:38
DOI 10.1038/s41377-018-0035-8

Official journal of the CIOMP 2047-7538
www.nature.com/lsa

ARTICLE Open Access

Observation of parity-time symmetry in microwave photonics

Yanzhong Liu[1,2], Tengfei Hao[1,2], Wei Li[1,2], Jose Capmany[3], Ninghua Zhu[1,2] and Ming Li[1,2]

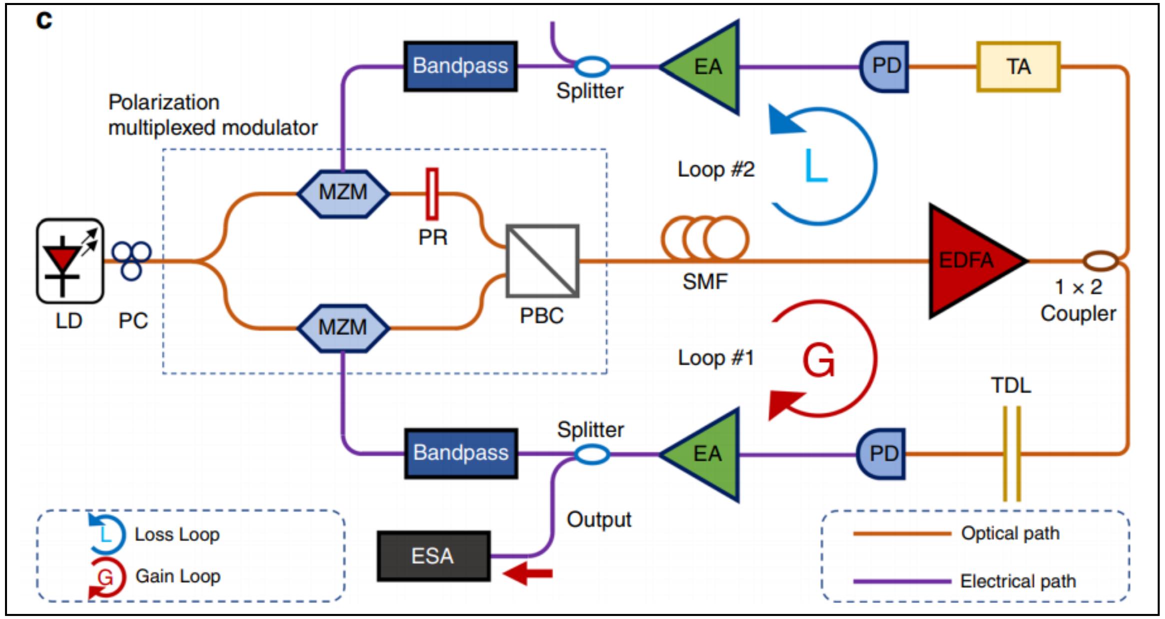

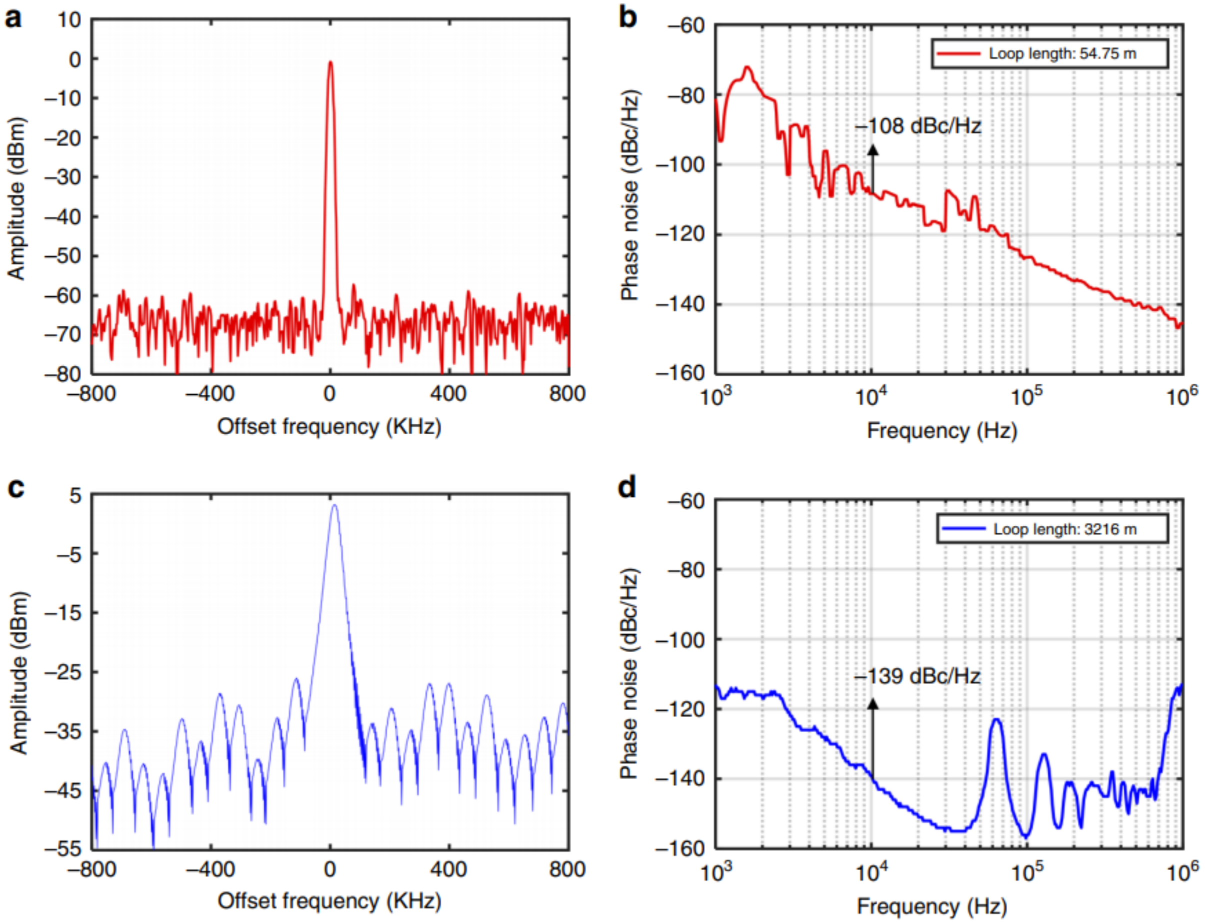

Y. Liu, T. Hao, W. Li, *et al. Light Sci Appl* **7,** 38 (2018)

ARTICLE

Check for updates

https://doi.org/10.1038/s41467-020-16705-8

OPEN

Parity-time symmetry in wavelength space within a single spatial resonator

Jiejun Zhang[1]✉, Lingzhi Li[1], Guangying Wang[1], Xinhuan Feng[1], Bai-Ou Guan[1] & Jianping Yao[1,2]✉

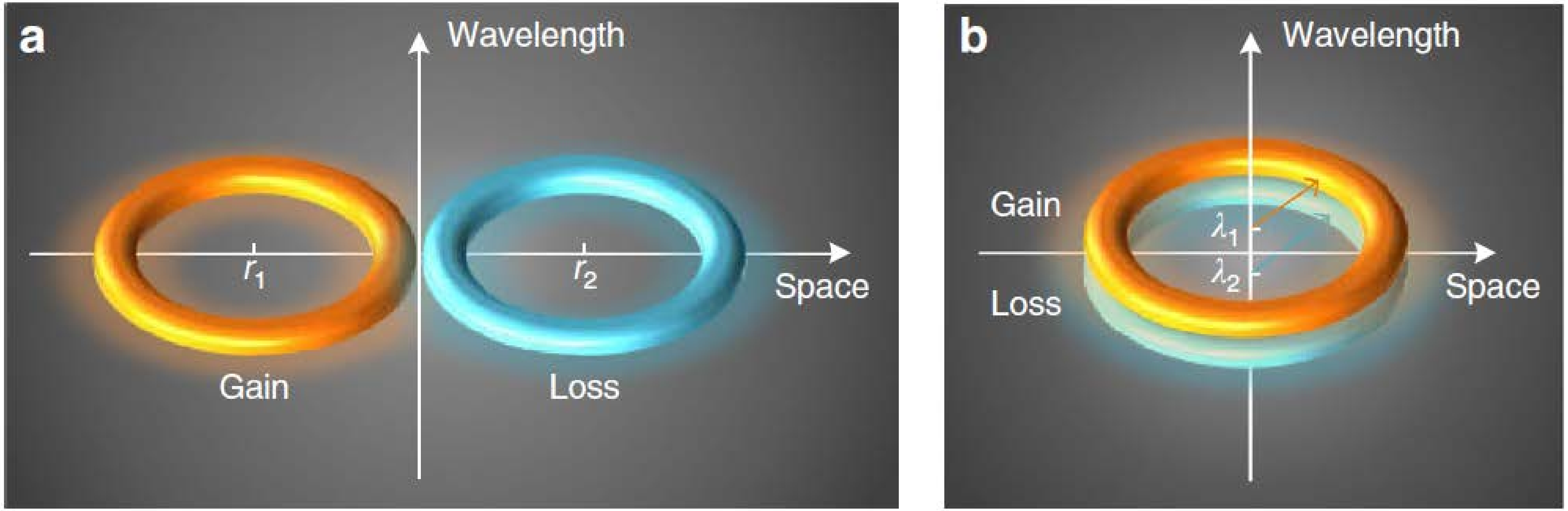

PT symmetry in wavelength space

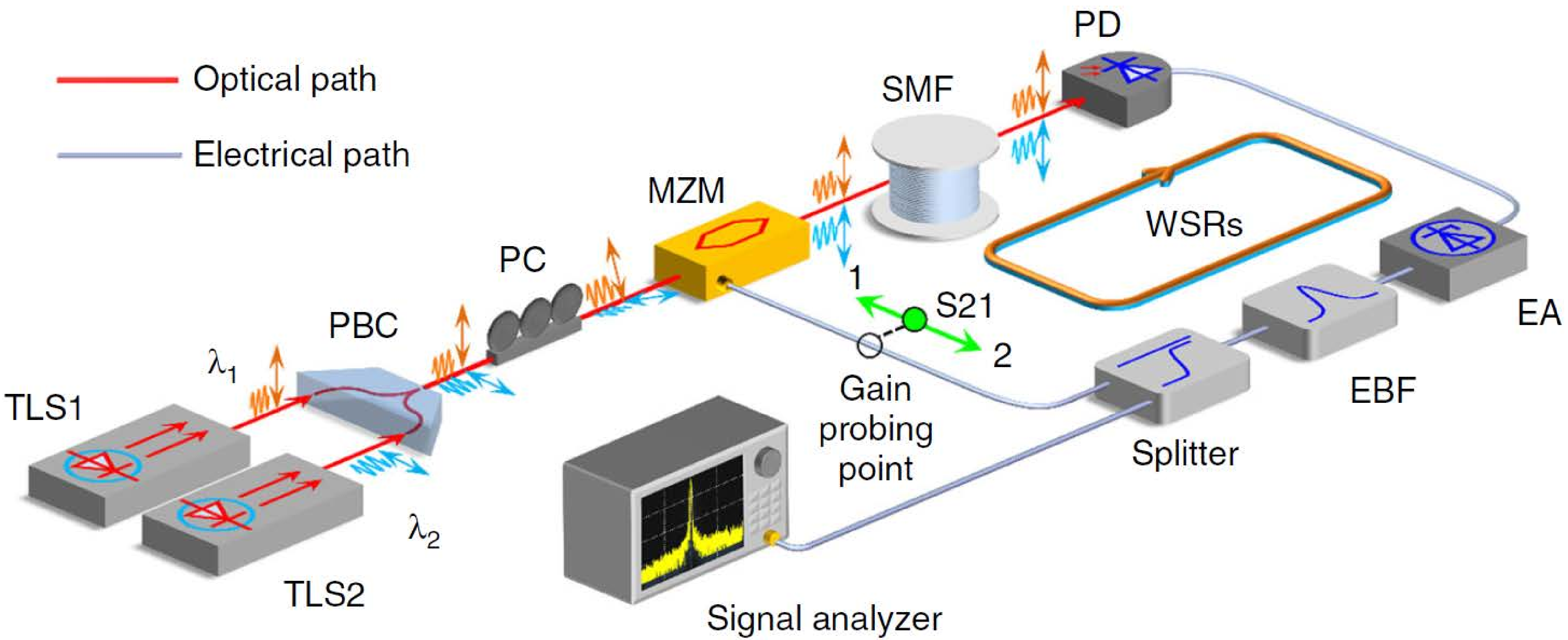

1）Two wavelengths, corresponding to the gain and loss loops

2）Gain and loss are controlled by tuning the polarization controllers

Experimental results

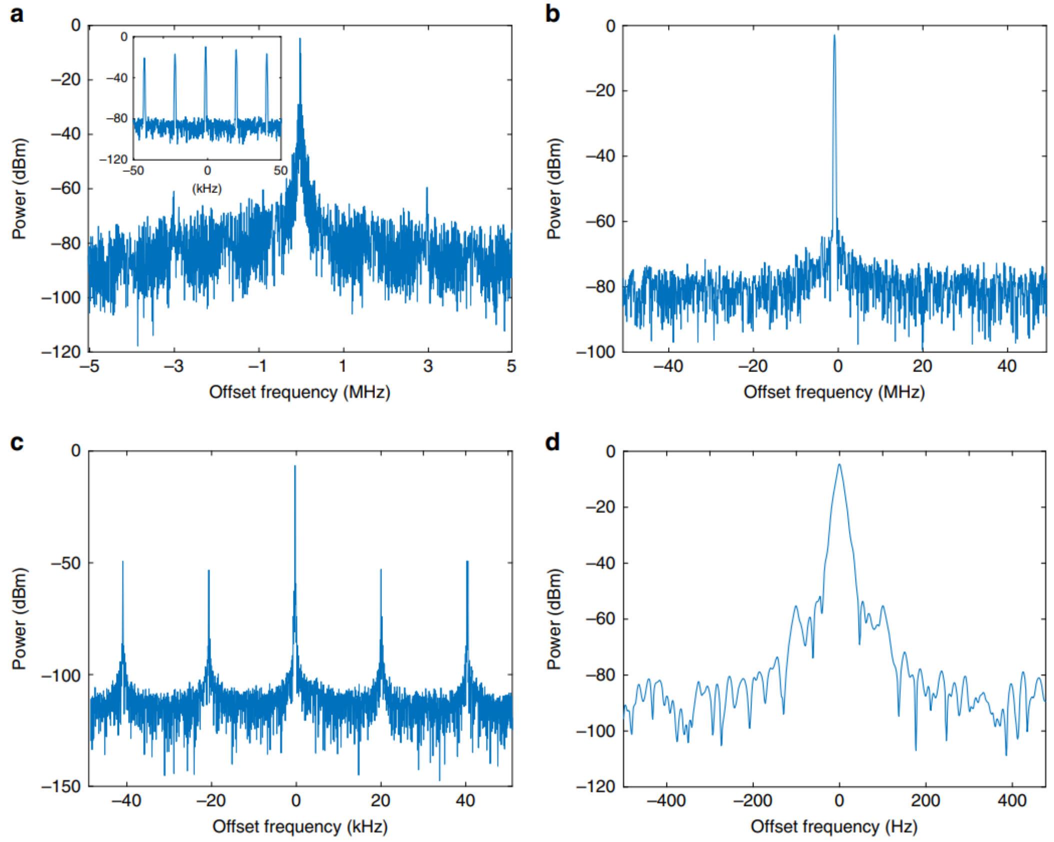

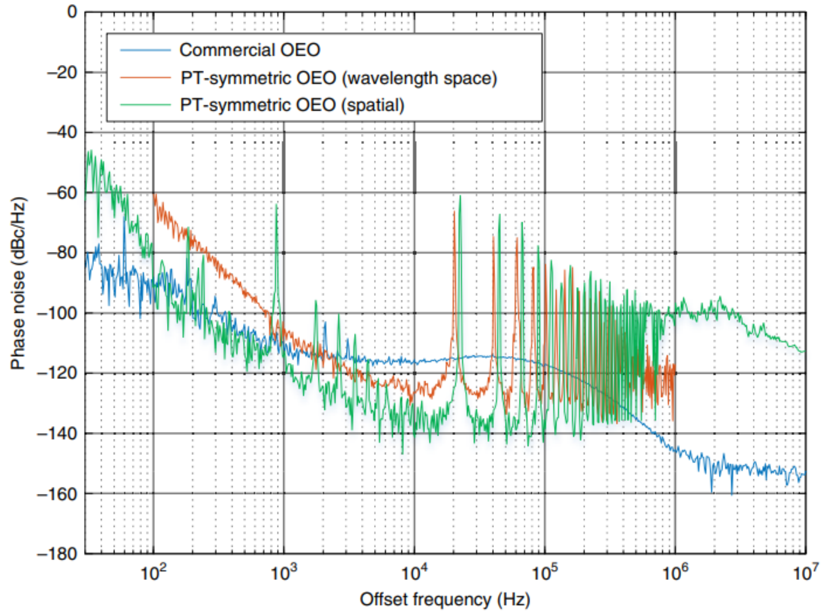

Phase noise: −129.3 dBc/Hz at an offset frequency of 10 kHz with sidemodes lower than −66.22 dBc/Hz with a 9.1-km loop length.

a) **(no PT symmetry)** Zoom-in view of the multimode spectrum showing multiple modes with comparable amplitudes

(With PT symmetry) Single-mode oscillation spectra measured with RBWs of **b)** 3 MHz, **c)** 100 kHz and **d)** 9 Hz. The spectrum in (c) shows a dominating mode with a sidemode suppression ration of 46.75 dB.

OEwaves OEOs

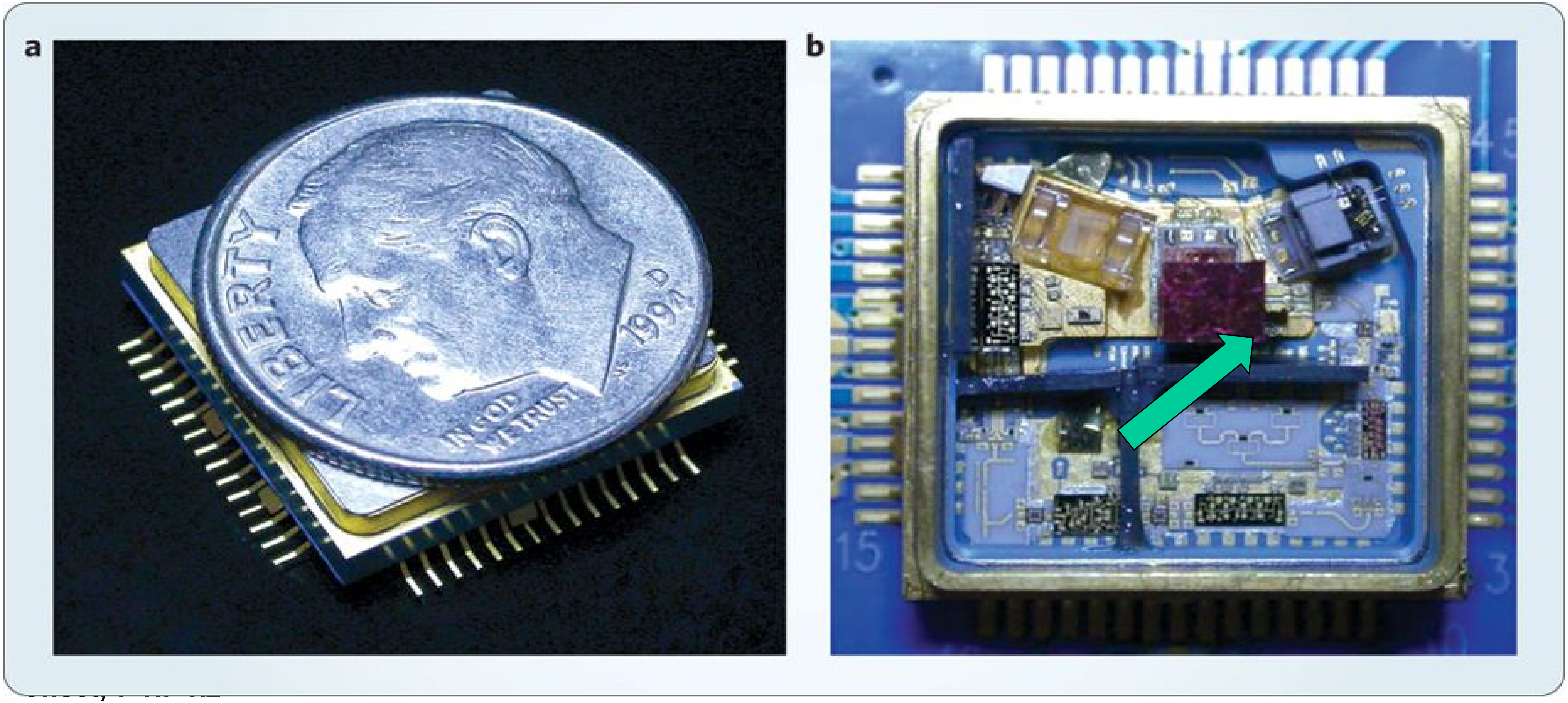

L. Maleki, Nat. Photonics 5(12), 728–730 (2011).

JOURNAL OF LIGHTWAVE TECHNOLOGY, VOL. 36, NO. 19, OCTOBER 1, 2018 4655

Silicon Photonic Integrated Optoelectronic Oscillator for Frequency-Tunable Microwave Generation

Weifeng Zhang, *Member, IEEE*, and Jianping Yao, *Fellow, IEEE, Fellow, OSA*

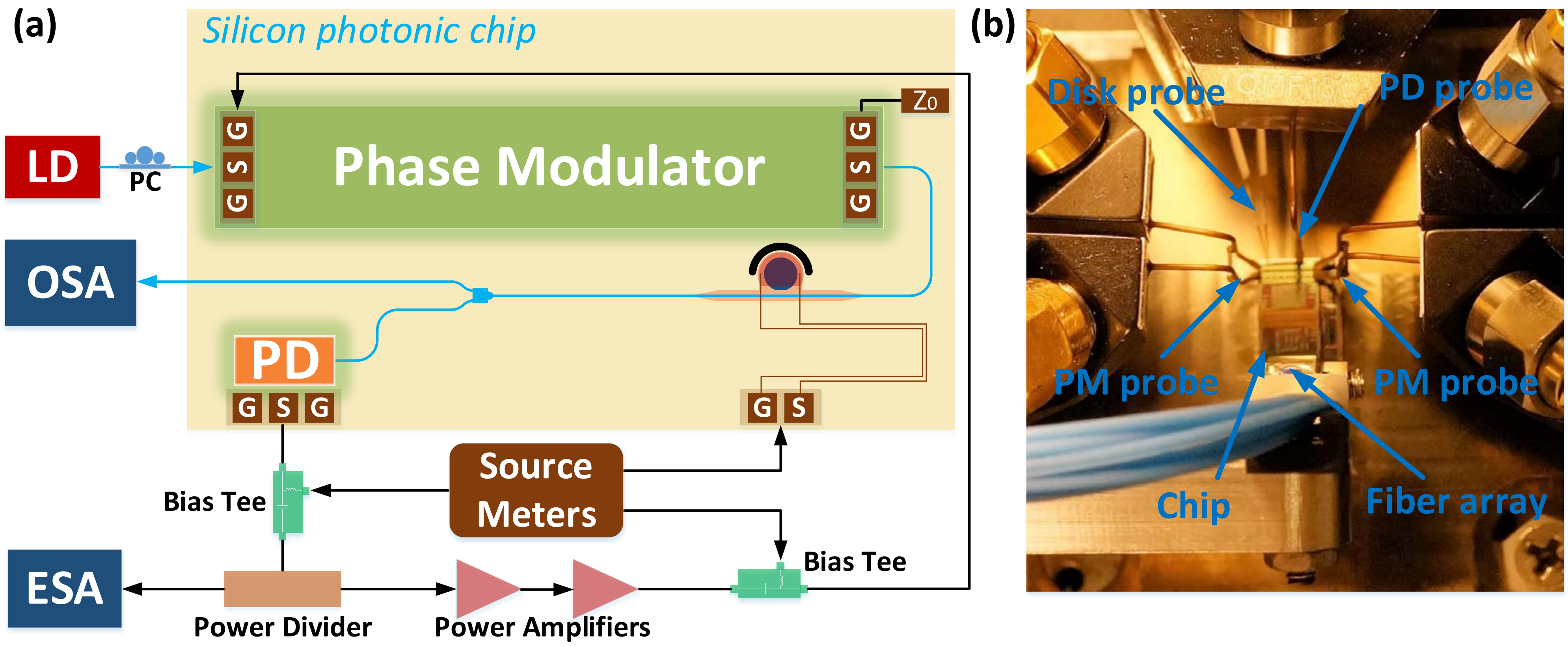

W. Zhang and J. P. Yao, *J. Lightw. Technol.*, vol. 36, no. 19, pp. 4655-4663, Oct. 2018. (MWP special issue 2018)

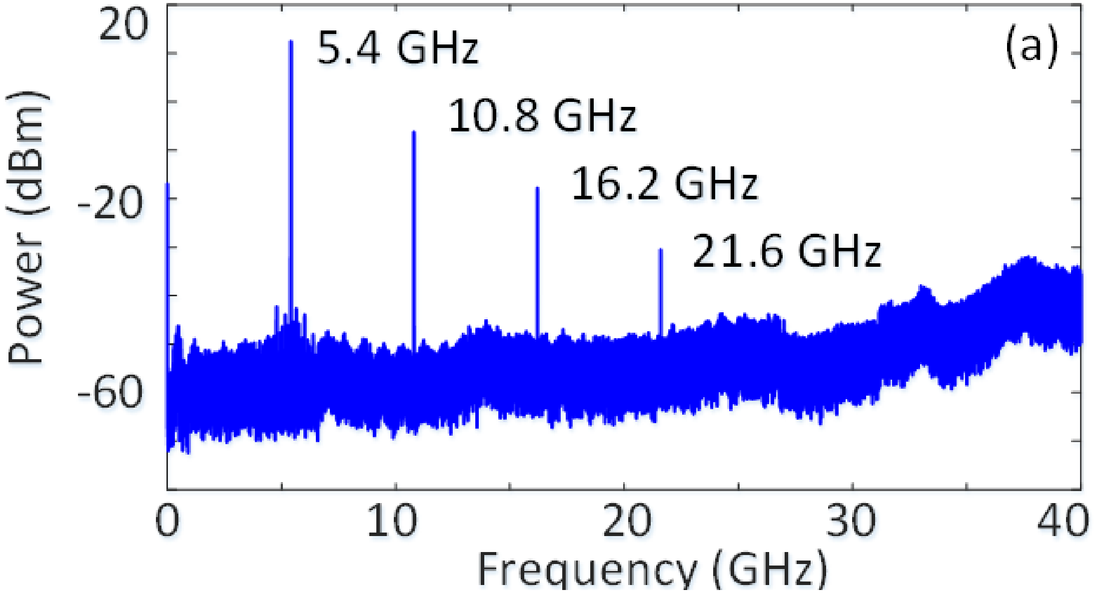

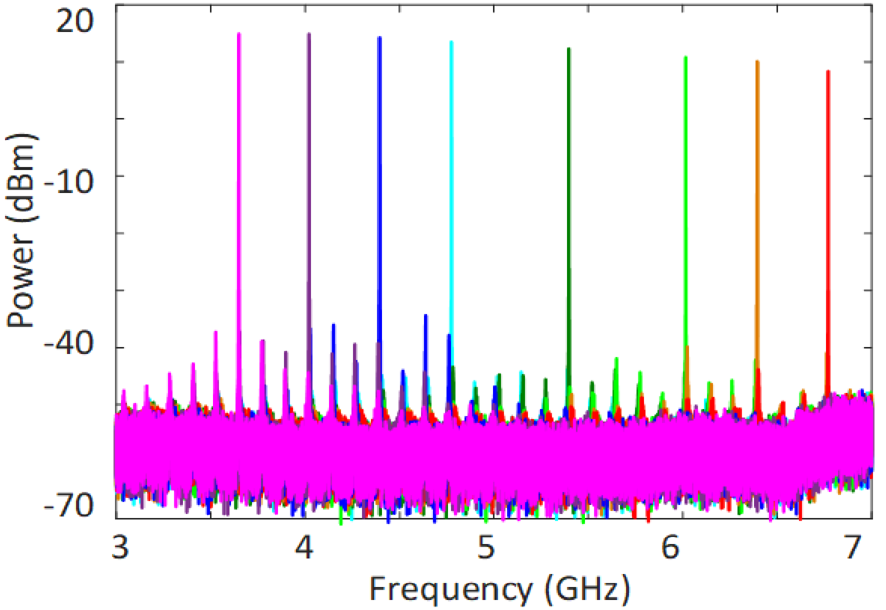

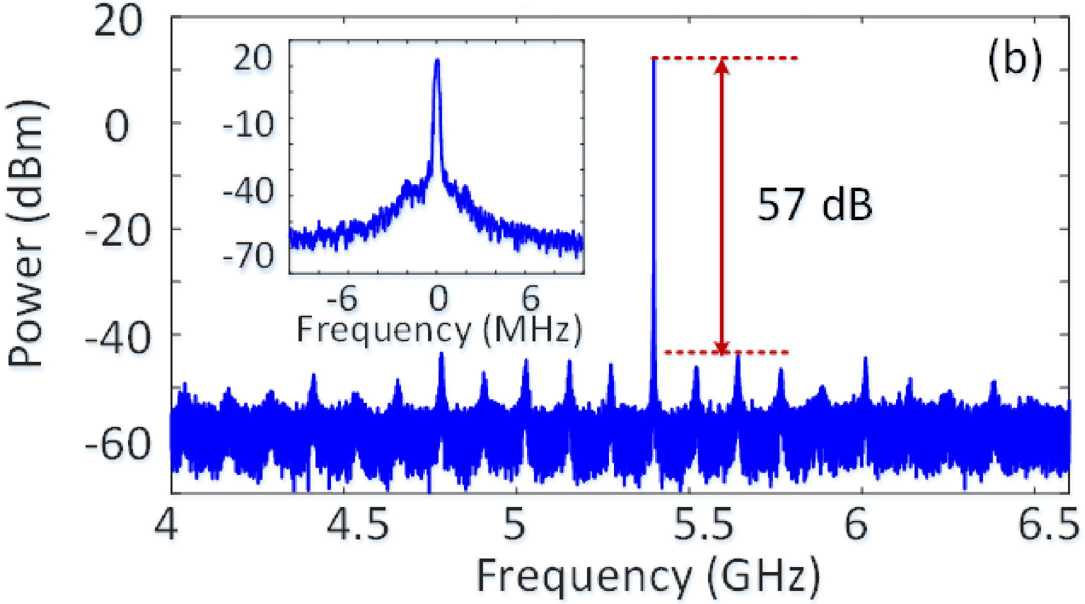

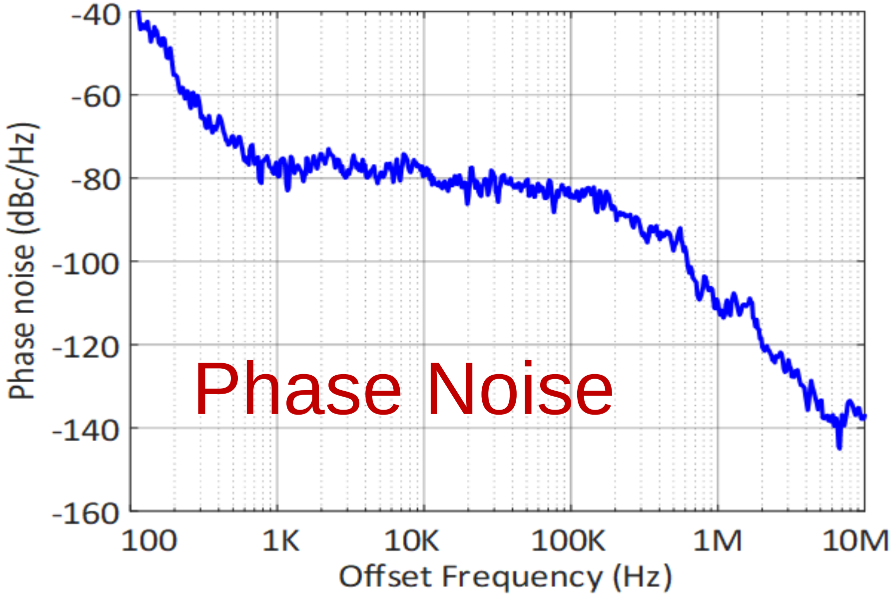

W. Zhang and J. P. Yao, *J. Lightw. Technol.*, vol. 36, no. 19, pp. 4655-4663, Oct. 2018. (MWP special issue 2018)

nature COMMUNICATIONS

OEO for chirped microwave waveform generation

ARTICLE

DOI: 10.1038/s41467-018-04240-6 OPEN

Breaking the limitation of mode building time in an optoelectronic oscillator

Tengfei Hao[1,2], Qizhuang Cen[3], Yitang Dai[3], Jian Tang[1,2], Wei Li[1,2], Jianping Yao[4], Ninghua Zhu[1,2] & Ming Li[1,2]

- A regular **frequency-tunable** OEO → poor phase noise performance →need of **building time** when tuned from one mode to another mode.
- A Fourier-domain mode locked OEO → **all modes co-exist** in the cavity → each time only one mode is selected → **no building time** problem.

T. Hao, Q. Cen, Y. Dai, J. Tang, W. Li, J. P. Yao, N. Zhu, and M. Li, *Nature Comm.*, vol. 9, 1839, May 2018.

FDML OEO for chirped microwave waveform generation

Synchronized tuning

$T_{\text{roundtrip}} = n \times T_{\text{filter drive}}$

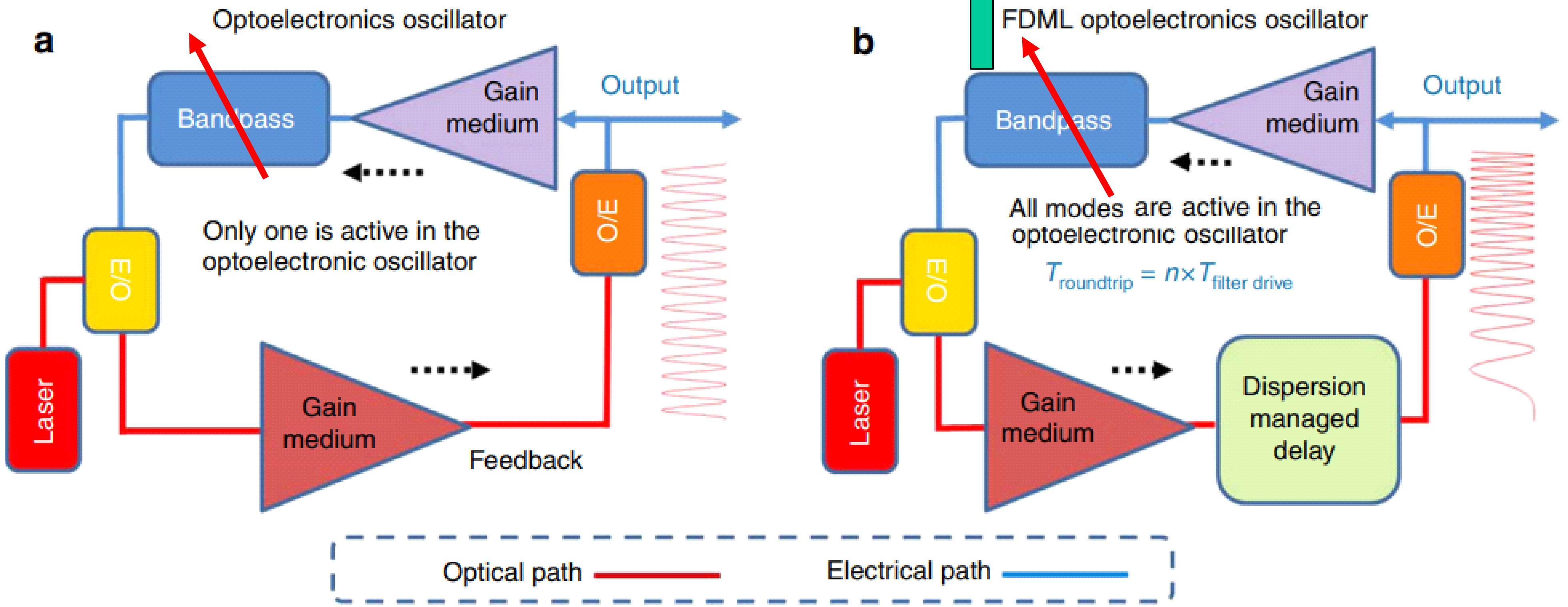

Fig. 1 Schematic to show the operations of a conventional OEO and an OEO based on FDML. **a** A conventional single-frequency OEO, only one mode is active in the cavity. **b** An OEO based on FDML for generation of a microwave signal with fast frequency tuning, all modes are active in the cavity. E/O electrical to optical conversion; O/E optical to electrical conversion

T. Hao, Q. Cen, Y. Dai, J. Tang, W. Li, J. P. Yao, N. Zhu, and M. Li, *Nature Comm.*, vol. 9, 1839, May 2018.

FDML OEO for chirped microwave waveform generation

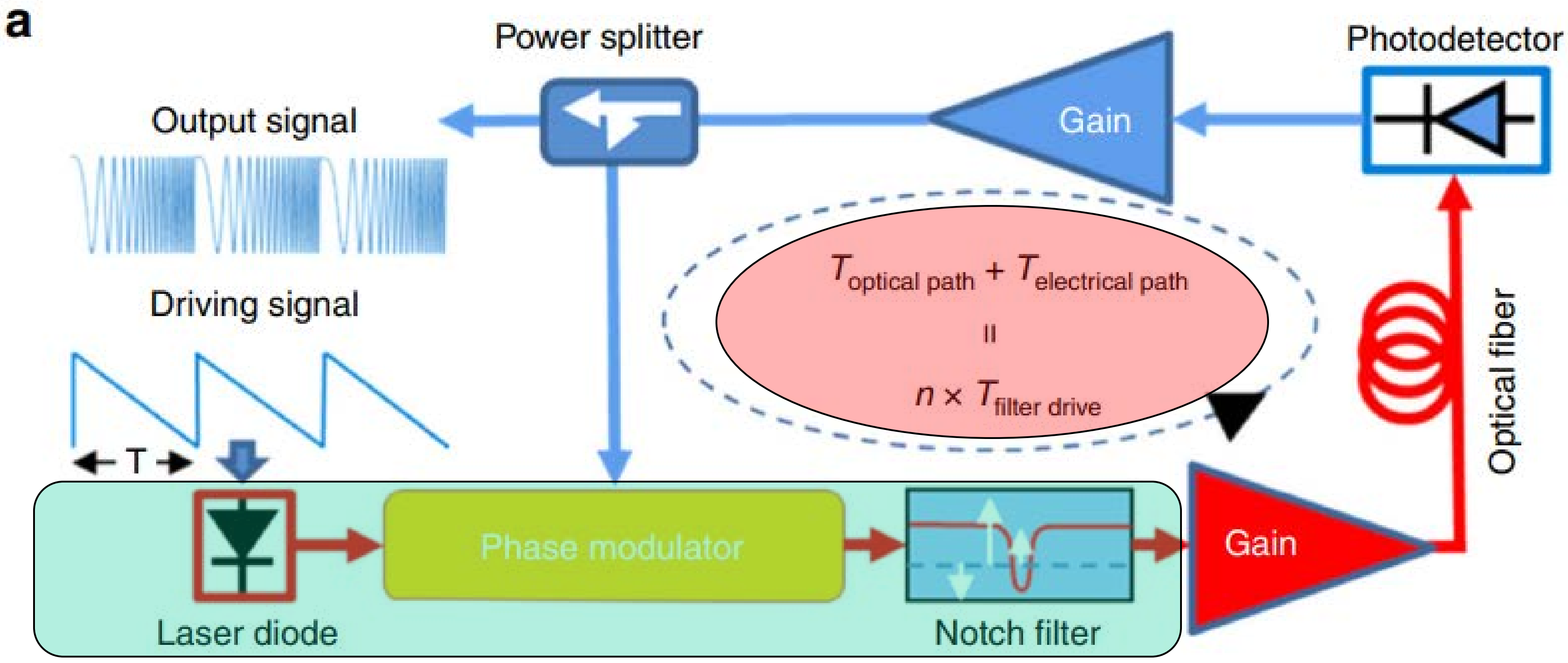

The fast-tunable bandpass filter for frequency-domain mode locking is implemented using **a tunable laser source, a phase modulator and a narrow-passband notch filter.**

T. Hao, Q. Cen, Y. Dai, J. Tang, W. Li, J. P. Yao, N. Zhu, and M. Li, *Nature Comm.*, vol. 9, 1839, May 2018.

Experimental results

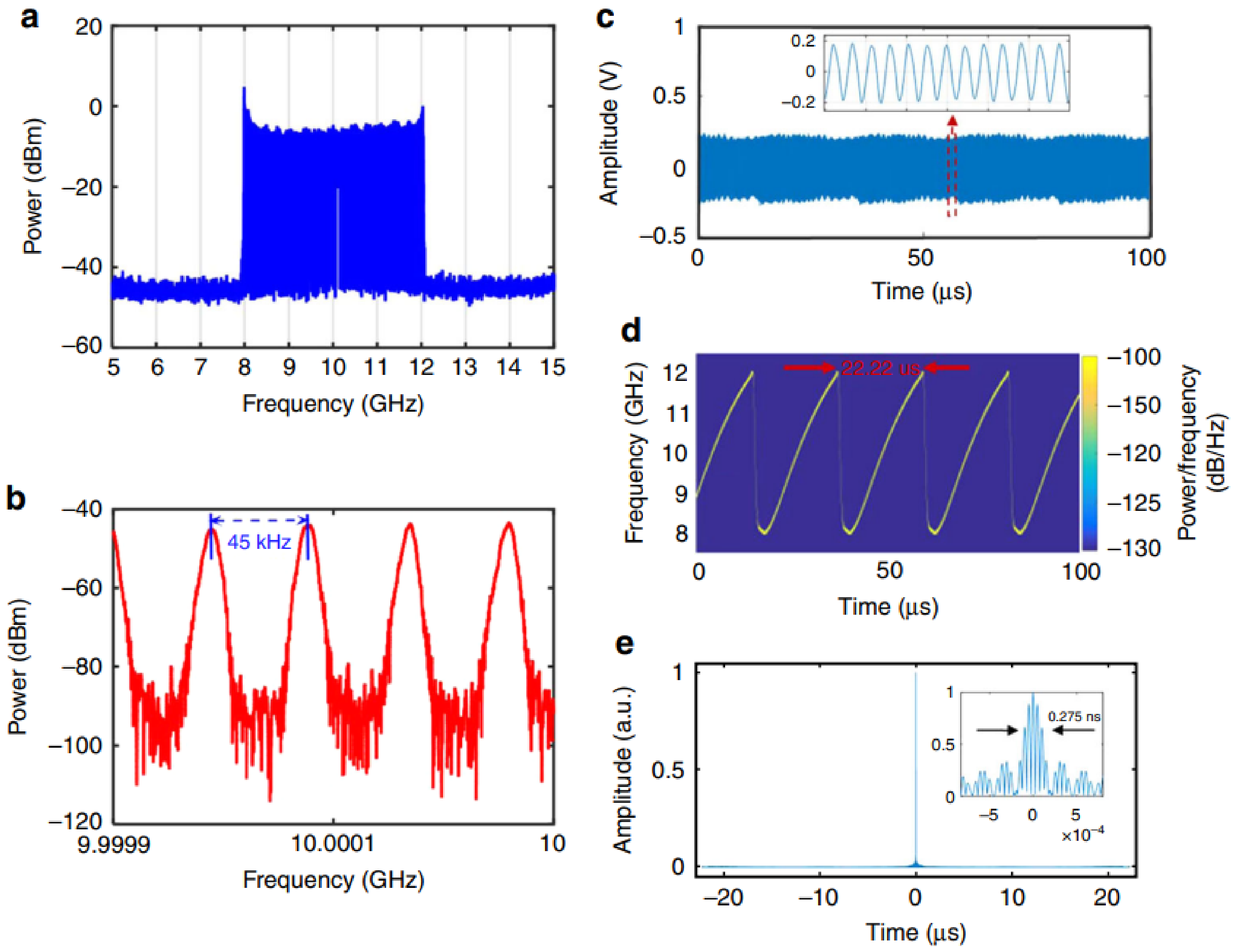

Fig. 3 Experimental results. **a** Spectrum of a generated X-band frequency-scanning microwave waveform with a span of 10 GHz. **b** Spectrum with a span of 200 kHz. **c** Temporal waveform of the periodically and continuously chirped microwave waveform, the inset shows a section of the waveform. **d** Real-time frequency distribution. **e** The compressed pulse by autocorrelation (inset: zoom-in display)

Challenge: an ultra-narrow bandpass filter is needed to ensure to select a single mode ar one time

T. Hao, Q. Cen, Y. Dai, J. Tang, W. Li, J. P. Yao, N. Zhu, and M. Li, *Nature Comm.*, vol. 9, 1839, May 2018.

Outline

- Recent research activities in MWP
- Microwave signal generation
- Microwave signal processing
- Radio over fiber based on coherent detection
- Microwave photonics for sensing
- Conclusion

Microwave photonic filters - Incoherent delay line MWP filters

Three examples:

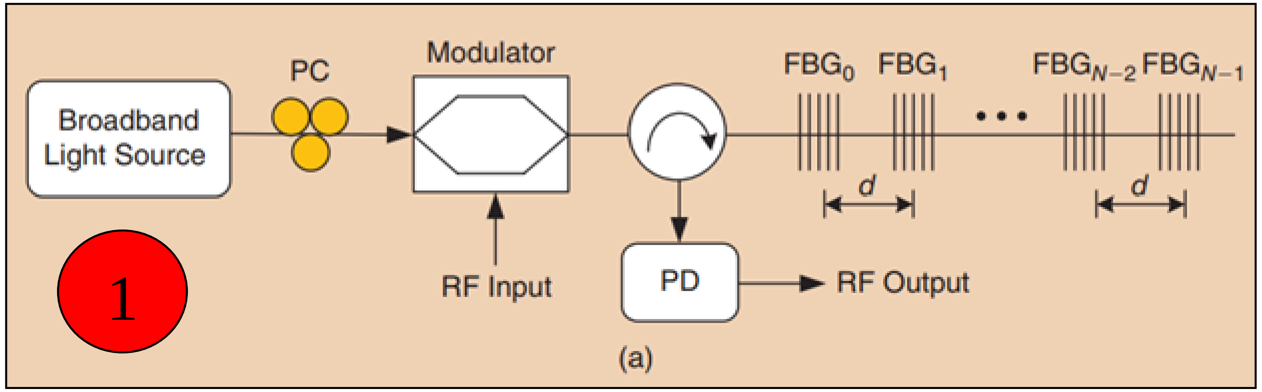

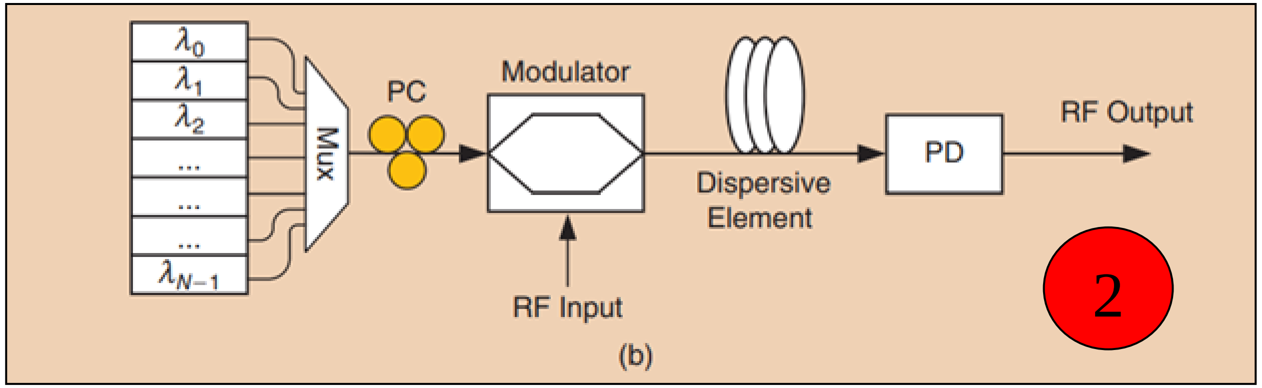

Two microwave photonic filter configurations operating in the incoherent regime based on (a) a broadband light source and (b) a laser array

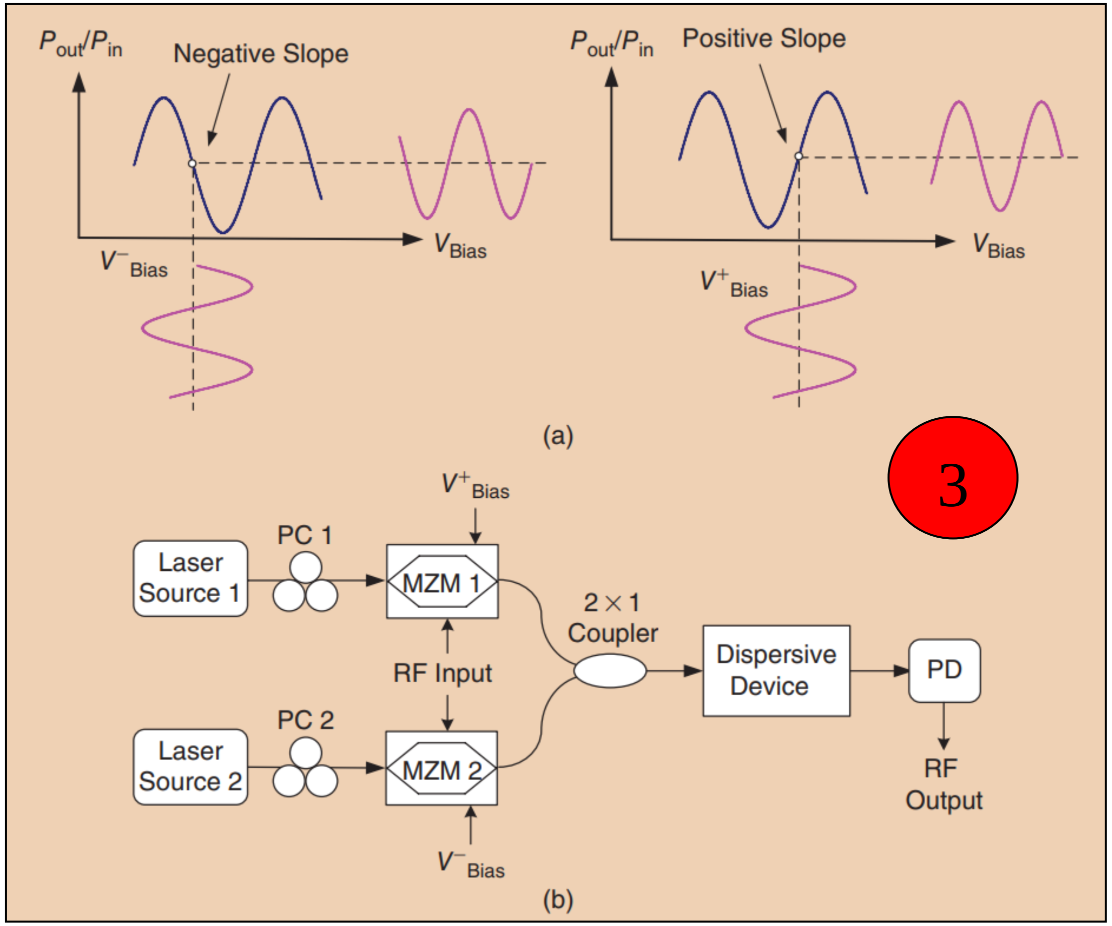

A microwave photonic filter with **negative coefficients** based on phase inversion using complementarily biased MZMs.

J. P. Yao, "A fresh look at microwave photonics filters," *IEEE Microwav. Mag.*, vo. 16, no. 8, pp. 46-60, Sept. 2015.

Microwave photonic filters - Coherent MWP filters

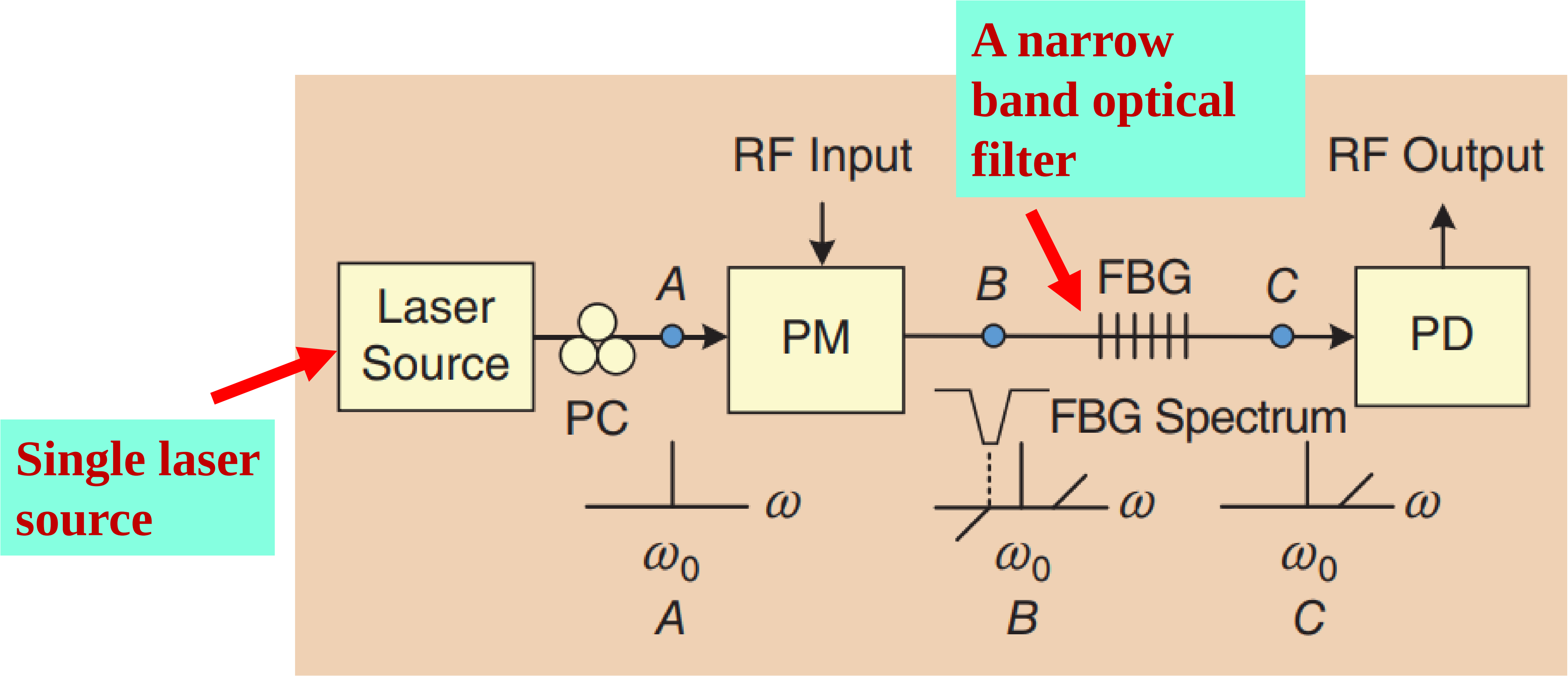

A coherent microwave photonic filter, in which an optical notch filter is used to filter out one sideband of a phase-modulated signal, thus achieving PM–IM conversion.

J. P. Yao, "A fresh look at microwave photonics filters," *IEEE Microwav. Mag.*, vo. 16, no. 8, pp. 46-60, Sept. 2015.

Microwave photonic filters - Coherent MWP filters

PS-FBG: phase shifted fiber Bragg grating

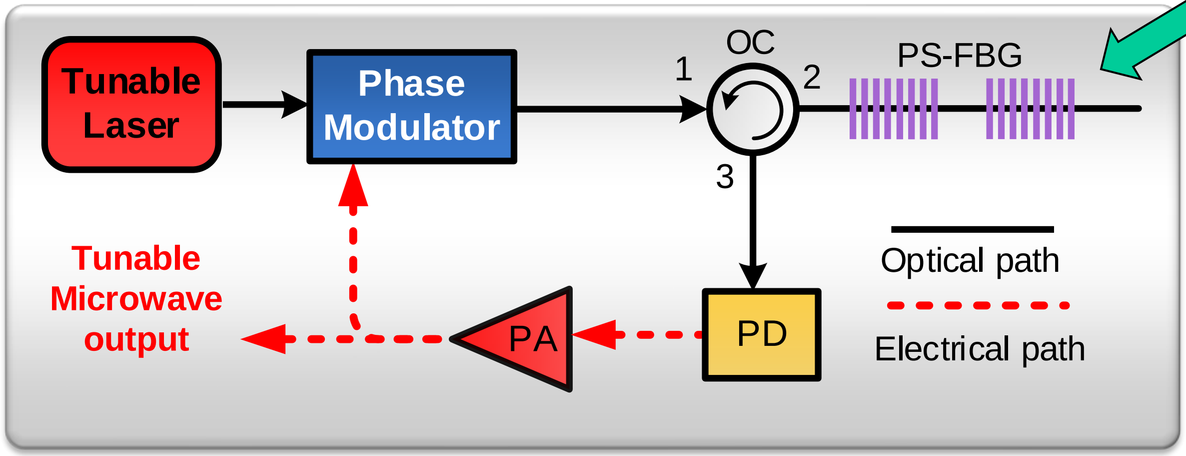

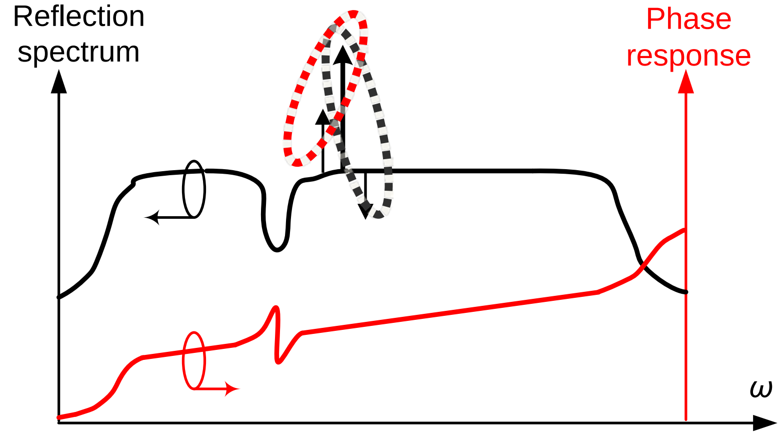

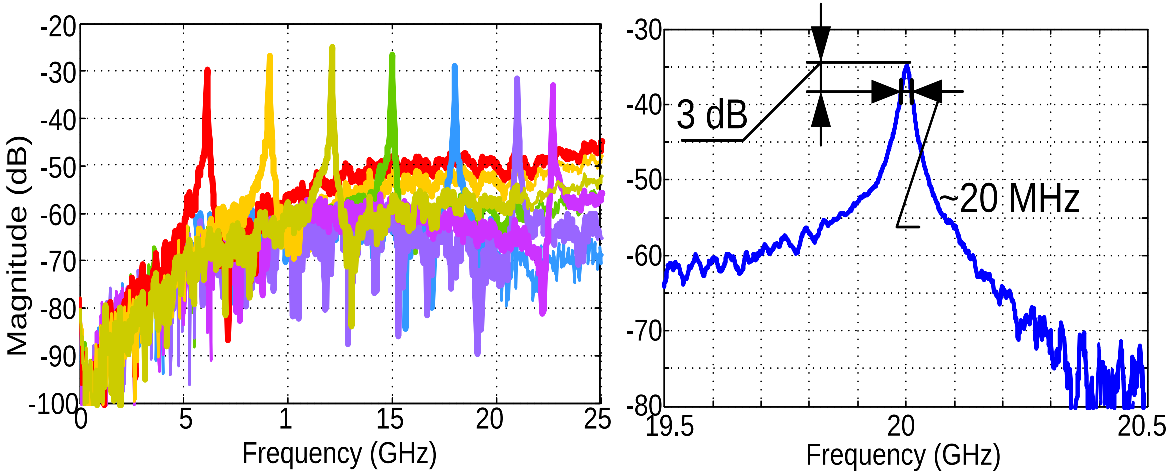

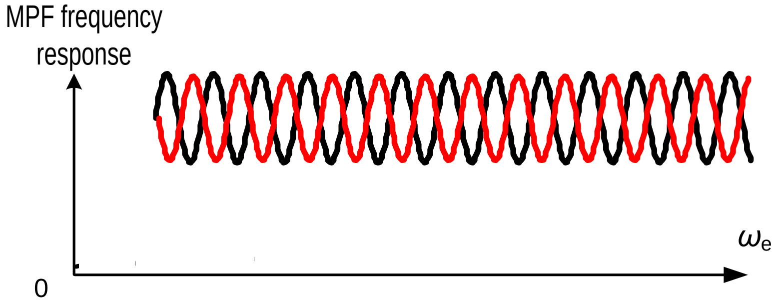

Size large, stability poor

W. Li and J. P. Yao, *IEEE Trans. Microw. Theory Tech.*, vol. 60, no. 6, pp. 1735-1742, June 2012.

Microwave photonic filters - Coherent MWP filters

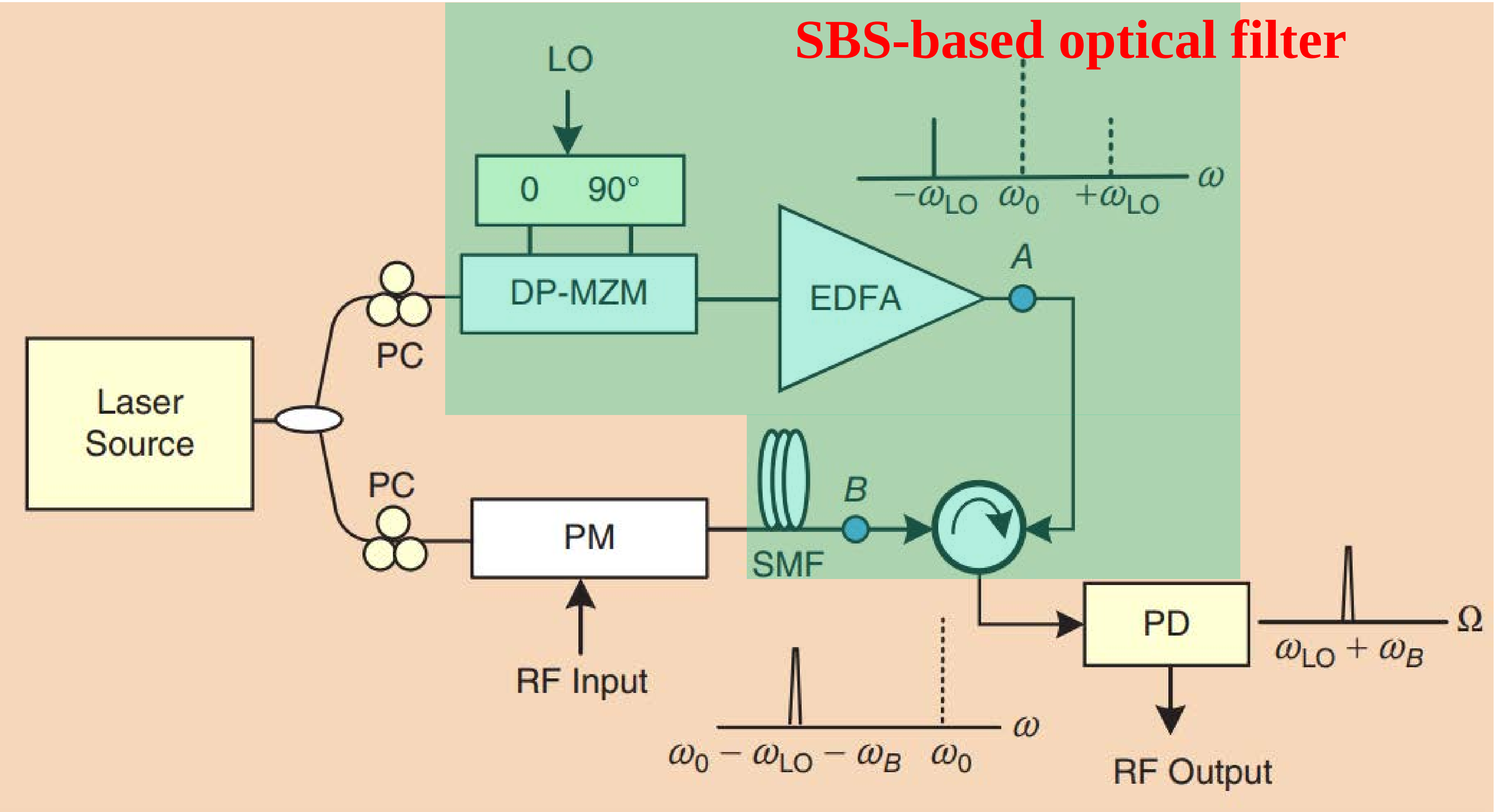

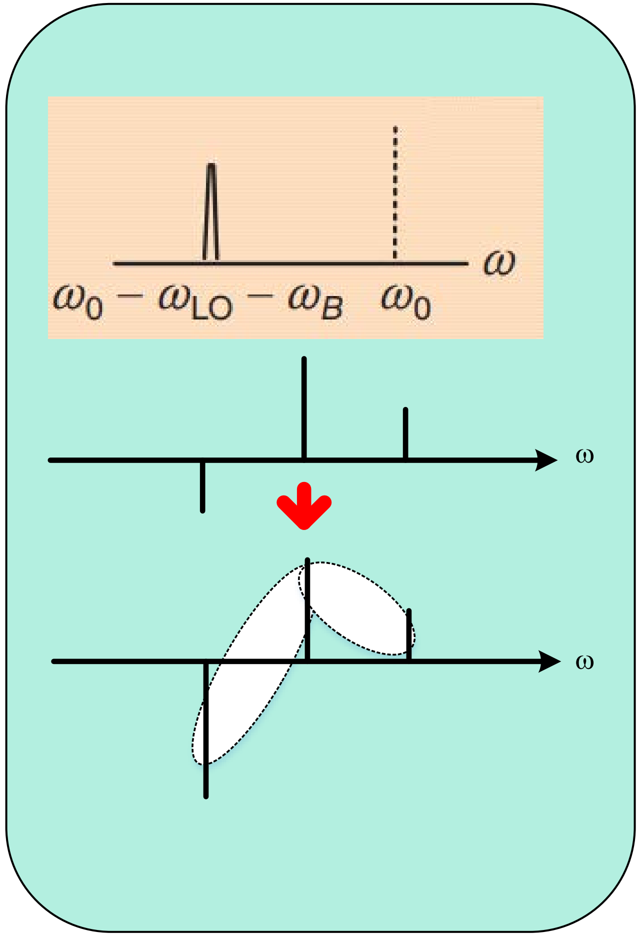

A coherent microwave photonic filter implemented based on phase modulation and PM–IM using SBS gain

J. P. Yao, “A fresh look at microwave photonics filters,” *IEEE Microwav. Mag.*, vo. 16, no. 8, pp. 46-60, Sept. 2015.

ARTICLES
PUBLISHED ONLINE: 5 DECEMBER 2016 | DOI: 10.1038/NPHOTON.2016.233
nature photonics

A monolithic integrated photonic microwave filter (InP)

Javier S. Fandiño[1], Pascual Muñoz[1,2], David Doménech[2] and José Capmany[1]*

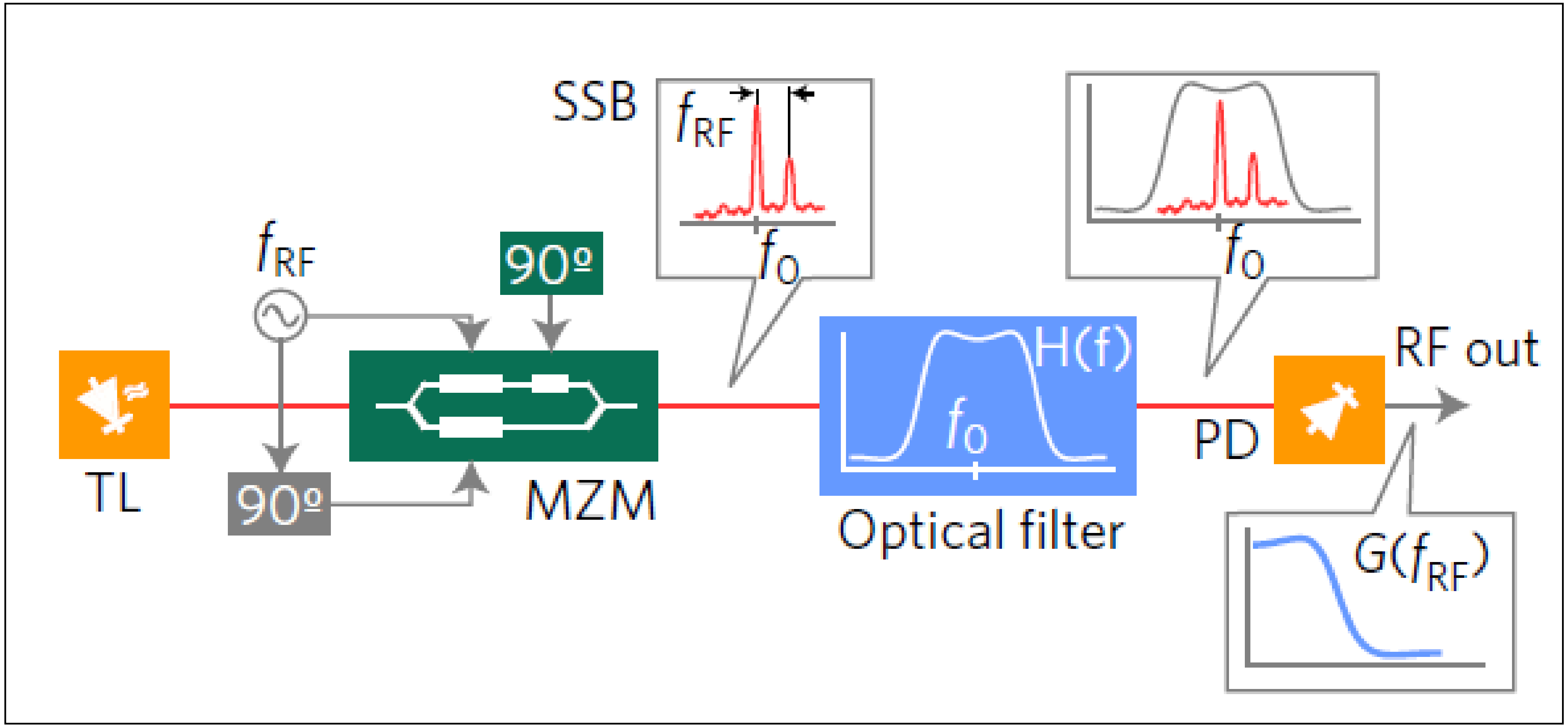

J. Fandno et al, Nature Photon. 2016

ARTICLES
PUBLISHED ONLINE: 5 DECEMBER 2016 | DOI: 10.1038/NPHOTON.2016.233
nature photonics

A monolithic integrated photonic microwave filter

Javier S. Fandiño[1], Pascual Muñoz[1,2], David Doménech[2] and José Capmany[1]*

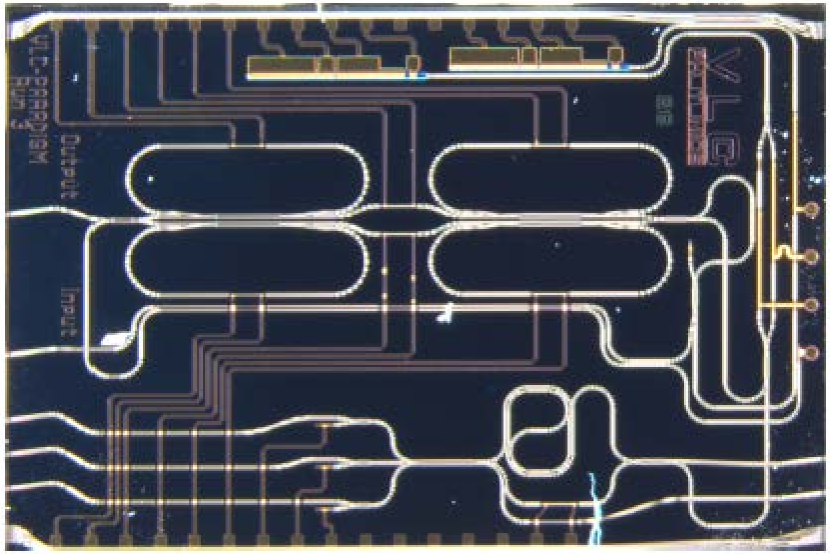

Image of a fabricated die

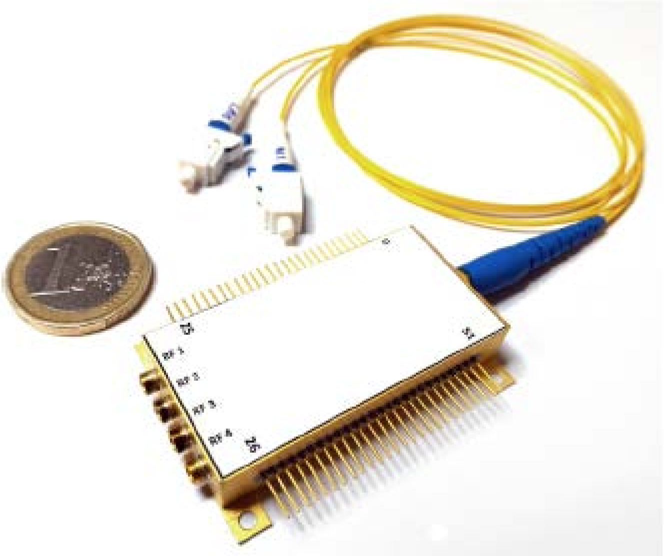

Packaged chip

A monolithic integrated photonic microwave filter

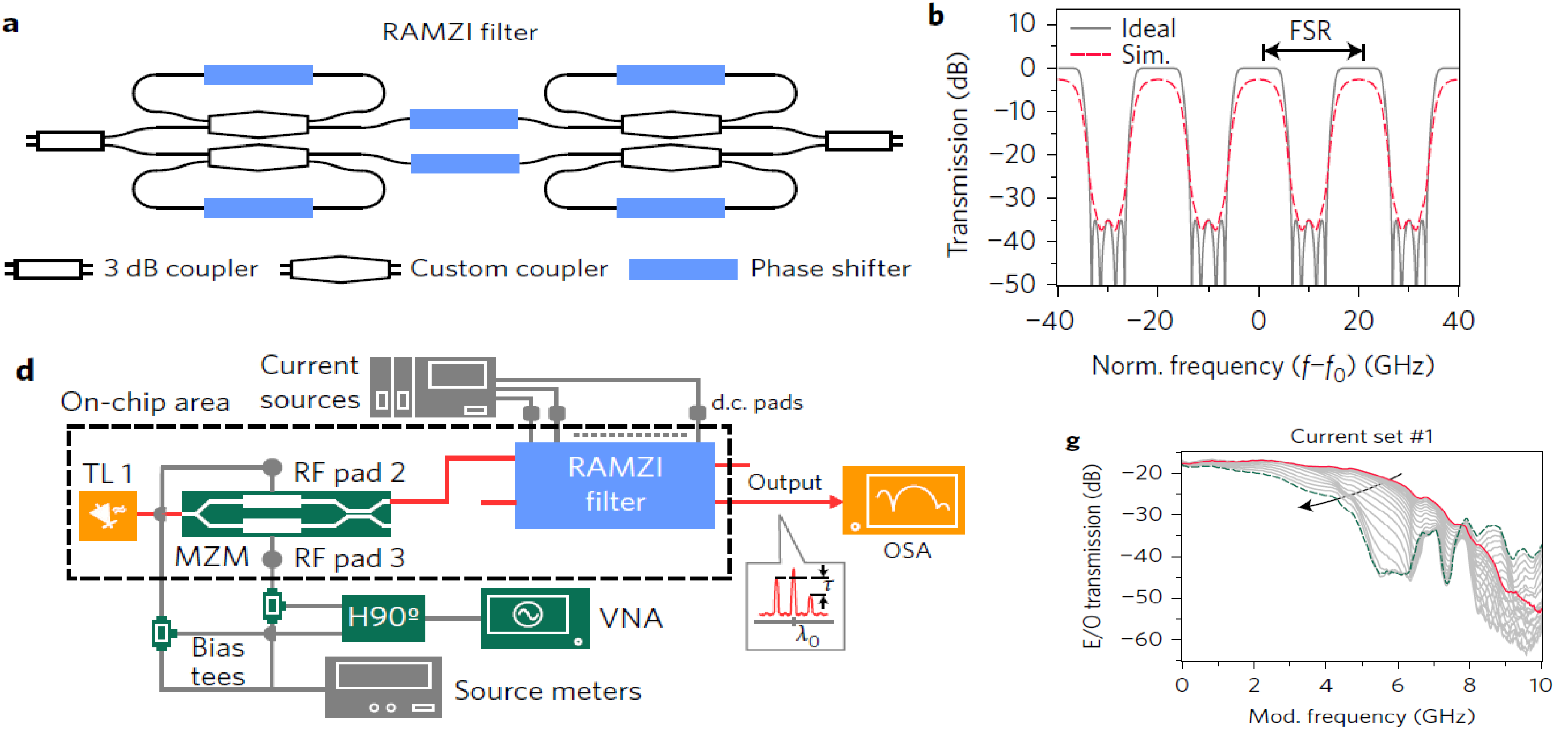

J. Fandno et al, Nature Photon. 2016

3622 Vol. 43, No. 15 / 1 August 2018 / *Optics Letters* **Letter**

Optics Letters

On-chip silicon photonic integrated frequency-tunable bandpass microwave photonic filter

WEIFENG ZHANG AND JIANPING YAO*

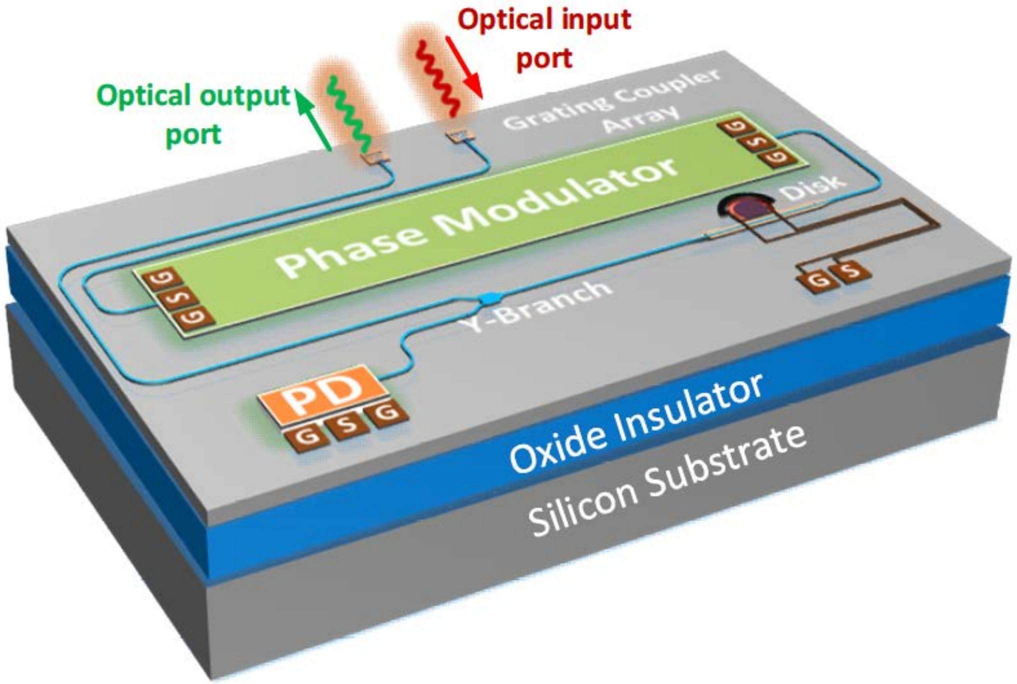

Fig. 1. Perspective view of the proposed IMPF on a silicon photonic chip

(SOI)

MWP2021

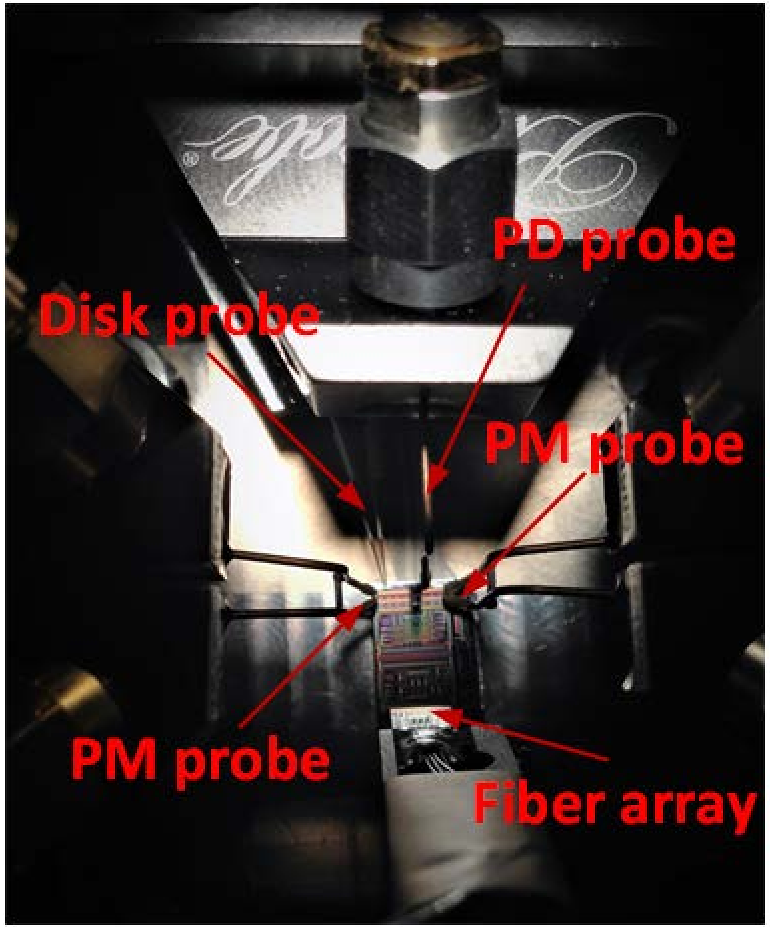

Image of the experimental set-up captured by a camera.

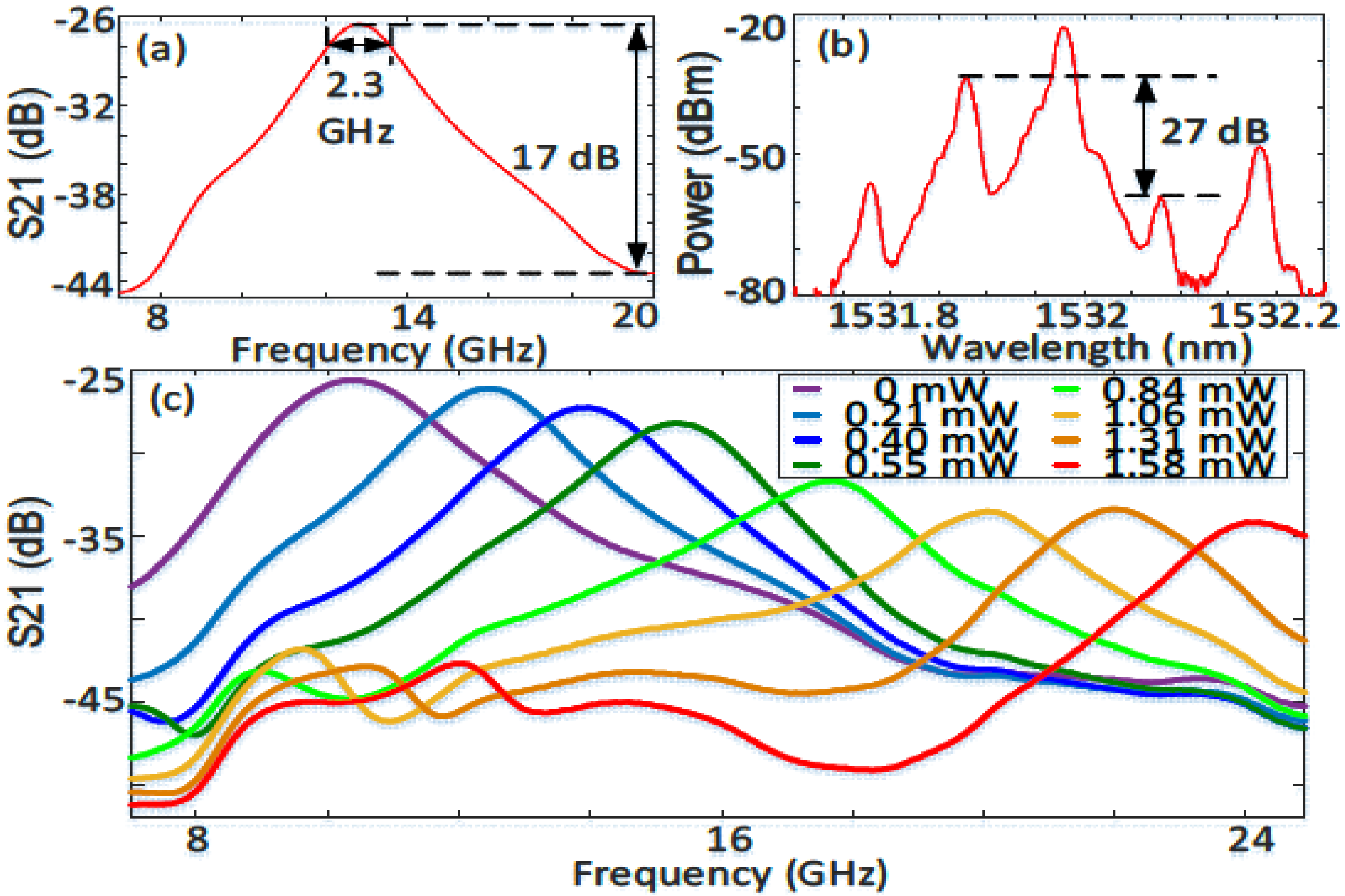

Fig. 7 Experimental result: (a) frequency response of the filter with a center frequency of 13 GHz; (b) optical spectrum of the modulated optical signal when the microwave signal frequency is 13 GHz; (c) measured frequency responses of the filter with the center frequency tuned from 7 to 25 GHz.

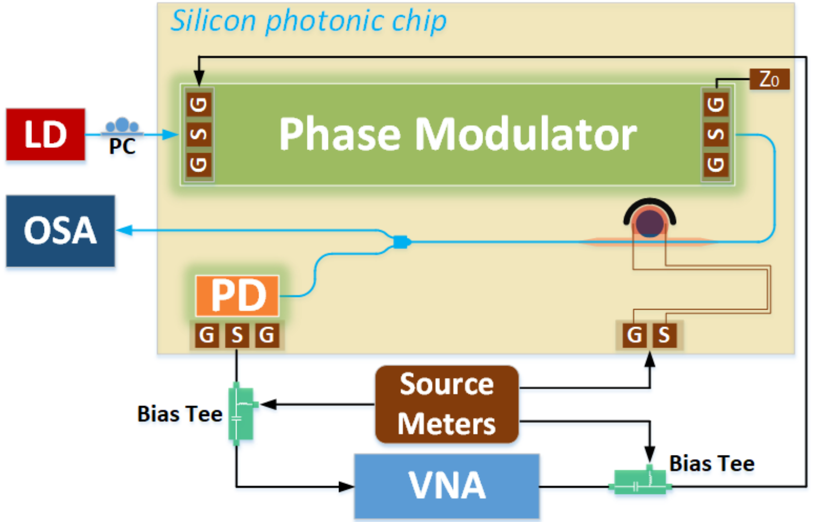

Tunable MWP filter - Measurements

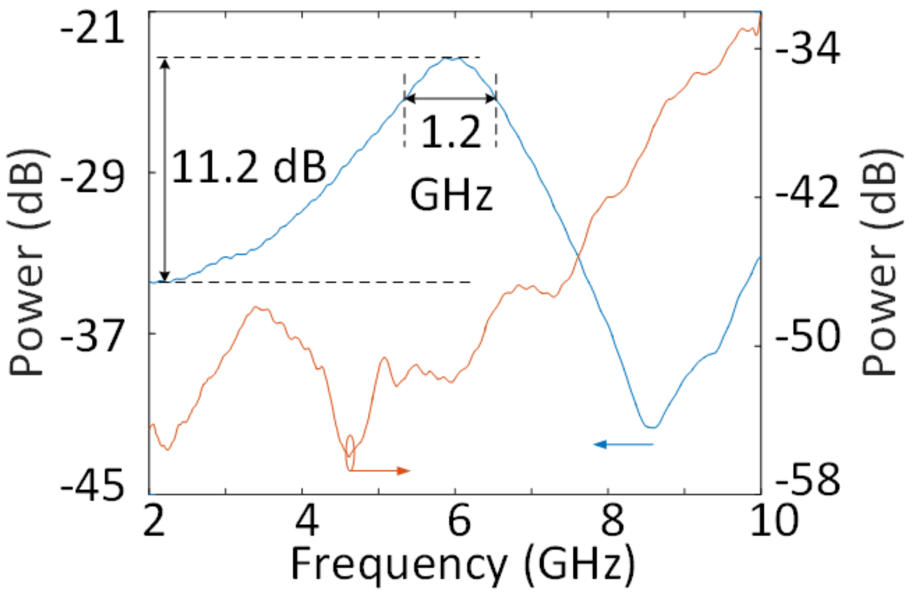

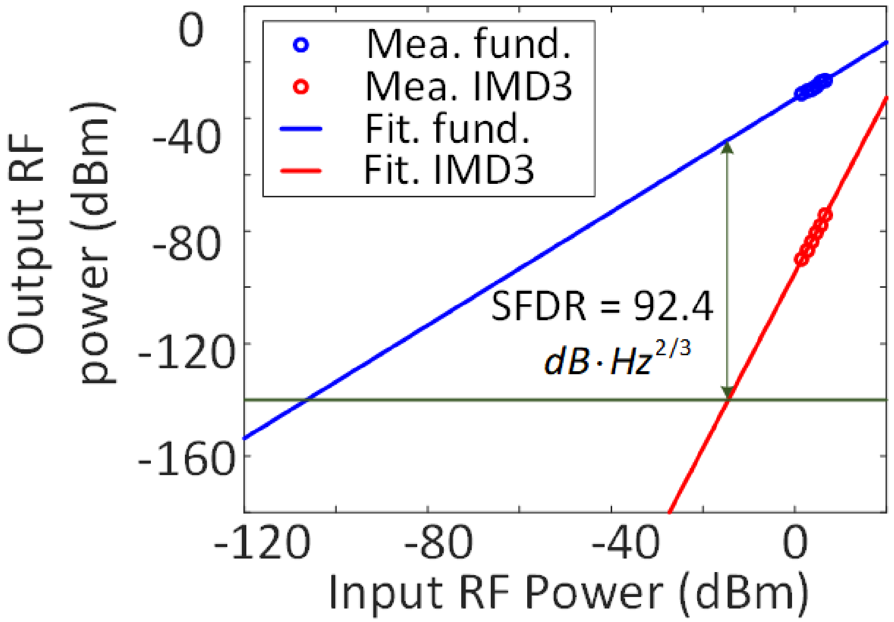

Frequency response of the filter (in blue) with a center frequency of 6 GHz and measured frequency response (in red) when no optical signal is coupled into the chip (to show the EMI)

Measurements of the fundamental signal power and that of the IMD3. Given a noise floor of -140 dBm/Hz, the measured **spurious-free dynamic range** (SFDR) of the filter are 92.4 dB·$Hz^{2/3}$.

nature COMMUNICATIONS

ARTICLE

DOI: 10.1038/s41467-017-00714-1 OPEN

Multipurpose silicon photonics signal processor core

Daniel Pérez[1], Ivana Gasulla[1], Lee Crudgington[2], David J. Thomson[2], Ali Z. Khokhar[2], Ke Li[2], Wei Cao[2], Goran Z. Mashanovich[2,3] & José Capmany[1]

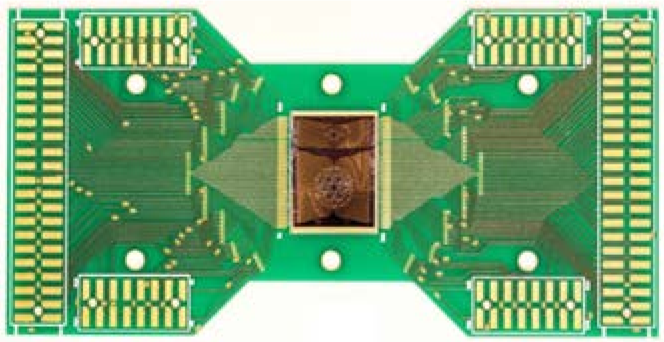

D. Perez et al., Nature Comm., Sep. 2017

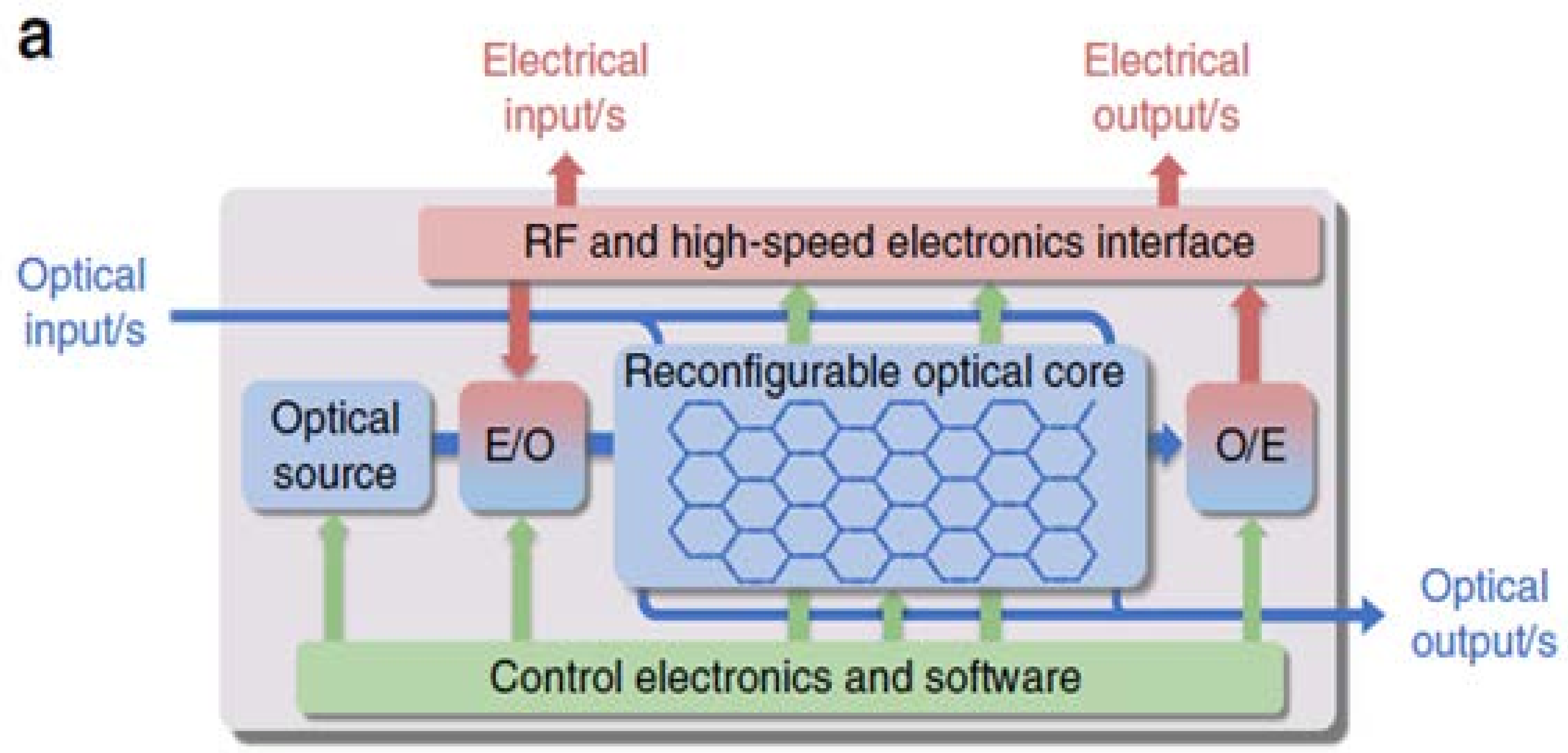

D. Perez et al., Nature Comm., Sep. 2017

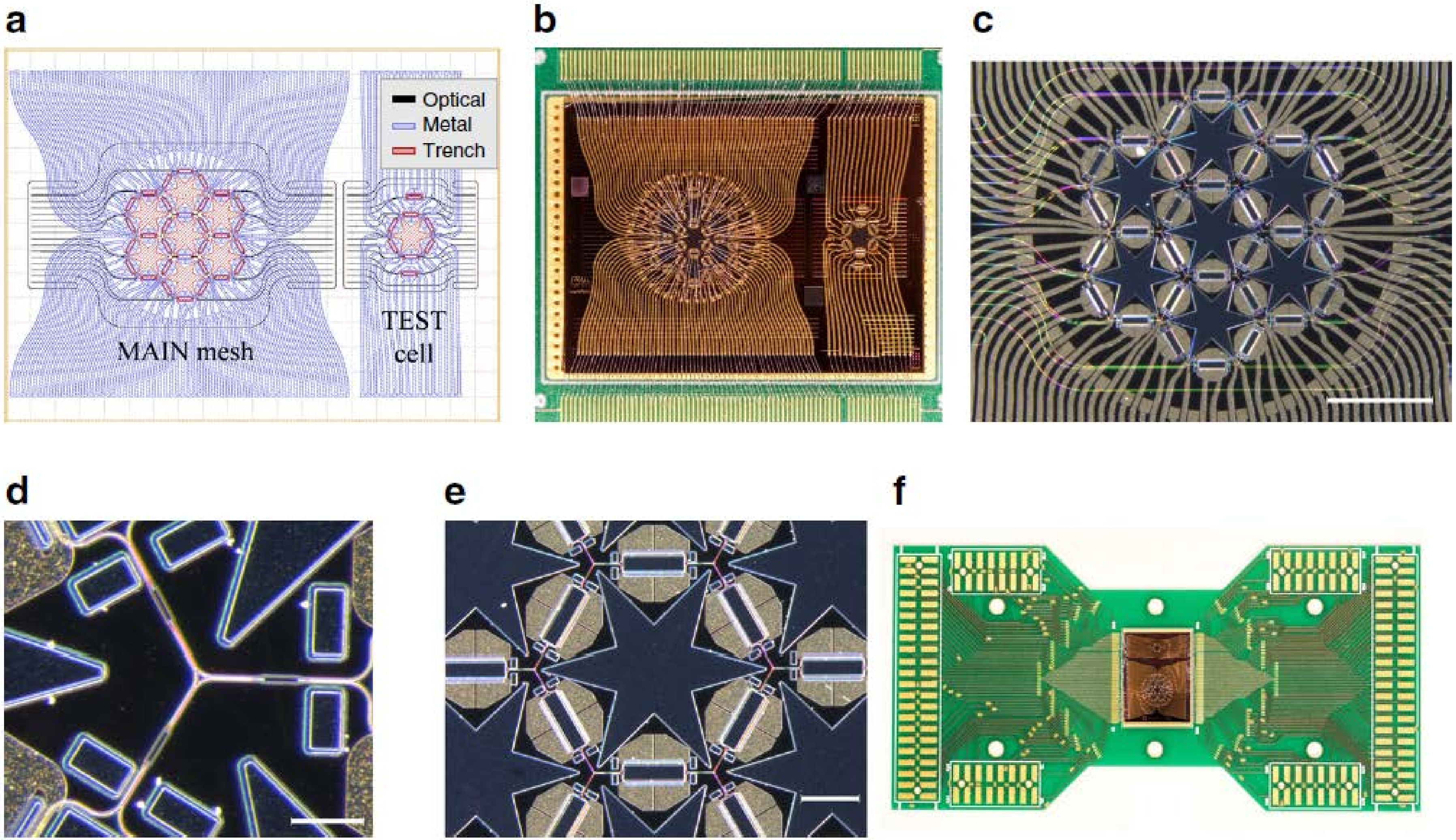

Fig. 2 Fabricated hexagonal waveguide mesh chip. **a** Design layers (optical, electrical, and thermal) of the 7-cell hexagonal waveguide mesh and the auxiliary test cell. **b** Fabricated silicon on insulator (*SOI*) chip of footprint 15 × 20 mm. **c** Zoomed vision of the 7-cell hexagonal waveguide mesh. *Scale bar* of 2 mm. In the *right bottom* corner **d** zoomed image of an optical interconnection node of three tuneable basic units (TBUs). *Scale bar* of 100 µm. In the *right bottom* corner **e** zoomed image of a single hexagonal cell showing the Mach Zehnder Interferometer (*MZI*). *Scale bar* of 500 µm. In the *right bottom* corner, tuning heaters, and star-type thermal isolation trenches. **f** Printed circuit board with the waveguide mesh chip mounted and wired bonded

D. Perez et al., Nature Comm., Sep. 2017

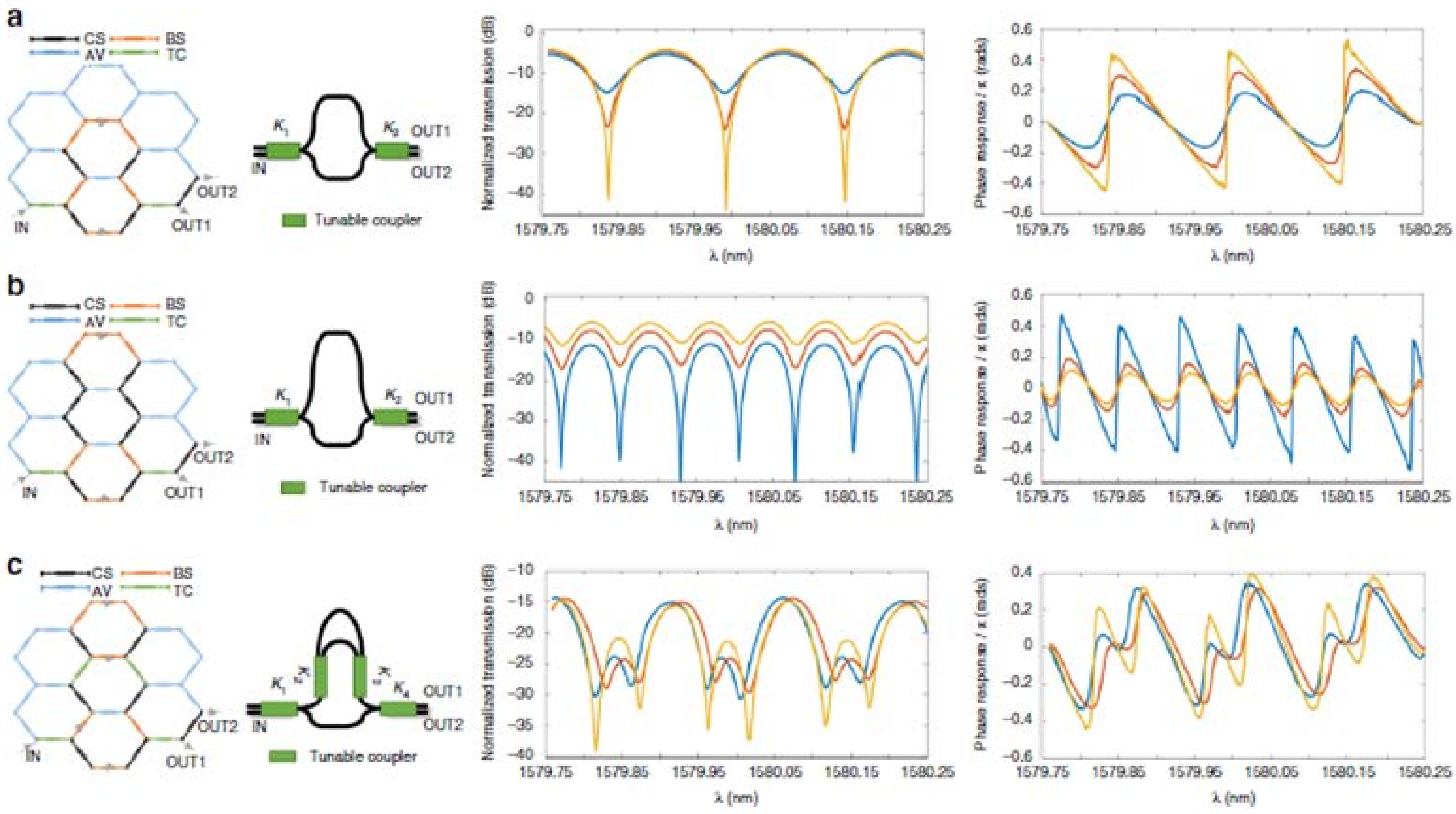
a
CS
BS
AV
TC
IN
OUT1
OUT2
Tunable coupler
Normalized transmission (dB)
λ (nm)
Phase response / π (rads)
b
c

ARTICLE

https://doi.org/10.1038/s41467-019-14249-0 OPEN

Similar to electronic FPGA

Photonic integrated field-programmable disk array signal processor

Weifeng Zhang[1] & Jianping Yao[1*]

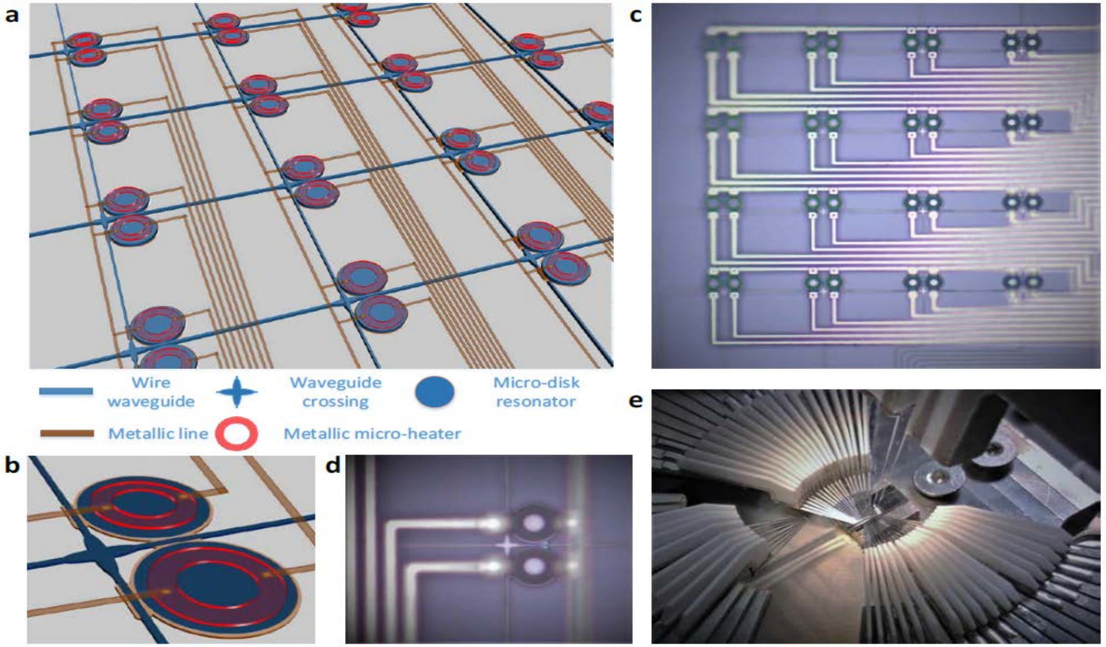

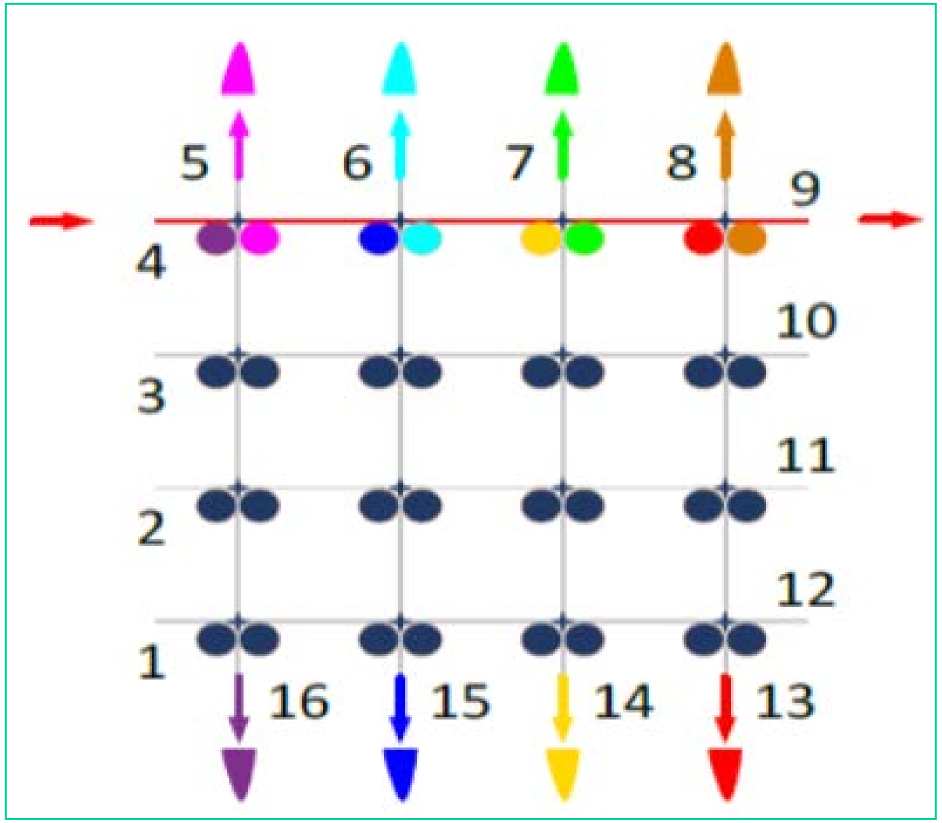

Photonic integrated field-programmable disk array signal processor

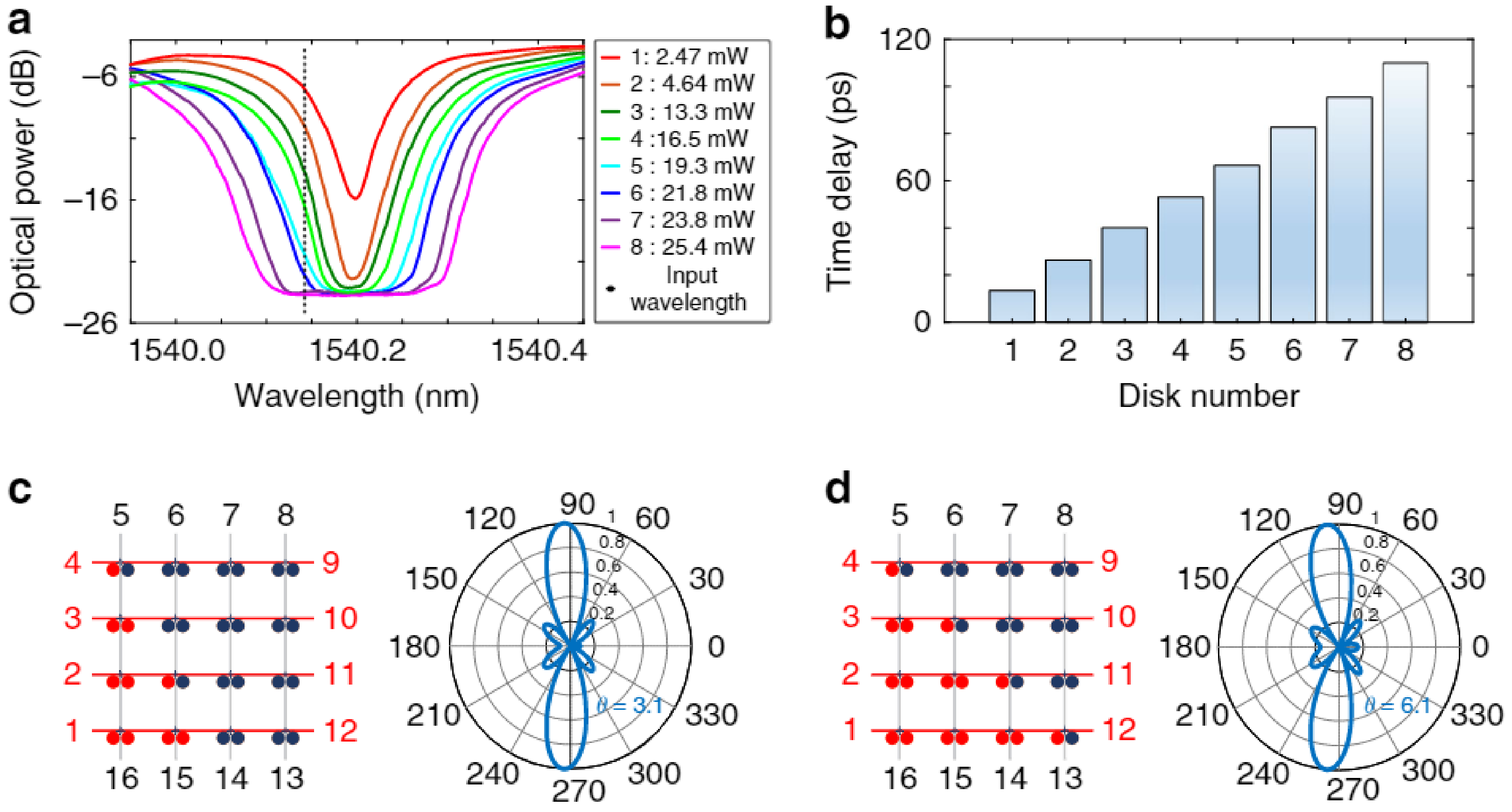

Fig. 4 Experimental results with photonic FPDA signal processor operating as optical beamforming network. a Measured transmission spectrum of the channel from port 4 to port 9 when the voltages are controlled to make resonance wavelength of each MDR aligned progressively. **b** Measured time delays with the number of the aligned MDRs increasing progressively. **c** Calculated array factors of a four-element linear PAA when the channel time delay is 13.5 ps. **d** Calculated array factors of a four-element linear PAA when the channel time delay is 26.4 ps.

W. Zhang and J. Yao, *Nat. Comm.*, **11**, Article number: 406 (2020)

Outline

- Recent research activities in MWP
- Microwave signal generation
- Microwave signal processing
- Radio over fiber based on coherent detection
- Microwave photonics for sensing
- Conclusion

RoF with coherent detection

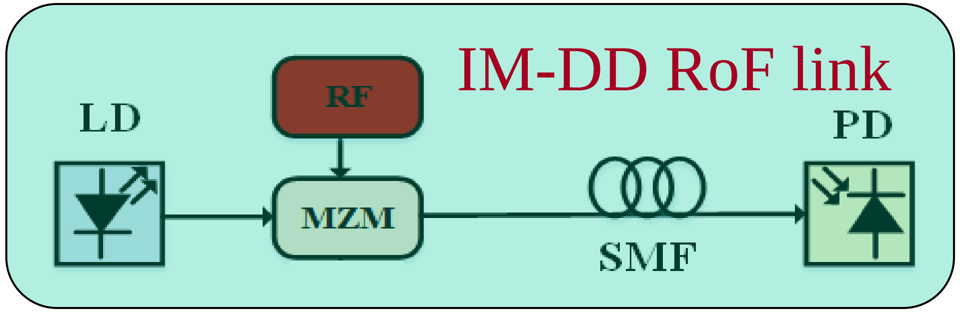

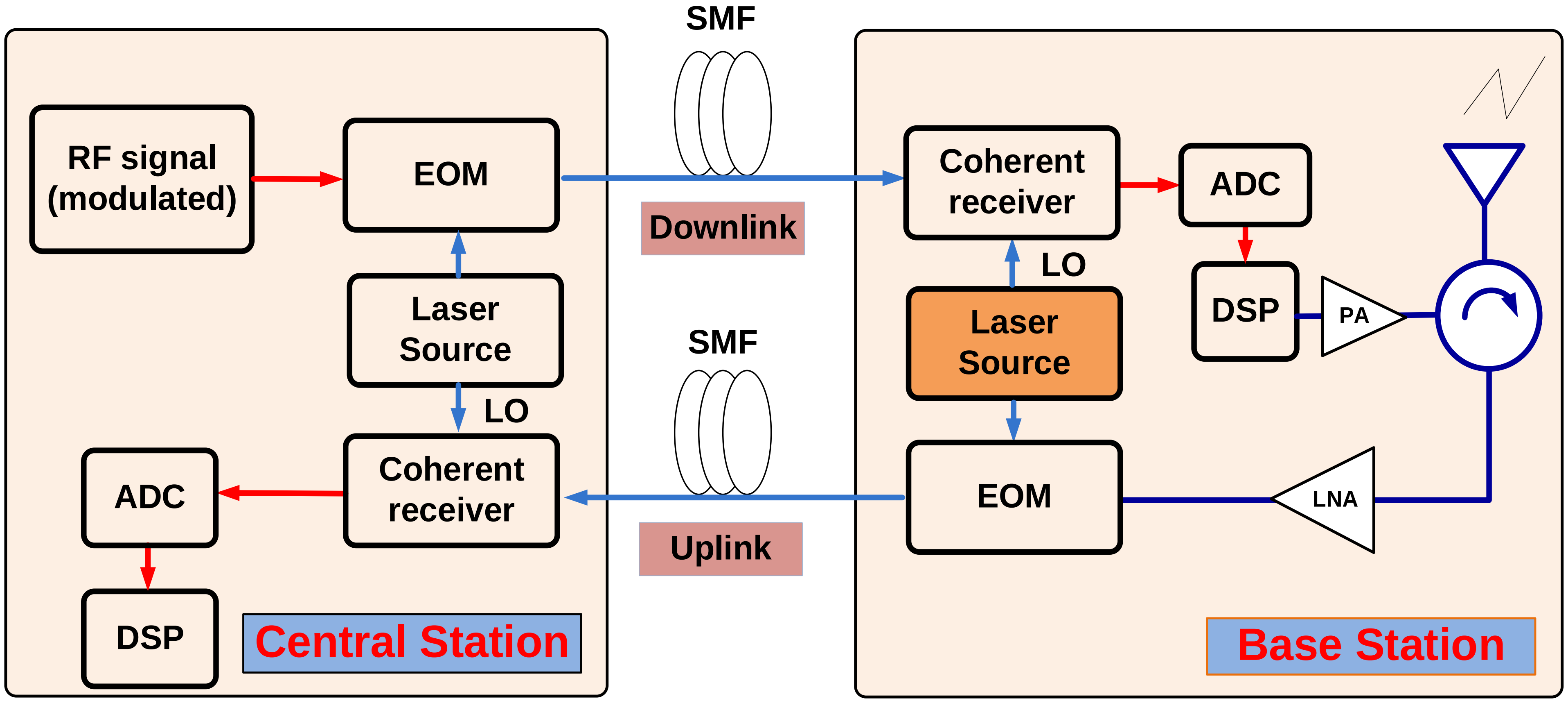

M. Nakazawa, K. Kikuchi and T. Miyazaki, High Spectral Density Optical Communication Technologies. New York: Springer-Verlag, 2010, pp. 11-50.

RoF with coherent detection

RoF with coherent detection:

- **Both amplitude and phase** can be modulated with increased spectral efficiency
- Demodulation achieved through coherent detection at a coherent receiver (**an LO needed**)
- Phase noise from the optical sources (the transmitter and LO) can be eliminated via a DSP algorithm

Advantages:

- High receiver sensitivity → **Increase the transmission distance**
- High spectral efficiency → **All information (phase and intensity) can be recovered via coherent detection and DSP**

Disadvantages:

- Complex structure and requires high speed DSP
- Receiver is sensitive to laser source **PHASE NOISE (high quality laser source and DSP)**.

Digital phase noise cancellation for an IM/CD RoF

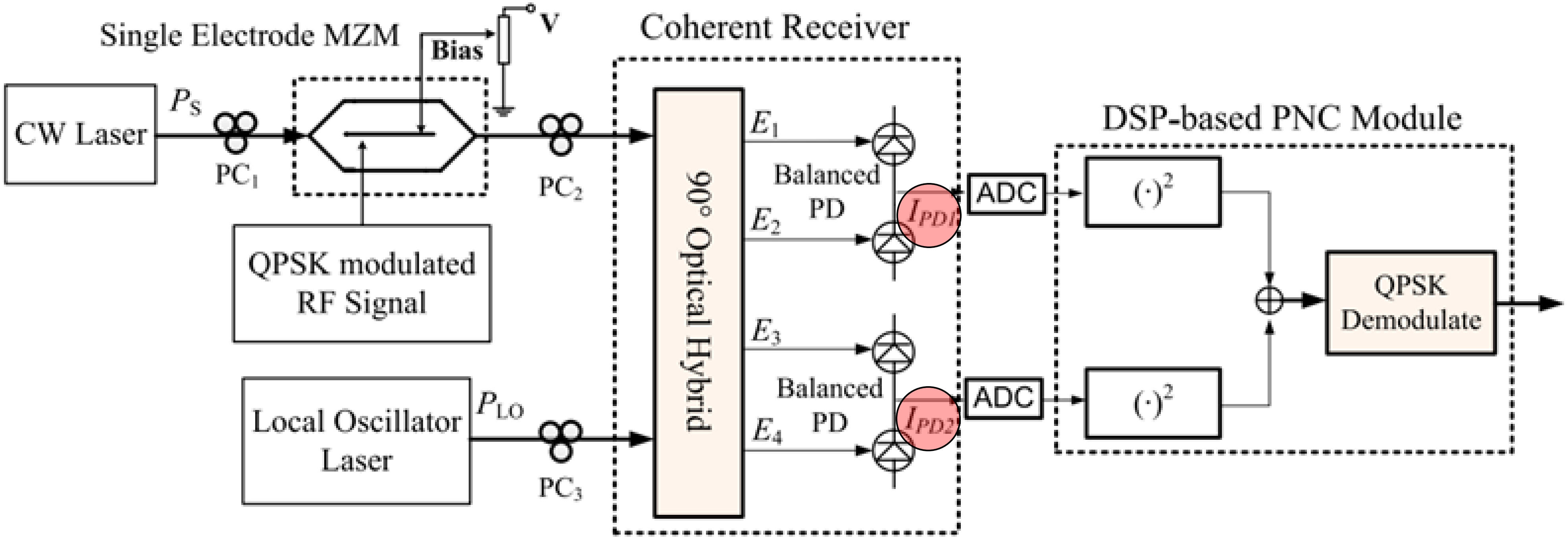

- **Demonstration of the effectiveness of coherent detection based on DSP**
- **Spectral efficiency is low due to the transmission of a single microwave signal**

X. Chen and J. Yao, *IEEE Photon. Lett.*, vol. 8, no. 26, 2014.

Digital phase noise cancellation for an IM/CD RoF

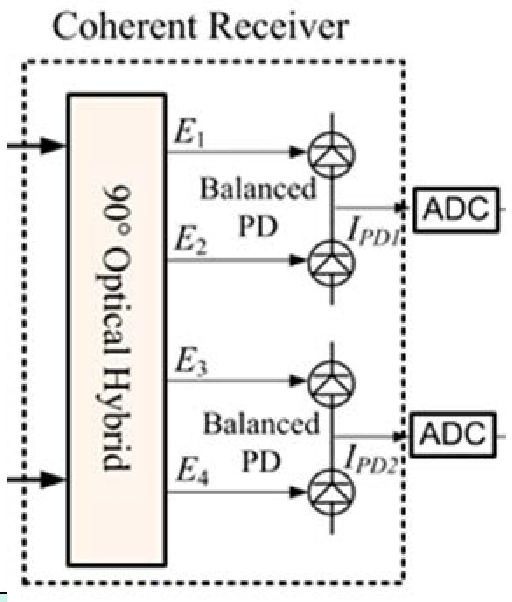

$$E_s(t) = \sqrt{2P_sL_s}\cos(\pi x(t)/2V_\pi + \pi/4)\,e^{j(\omega_c t + \varphi_c(t))} \quad (1)$$

$$E_{LO}(t) = \sqrt{2P_{LO}}e^{j(\omega_{LO}t + \varphi_{LO}(t))} \quad (2)$$

$$E_1 = \sqrt{L}(E_s + E_{LO}) \quad (3)$$

$$E_2 = \sqrt{L}(E_s - E_{LO}) \quad (4)$$

$$E_3 = \sqrt{L}(E_s + E_{LO}e^{j\pi/2}) \quad (5)$$

$$E_4 = \sqrt{L}(E_s - E_{LO}e^{j\pi/2}) \quad (6)$$

$$I_{PD1} = 4RL\sqrt{P_sP_{LO}L_s}\left[\cos(\pi x(t)/2V_\pi + \pi/4) \times \cos((\Delta\omega)t + \varphi(t))\right] \quad (7)$$

$$I_{PD2} = 4RL\sqrt{P_sP_{LO}L_s}\left[\cos(\pi x(t)/2V_\pi + \pi/4) \times \sin((\Delta\omega)t + \varphi(t))\right] \quad (8)$$

$$I_o^2 = I_{PD1}^2 + I_{PD2}^2 = 8R^2L^2P_sP_{LO}L_s(1 - \sin(\pi x(t)/V_\pi)) \approx 8R^2L^2P_sP_{LO}L_s(1 - (\pi x(t)/V_\pi)) \quad (9)$$

$$\Delta\omega = \omega_C - \omega_{LO}$$

Offset frequency

$$\varphi(t) = \varphi_c(t) - \varphi_{LO}(t)$$

Joint phase noise

Recovered microwave signal free from the phase noise and offset frequency

Digital phase noise cancellation for an IM/CD RoF

- Experimental Results (1/3)

$$I_{PD1} = -4RL\sqrt{P_s P_{LO} L_s}\left[\sin\left(\pi x(t)/2V_\pi\right) \times \cos\left((\Delta\omega)t + \varphi(t)\right)\right]$$

$$I_{PD2} = -4RL\sqrt{P_s P_{LO} L_s}\left[\sin\left(\pi x(t)/2V_\pi\right) \times \sin\left((\Delta\omega)t + \varphi(t)\right)\right]$$

$$I_o^2 = I_{PD1}^2 + I_{PD2}^2 = 8R^2L^2P_sP_{LO}L_s\left(1-\cos\left(\pi x(t)/V_\pi\right)\right)$$

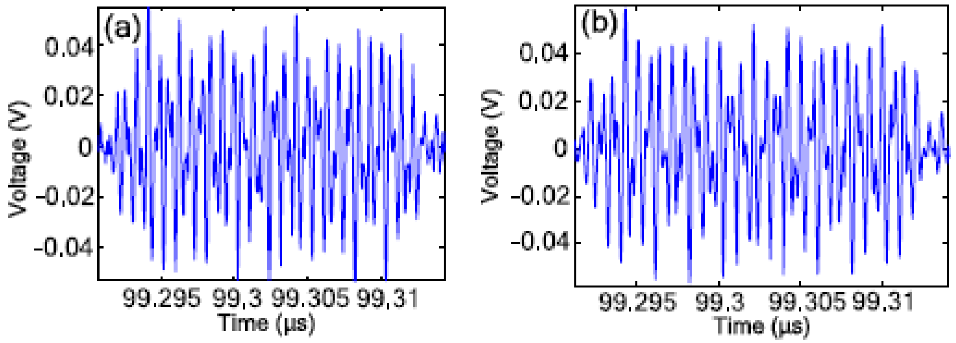

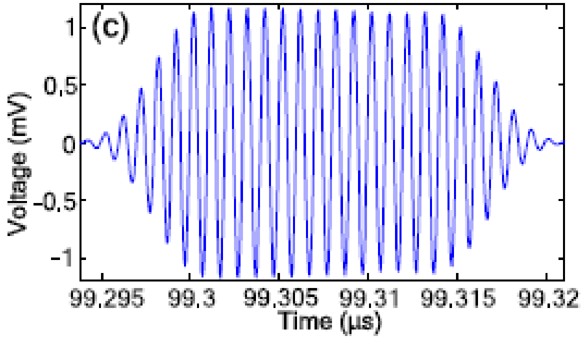

Fig. 4. Temporal waveform when the RF input signal is an ASK modulated RF signal with a center frequency of 500 MHz. (a) The in-phase component from the coherent receiver, (b) the quadrature component from the coherent receiver, and (c) the signal at the output of the DSP-based PNC module.

Digital phase noise cancellation for an IM/CD RoF

- Experimental Results (2/3)

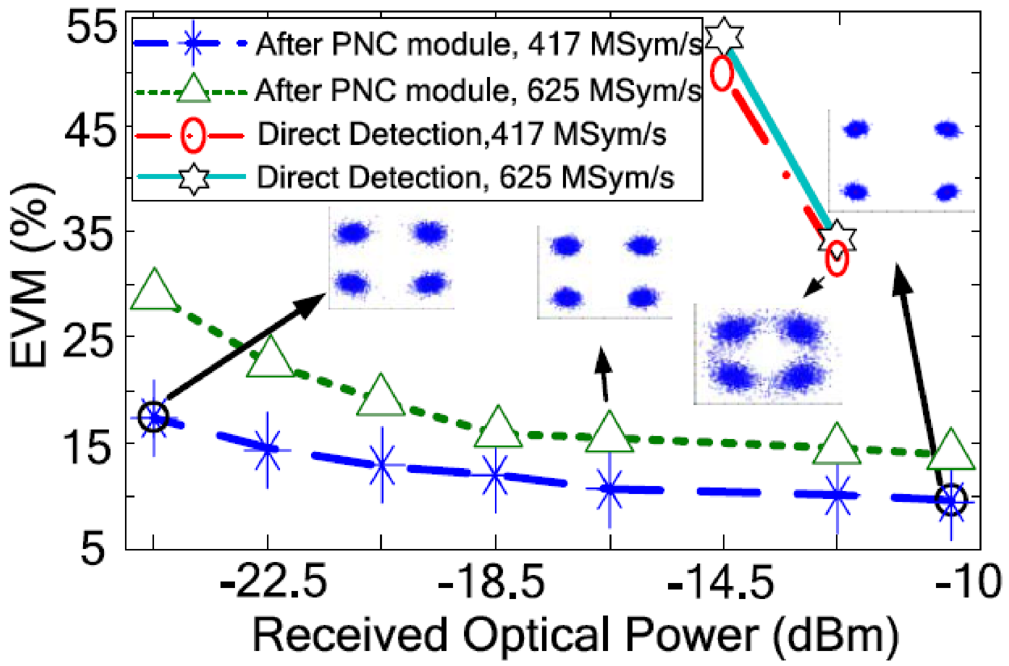

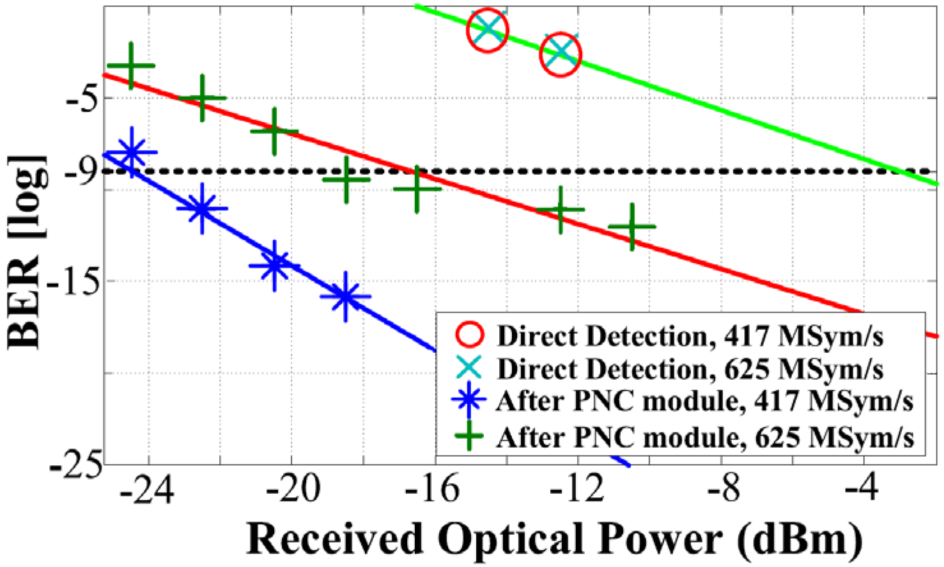

Comparison of the EVMs and BERs for the transmission of a QPSK-modulated RF signal based on coherent detection and direct detection. **PNC-phase noise cancellation**

Digital phase noise cancellation for an IM/CD RoF

- Experimental Results (3/3)

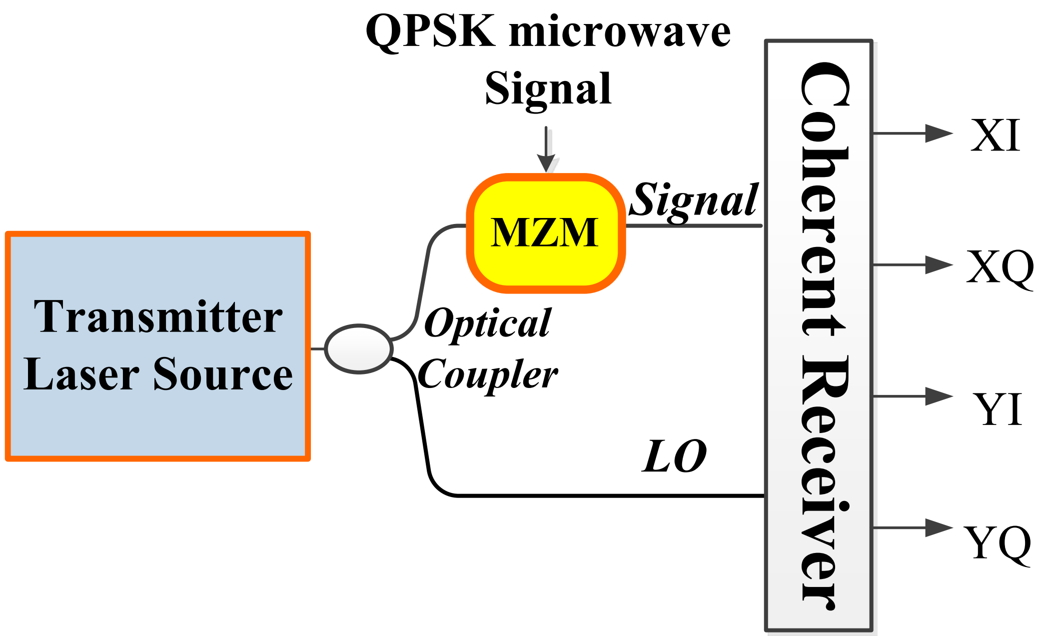

Schematic diagram of an Intensity modulation/coherent detection MPL without digital PNC module

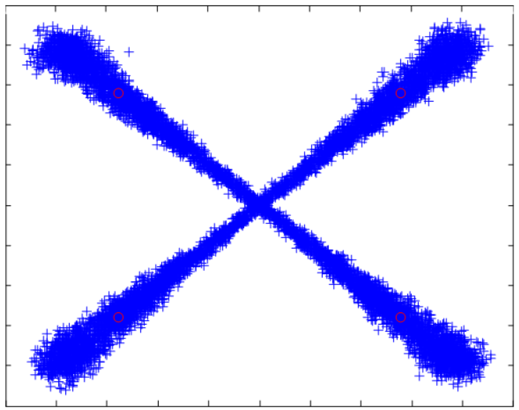

Constellation of the detected QPSK microwave vector signal (XI port)

- **Demonstration of the effectiveness of coherent detection based on DSP**
- **Spectral efficiency is low due to the transmission of a single microwave signal**

A High Spectral Efficiency Radio Over Fiber Link Based on Coherent Detection and Digital Phase Noise Cancellation

Peng Li, Ruoshi Xu, Zheng Dai, Zhenguo Lu, *Member, IEEE, Member, OSA*, Lianshan Yan, *Senior Member, IEEE, Fellow, OSA*, and Jianping Yao, *Fellow, IEEE, Fellow, OSA*

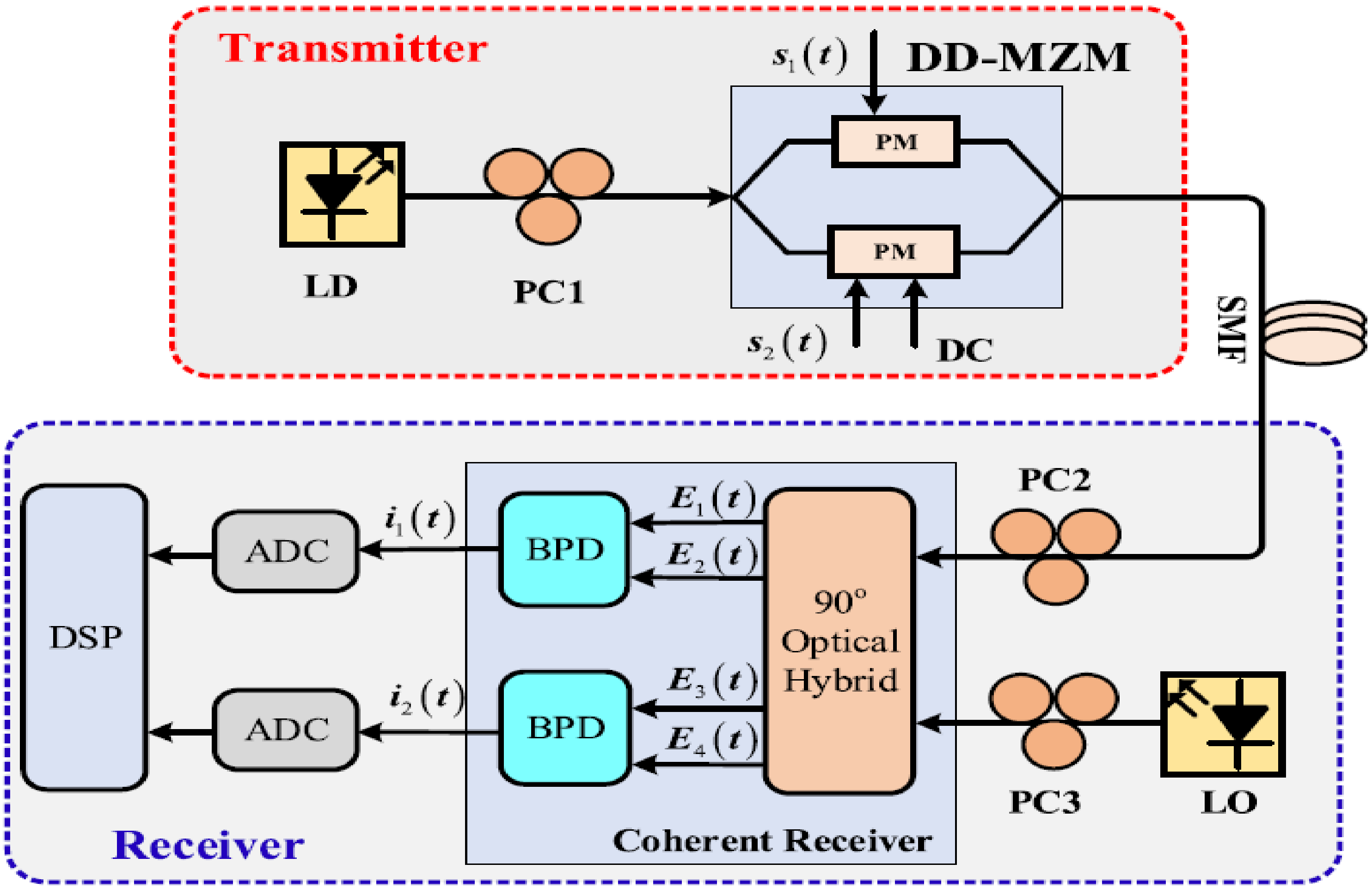

- ✓ Two microwave signals
- ✓ Single polarization
- ✓ Single optical carrier

Two microwave vector signal transmission

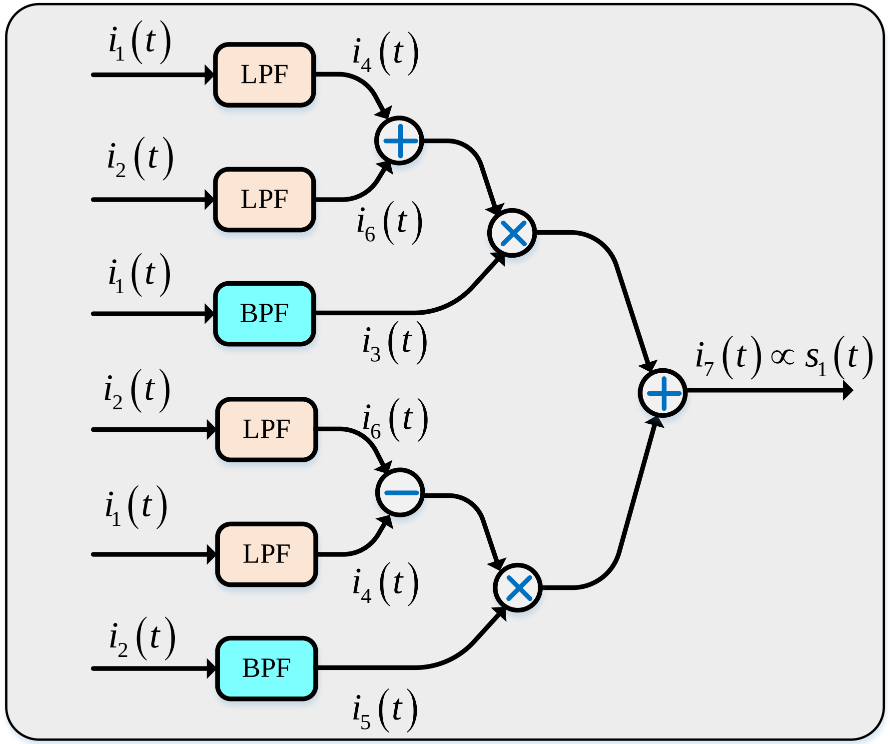

Flow chart to show the DSP algorithm. **LPF**: low-pass filter; **BPF**: bandpass filter.

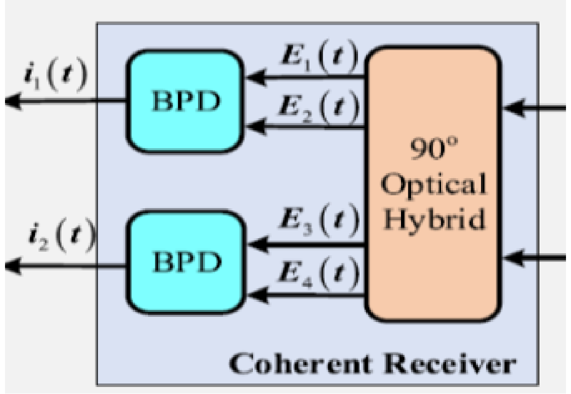

$$i_1(t) = E_1(t)E_1^*(t) - E_2(t)E_2^*(t)$$

$$= \sqrt{2P_sLP_{LO}}R\begin{pmatrix}\cos[\Delta\omega t + \varphi(t)] \\ -\sin[\Delta\omega t + \varphi(t)]\end{pmatrix}$$

$$+\sqrt{2P_sLP_{LO}}R\frac{\pi}{V_\pi}\begin{pmatrix}s_1(t)\cos[\Delta\omega t + \varphi(t)] \\ -s_2(t)\sin[\Delta\omega t + \varphi(t)]\end{pmatrix}$$

After DSP

$S_1(t)$

$$i_7(t) = (i_4(t) + i_6(t)) * i_3(t) + (i_6(t) - i_4(t)) * i_5(t)$$

$$= 4P_sLP_{LO}R^2\frac{\pi}{V_\pi}s_1(t)$$

Experimental results

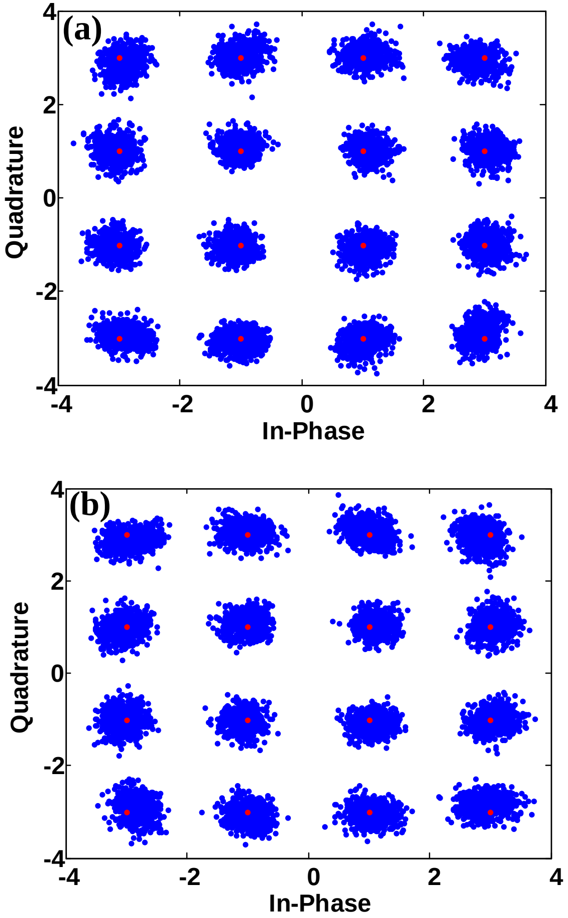

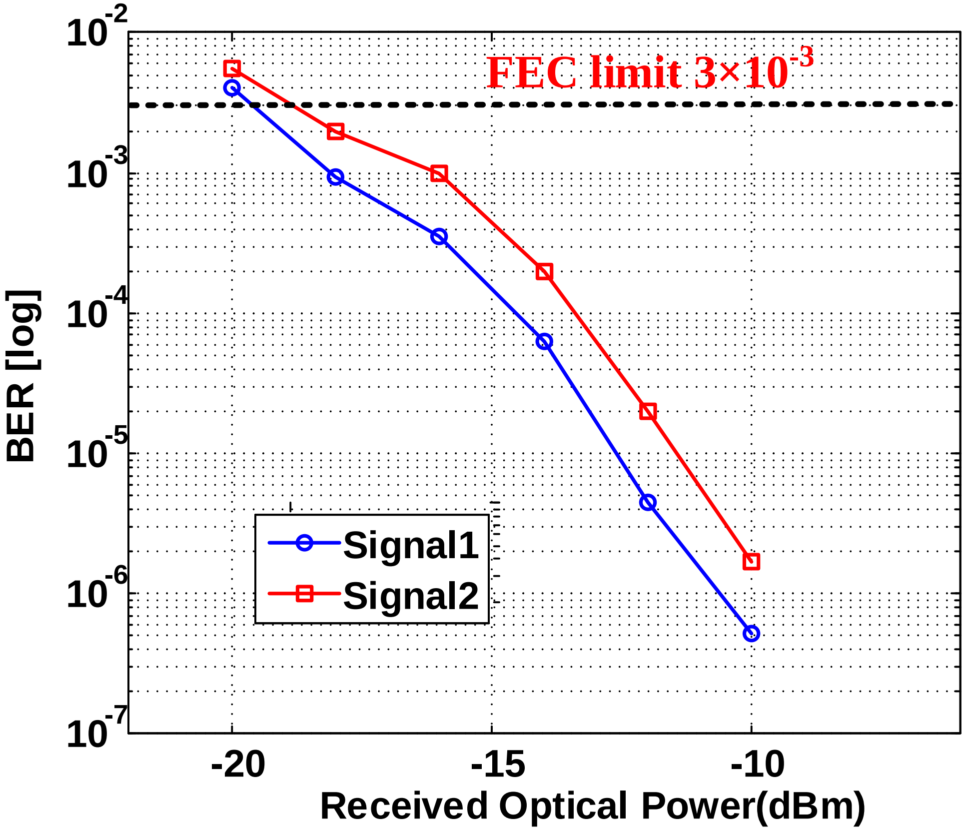

When the received optical power is beyond -18 dBm, **Error-free transmission** is achieved with forward error correction (FEC).

Measured constellations of the two recovered 16-QAM microwave vector signals (fiber length: 9 km, received optical power :-10 dBm)

Four microwave vector signal transmission

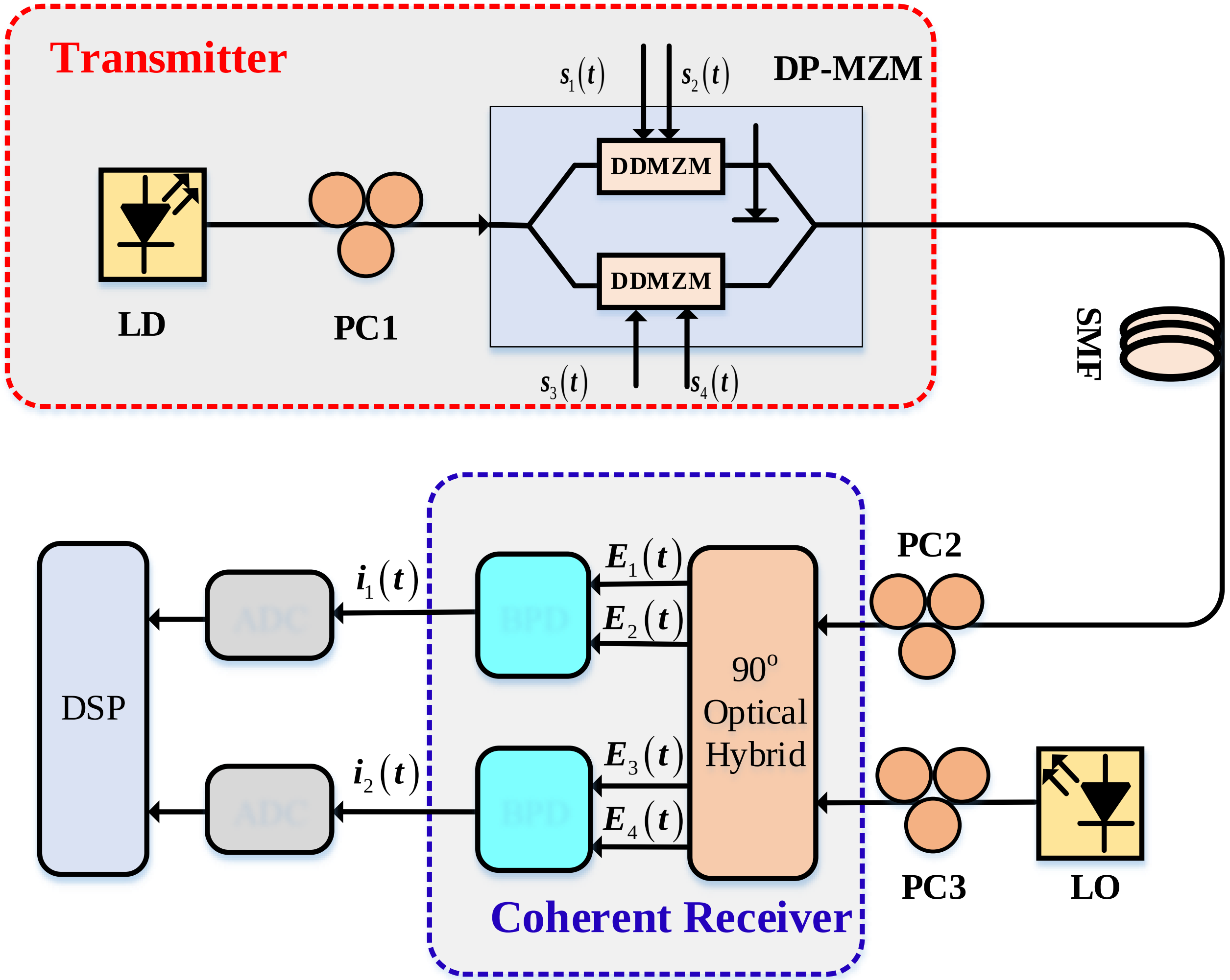

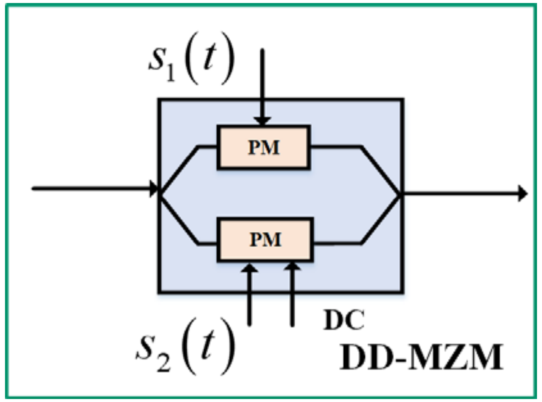

- ✓Four microwave vector signals
- ✓Single polarization
- ✓Single optical carrier

Four microwave vector signal transmission

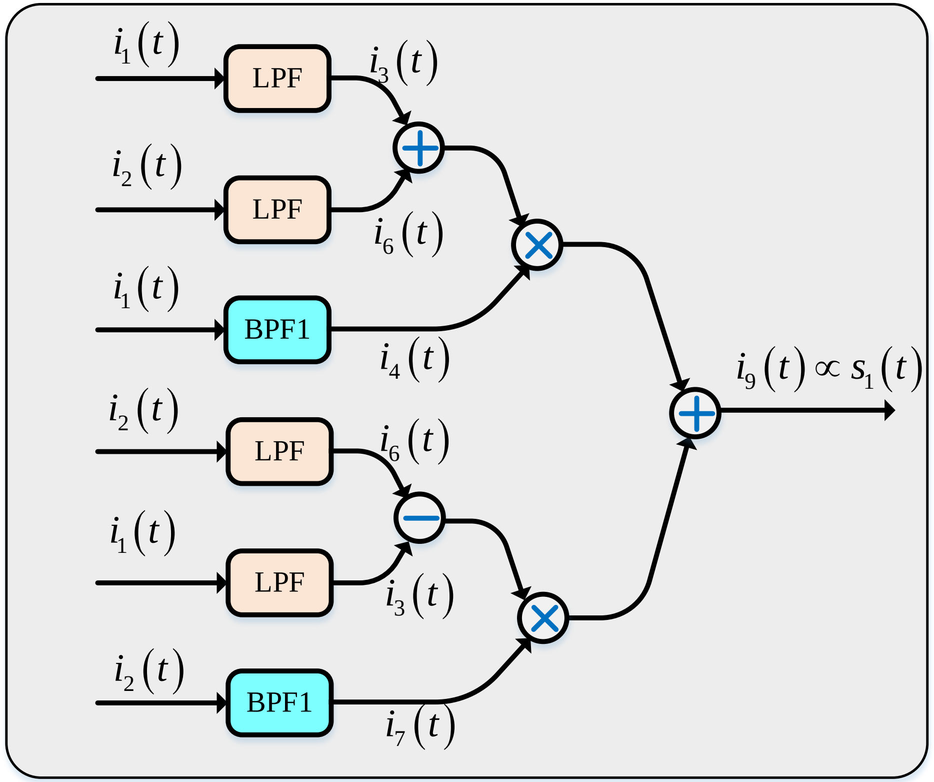

Flow chart to show the DSP algorithm.
LPF: low-pass filter; **BPF**: bandpass filter.

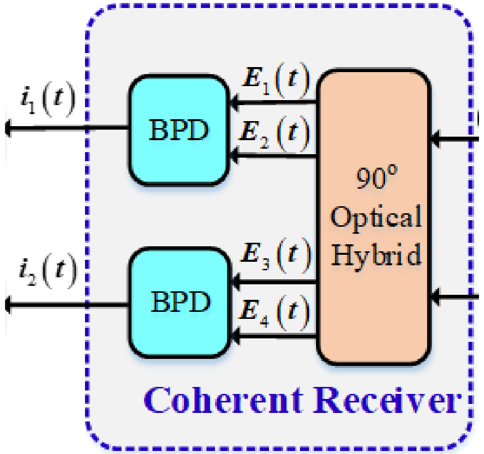

$$
\begin{aligned}
i_1(t) &= \frac{1}{2}R\left(E_1(t)E_1^*(t) - E_2(t)E_2^*(t)\right) \\
&= \frac{R\sqrt{2P_sLP_{LO}}}{2}\begin{pmatrix}\cos[\Delta\omega t+\varphi(t)] \\ -\sin[\Delta\omega t+\varphi(t)]\end{pmatrix} + \\
&\quad \frac{\pi R\sqrt{2P_sLP_{LO}}}{4V_\pi}\begin{pmatrix}s_1(t)\cos[\Delta\omega t+\varphi(t)] \\ -s_2(t)\sin[\Delta\omega t+\varphi(t)]\end{pmatrix} + \\
&\quad \frac{\pi R\sqrt{2P_sLP_{LO}}}{4V_\pi}\begin{pmatrix}s_3(t)\cos[\Delta\omega t+\varphi(t)] \\ -s_4(t)\sin[\Delta\omega t+\varphi(t)]\end{pmatrix}
\end{aligned}
$$

After DSP

$S_1(t)$

$$
\begin{aligned}
i_9(t) &= (i_3(t)+i_6(t))*i_4(t)+(i_6(t)-i_3(t))*i_7(t) \\
&= \frac{\pi P_sLP_{LO}R^2}{2V_\pi}s_1(t)
\end{aligned}
$$

Four microwave vector signal transmission

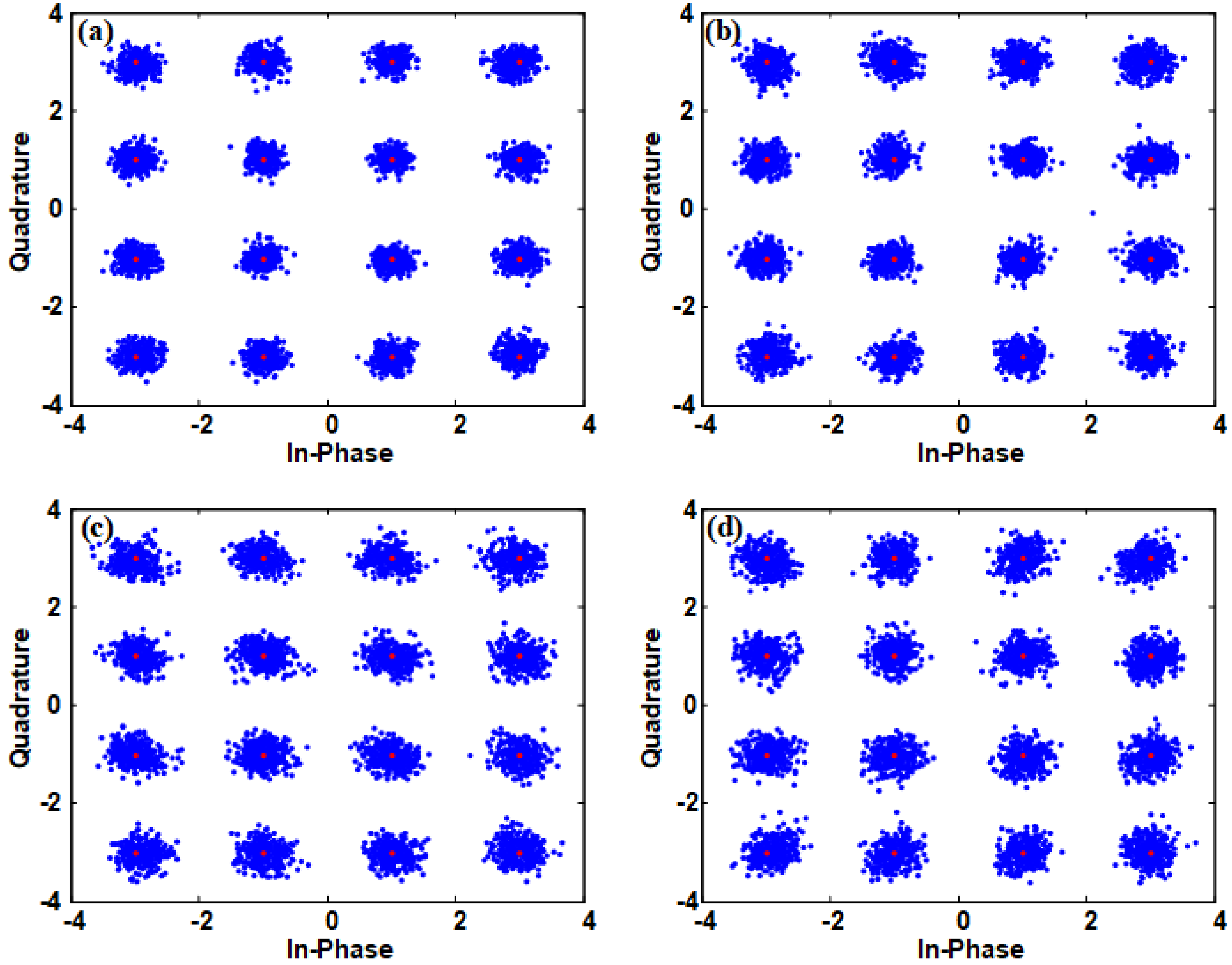

Measured constellations of the four recovered 16-QAM microwave vector signals at the output of the DSP unit (fiber length: 9 km, the received optical power: -10 dBm

Experimental results

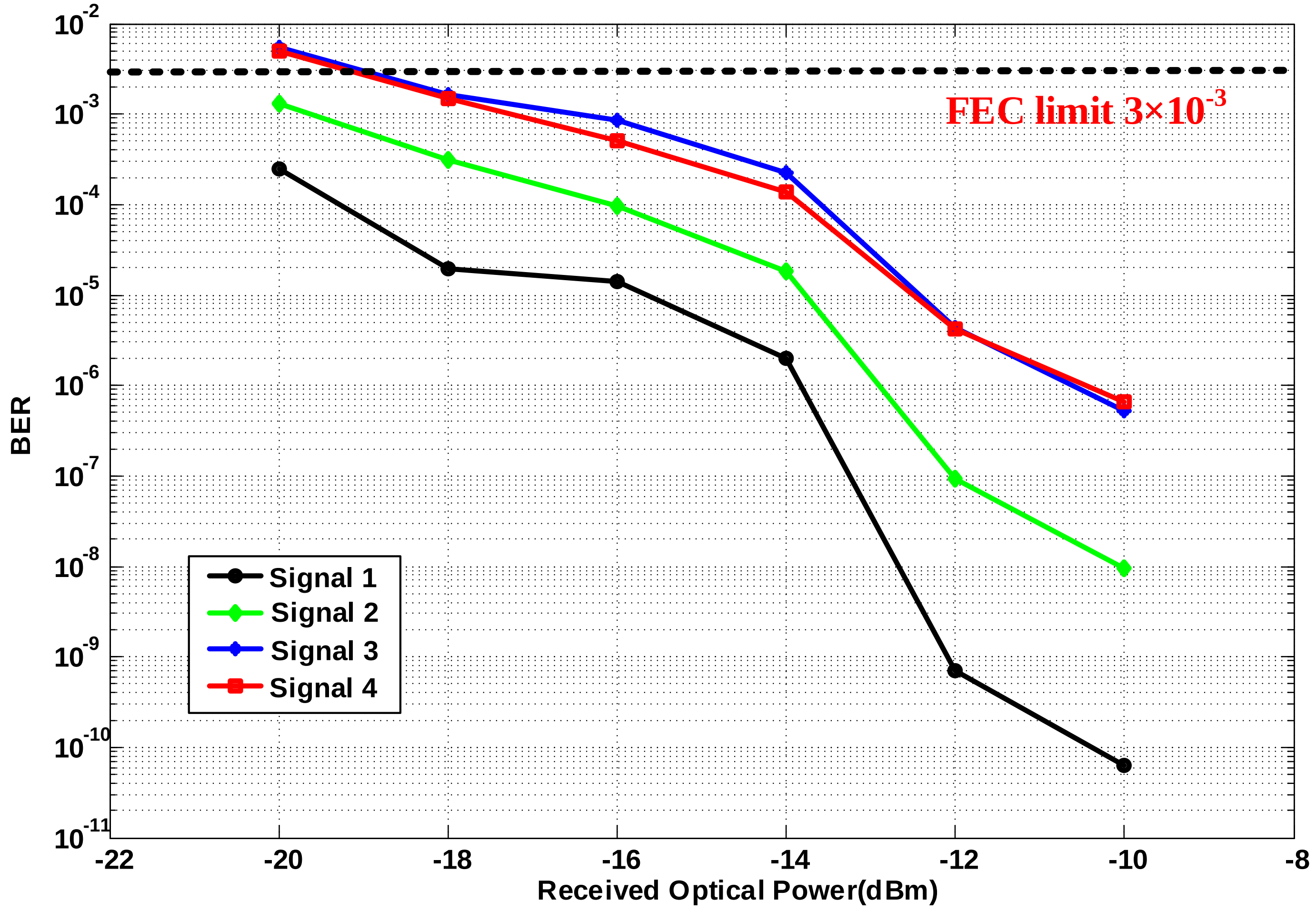

When the received optical power is beyond -19 dBm, **Error free transmission** is achieved with forward error correction (FEC).

Outline

- Recent research activities in MWP
- Microwave signal generation
- Microwave signal processing
- Radio over fiber based on coherent detection
- Microwave photonics for sensing
- Conclusion

Microwave photonics for sensing - Motivation

Broadband light

Transmission

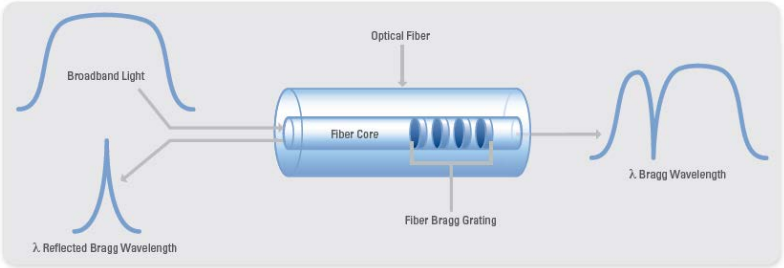

Reflected λ_B

FBG

$$\lambda_B = 2\boxed{n_{eff}}\boxed{\Lambda}$$

Major source is temperature.

Major source is strain.

Conventional Interrogation of FBG sensors

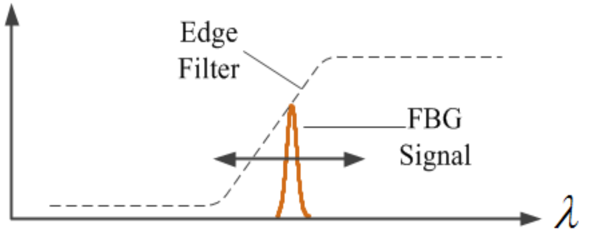

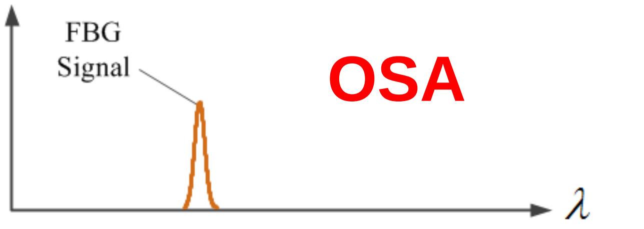

OSA

High Interrogation Speed	Low Interrogation Speed
Low Accuracy (power drifting)	Low Resolution (limited by OSA)

There is a trade-off between resolution and interrogation speed! Solution → Microwave Photonics → to convert the spectral information to the time domain.

Wavelength-to-time mapping and chirped pulse compression

- **Wavelength-to-time mapping**

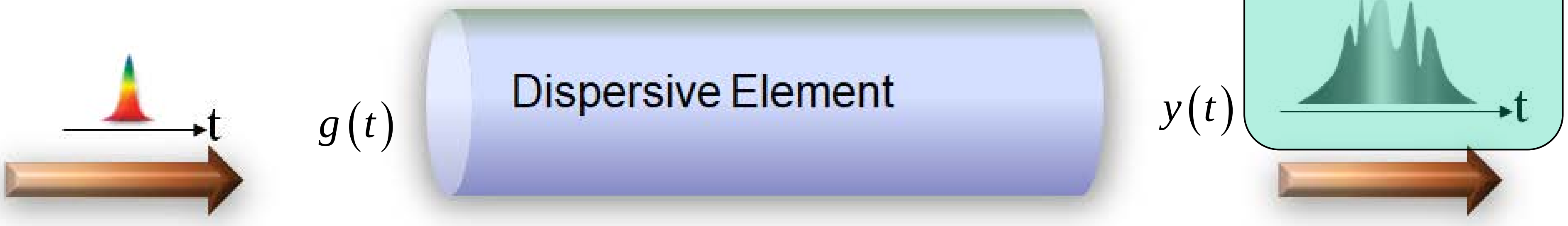

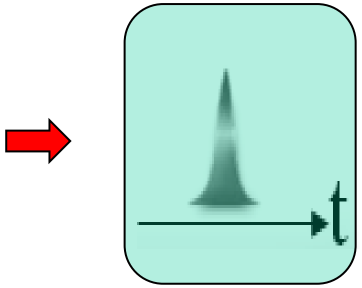

pulse compression
(waveform should be linearly chirped or randomly distributed)

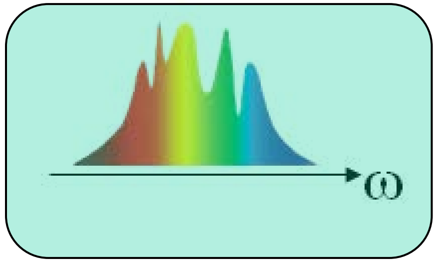

$$
\begin{aligned}
y(t) &= g(t) * \exp\left(j\frac{t^2}{2\ddot{\Phi}}\right) = \int_{-\infty}^{\infty} g(\tau) \times \exp\left[j\frac{(t-\tau)^2}{2\ddot{\Phi}}\right] d\tau \\
&= \exp\left(j\frac{t^2}{2\ddot{\Phi}}\right) \times \int_{-\infty}^{\infty} g(\tau) \times \exp\left(j\frac{\tau^2}{2\ddot{\Phi}}\right) \times \exp\left[-j\left(\frac{t}{\ddot{\Phi}}\right)\tau\right] d\tau \\
&\approx \exp\left(j\frac{t^2}{2\ddot{\Phi}}\right) \times \int_{-\infty}^{\infty} g(\tau) \times \exp\left[-j\left(\frac{t}{\ddot{\Phi}}\right)\tau\right] d\tau \\
&= \exp\left(j\frac{t^2}{2\ddot{\Phi}}\right) \times G(\omega)\Big|_{\omega=\frac{t}{\ddot{\Phi}}}
\end{aligned}
$$

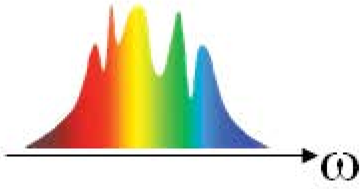

Wavelength-to-time mapping, namely dispersive Fourier transformation, is a fast and effective way to **measure optical spectrum in the time domain**.

J. P. Yao, "Photonic generation of microwave arbitrary waveforms," *Opt. Comm.*, vol. 284, no. 15, pp. 3723-3736, Jul. 2011.

Wavelength-to-time mapping and chirped pulse compression

- **Chirped pulse compression**

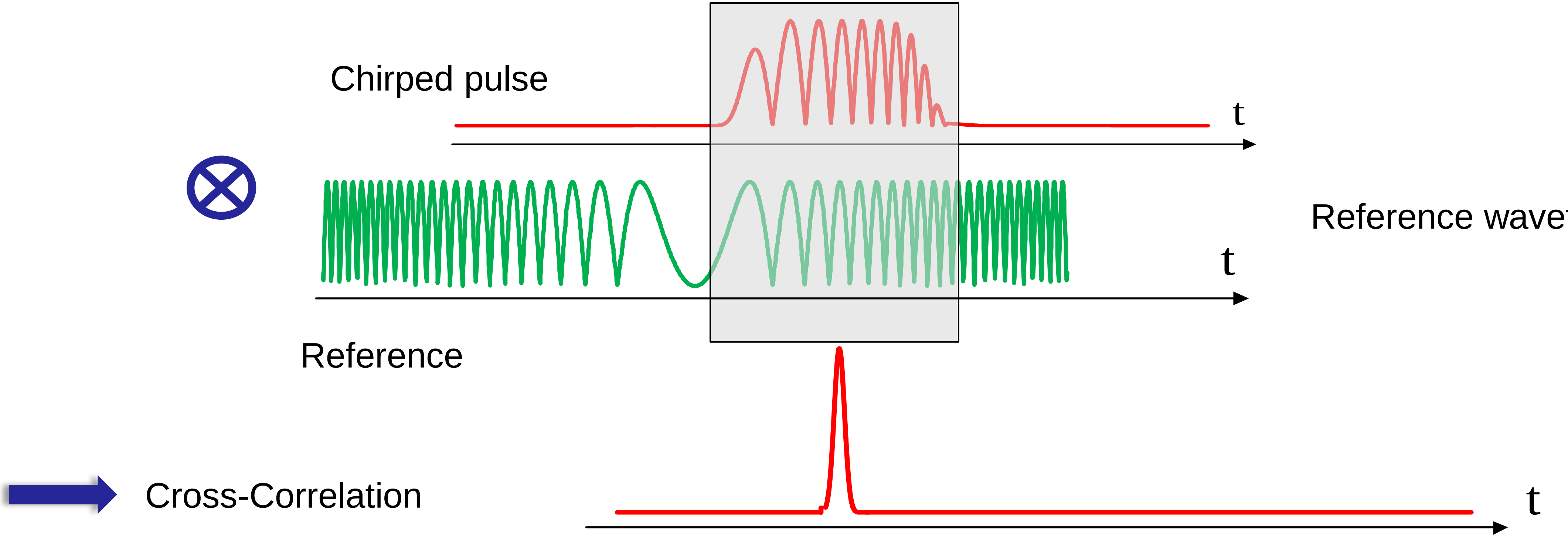

$$R_{12}(\tau)=\frac{1}{2}w(\tau)\,sinc\left\{\pi k\left[\tau+\frac{\Delta t_c(z)}{2}\right]w(\tau)\right\}\cos\left(2\pi f_e\tau+\varphi\right)$$

W. Liu, M. Li, C. Wang, and J. P. Yao, *J. Lightwave Technol.*, vol. 29, no. 9, pp. 1239-1247, May 2011.

Wavelength-to-time mapping and chirped pulse compression

Temperature/Strain Measurement

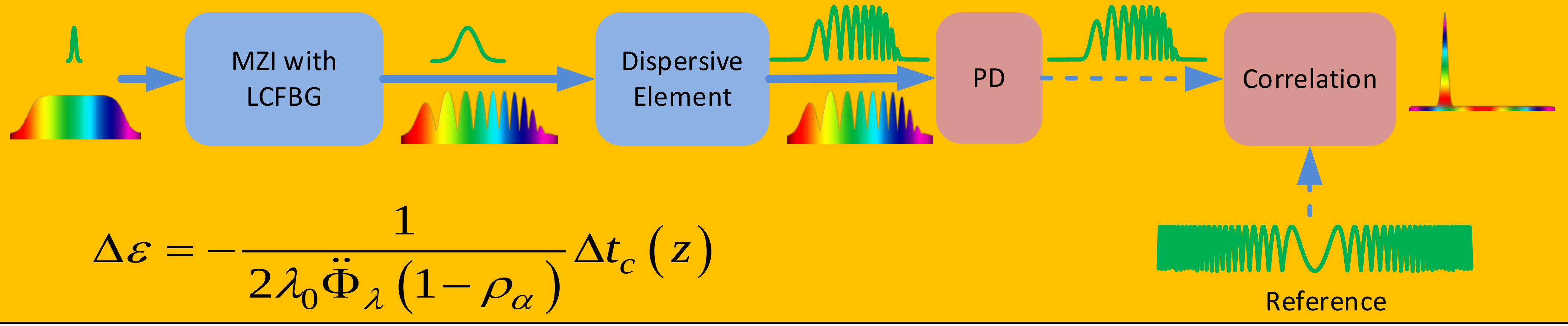

$$\Delta\varepsilon = -\frac{1}{2\lambda_0\ddot{\Phi}_\lambda\left(1-\rho_\alpha\right)}\Delta t_c\left(z\right)$$

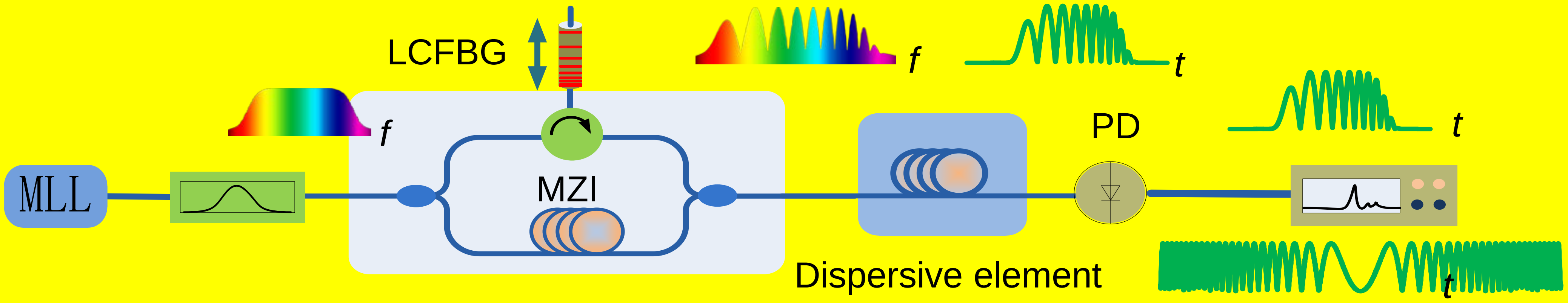

W. Liu, M. Li, C. Wang, and J. P. Yao, *J. Lightwave Technol.*, vol. 29, no. 9, pp. 1239-1247, May 2011.

Wavelength-to-time mapping and chirped pulse compression

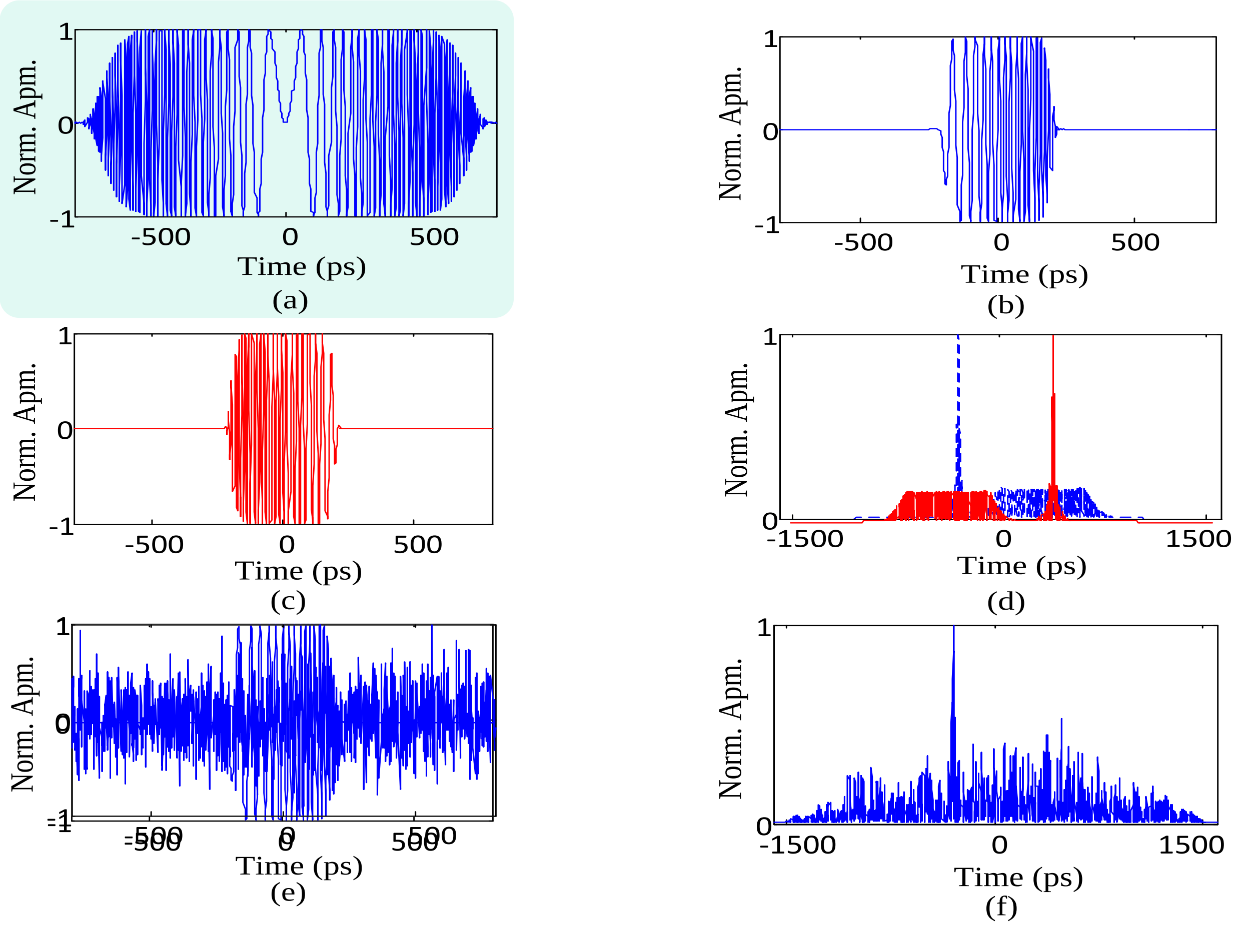

Simulation Results

(**a**) Special reference signal.

(**b**) Sensor signal with a wavelength shift of 0.185 nm.

(**c**) Sensor signal with a wavelength shift of 0.740 nm.

(**d**) The correlation outputs.

(**e**) The waveform in (b) with an added stationary white noise.

(**f**) The correlation with the noisy waveform shown in (e).

W. Liu, M. Li, C. Wang, and J. P. Yao, *J. Lightwave Technol.*, vol. 29, no. 9, pp. 1239-1247, May 2011.

Experimental results

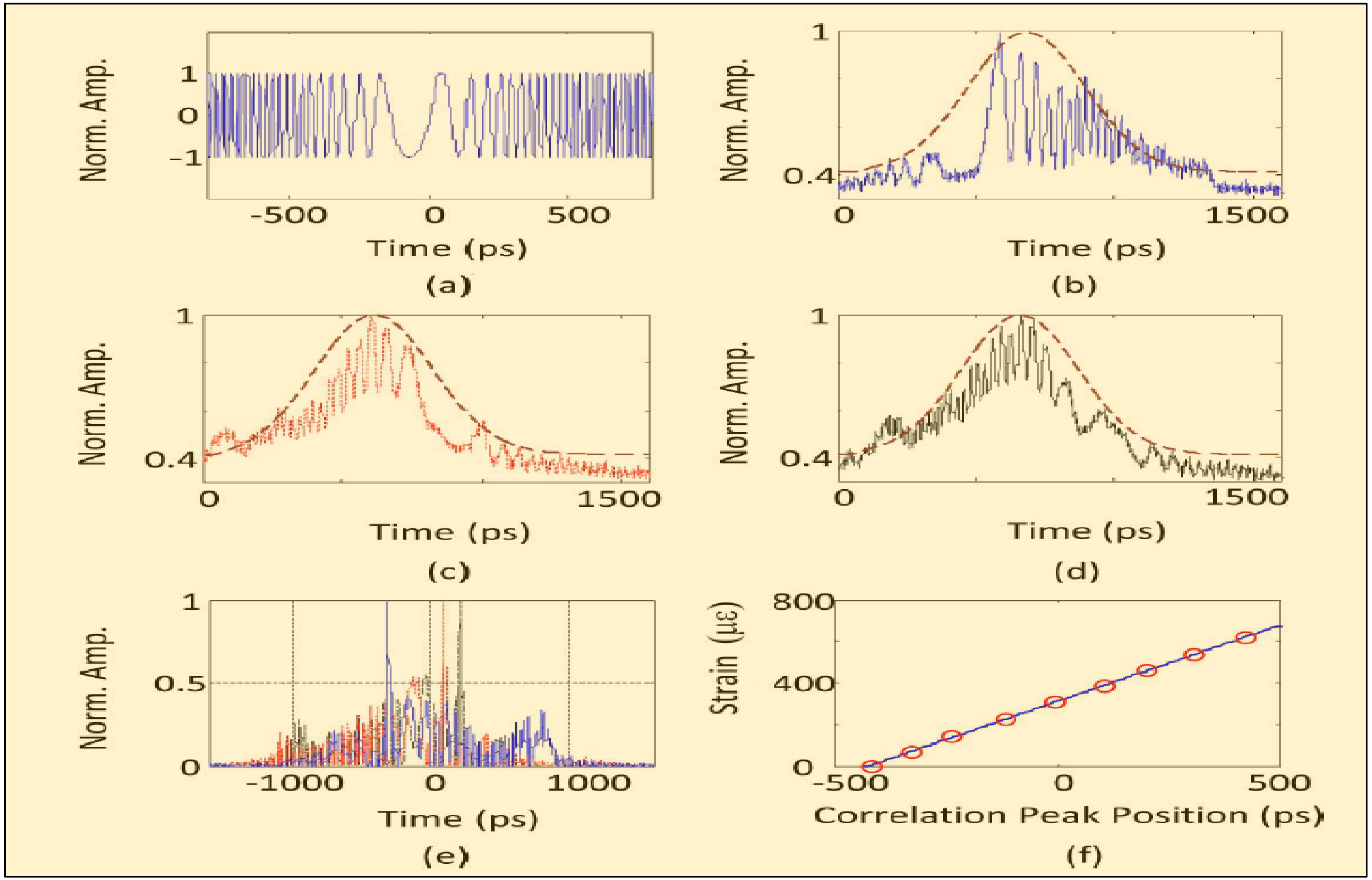

a) Reference waveform

b) When a strain of 71.5 με is applied to the LCFBG.

c) When a strain of 406.9με is applied to the LCFBG.

d) When a strain of 484.2 με is applied to the LCFBG.

e) Correlation results for the detected microwave waveforms as show in (b), (c) and (d).

f) The measured strain vs the peak position. The circles are the experimental data, and the solid curve is linear fitting of the experimental data.

W. Liu, M. Li, C. Wang, and J. P. Yao, *J. Lightwave Technol.*, vol. 29, no. 9, pp. 1239-1247, May 2011.

Simultaneous measurement of temperature and strain – replace the chirped FBG by a chirped FBG written in a highly birefringent fiber (Hi Fi)

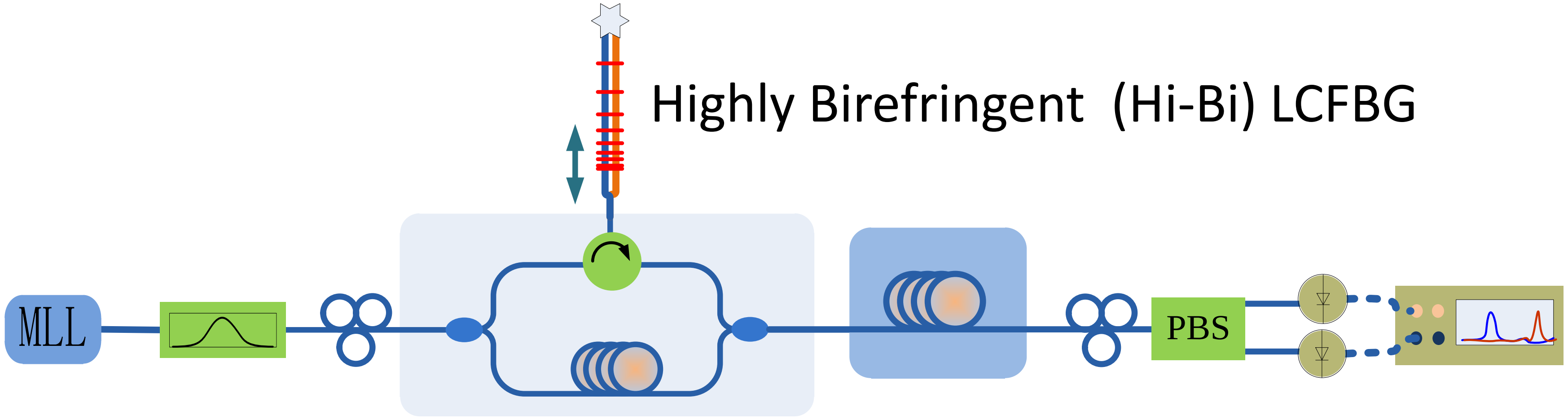

Perform chirped pulse compression, calculate the sensor function

$$\begin{bmatrix} \Delta T \\ \Delta \varepsilon \end{bmatrix} = -2 \begin{bmatrix} f_1 & g \\ f_2 & g \end{bmatrix}^{-1} \begin{bmatrix} \tau_f \\ \tau_s \end{bmatrix}$$

Wavelength-to-time mapping and chirped pulse compression

Experimental Results

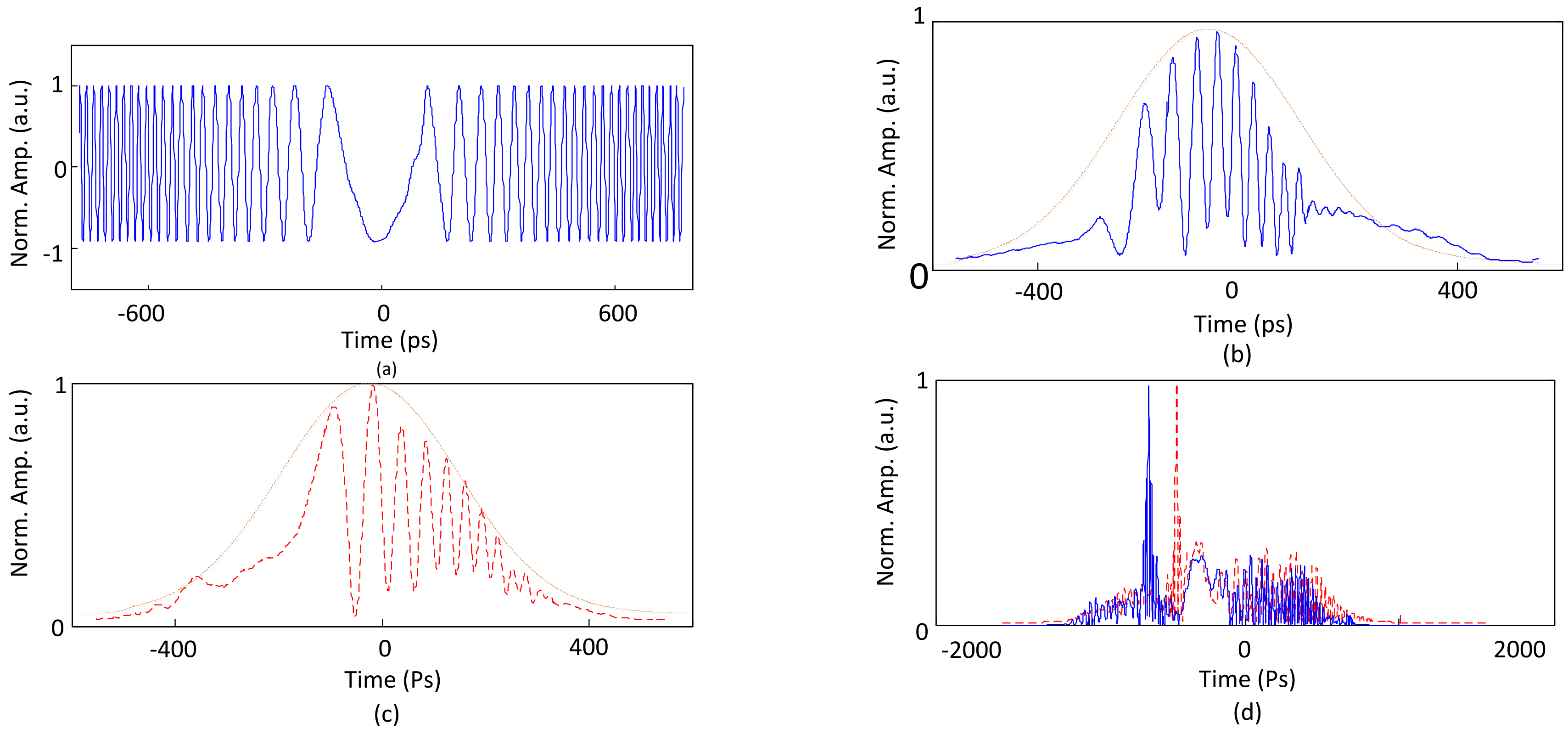

(a) Reference A linearly chirped microwave waveform corresponding to the polarization direction of the ultrashiort pulse aligned with (b) the fast axis and (c) the slow axis, when a strain of 50 $\mu\varepsilon$ is applied to the LCFBG at 25 ºC.

(d) Correlation of the waveforms shown in (b) and (c) with the special reference waveform.

W. Liu, W. Li, and J. P. Yao, *IEEE Photon. Technol. Lett.*, vol. 23, no. 18, pp. 1340-1342, Sep 2011.

Wavelength-to-time mapping and chirped pulse compression

Wavelength-to-time mapping & chirped pulse compression

Experimental Results

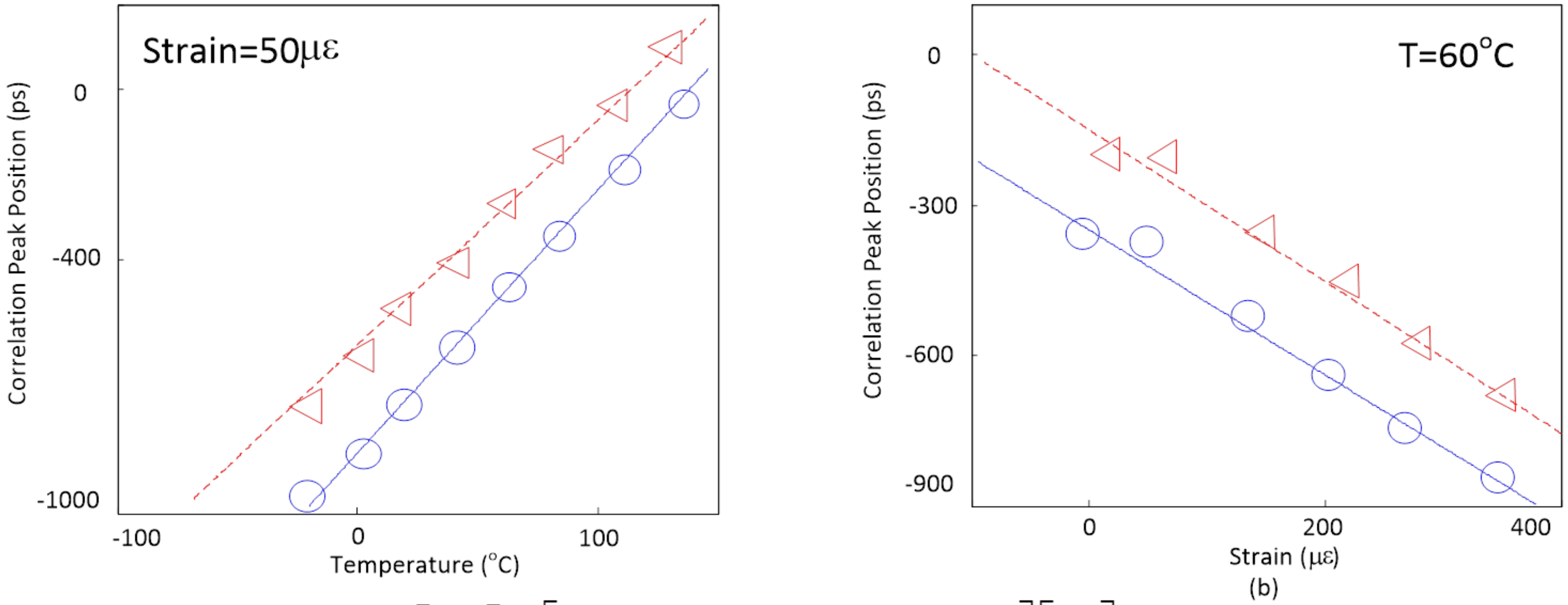

$$\begin{bmatrix}\Delta T\\ \Delta\varepsilon\end{bmatrix}=\begin{bmatrix}1.3152\,^{\circ}\mathrm{C/ps} & -1.3152\,^{\circ}\mathrm{C/ps}\\ 7.6242\ \mu\varepsilon/\mathrm{ps} & -8.4927\,\mu\varepsilon/\mathrm{ps}\end{bmatrix}\begin{bmatrix}\tau_f\\ \tau_s\end{bmatrix}$$

JOURNAL OF LIGHTWAVE TECHNOLOGY, VOL. 36, NO. 23, DECEMBER 1, 2018 5587

High-Speed and High-Resolution Interrogation of a Strain and Temperature Random Grating Sensor

Hong Deng, *Student Member, IEEE*, Ping Lu, Stephen J. Mihailov, *Member, IEEE*, and Jianping Yao, *Fellow, IEEE, Fellow, OSA*

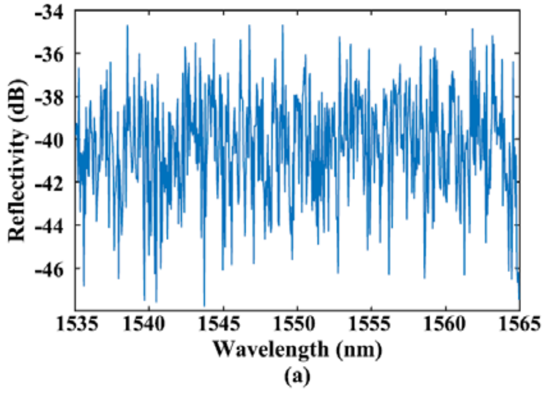

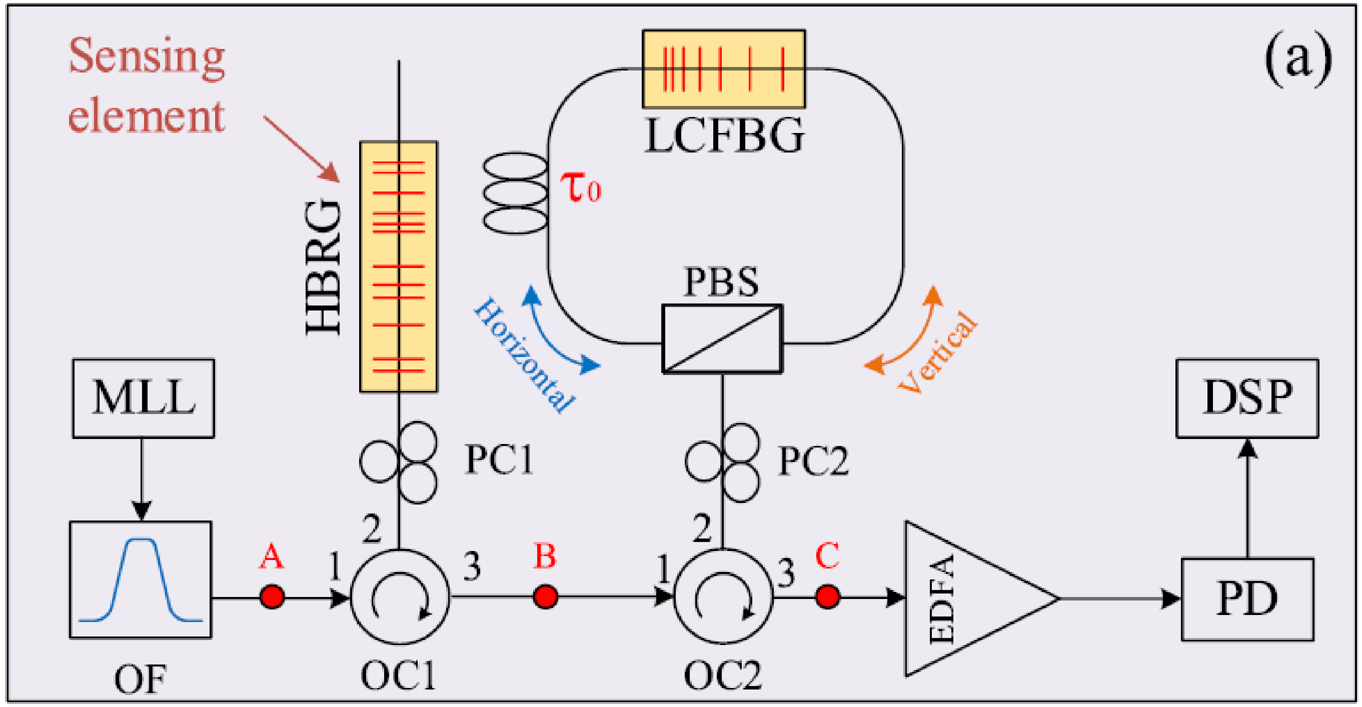

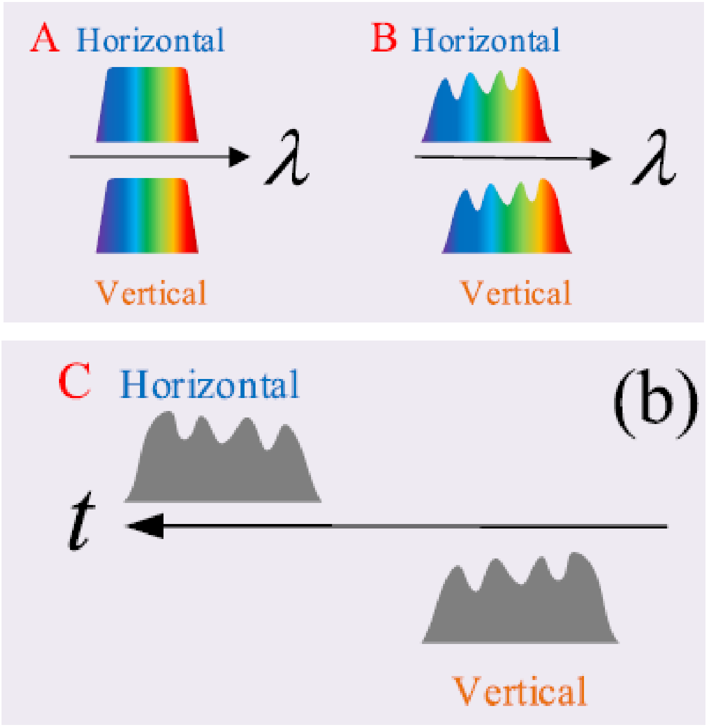

Experimental results

$$\begin{bmatrix}\Delta\varepsilon \\ \Delta T\end{bmatrix} = \begin{bmatrix} 0.398\ \mu\varepsilon/\mathrm{ps} & -0.422\ \mu\varepsilon/\mathrm{ps} \\ -3.291\ ^\circ\mathrm{C}/\mathrm{ps} & 3.793\ ^\circ\mathrm{C}/\mathrm{ps}\end{bmatrix}\begin{bmatrix}\Delta\tau_x \\ -\Delta\tau_y\end{bmatrix}$$

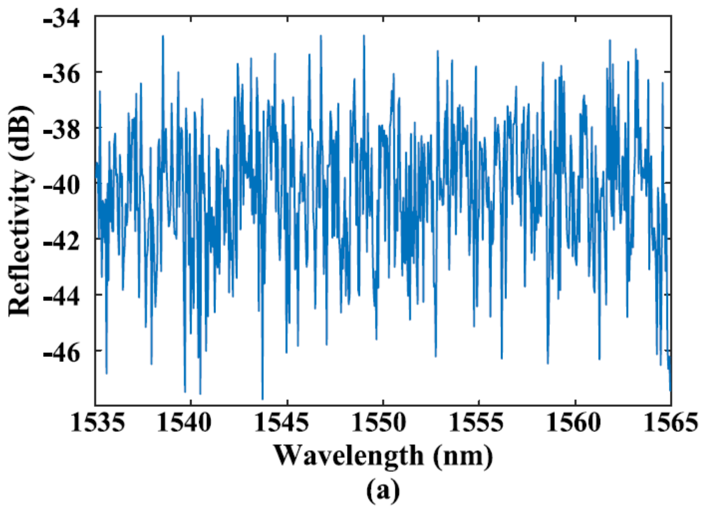

Random grating spectrum

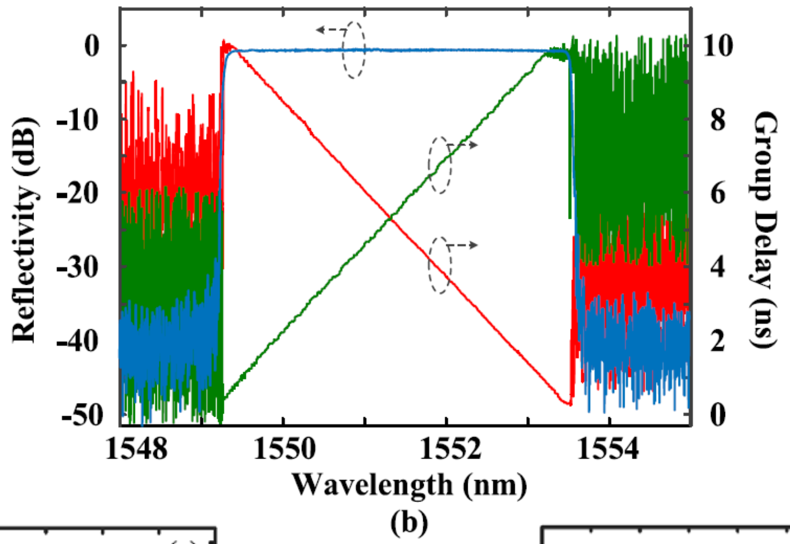

Chirped FBG spectrum

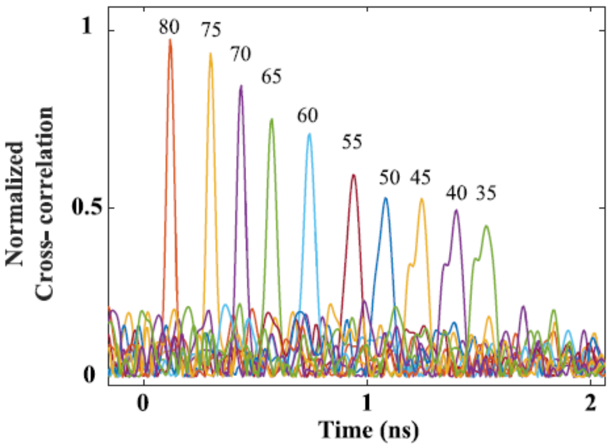

Compressed pulse

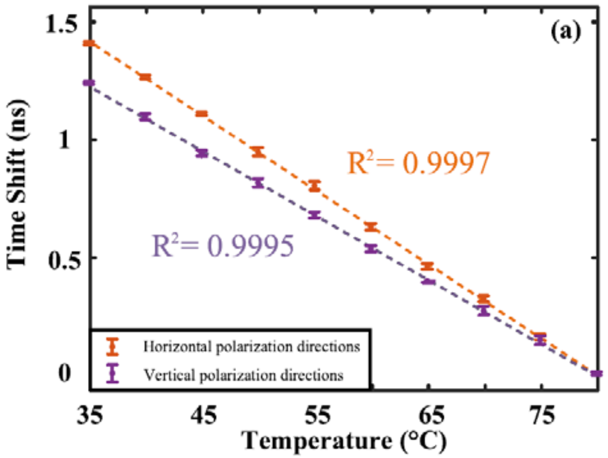

Temperature sensing

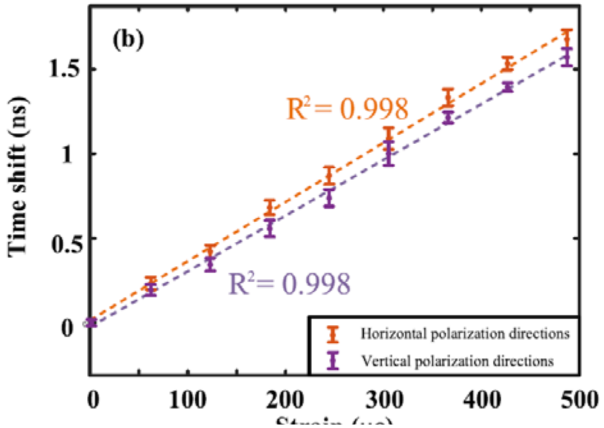

Strain sensing

Optical sensors based on an optoelectronic oscillator

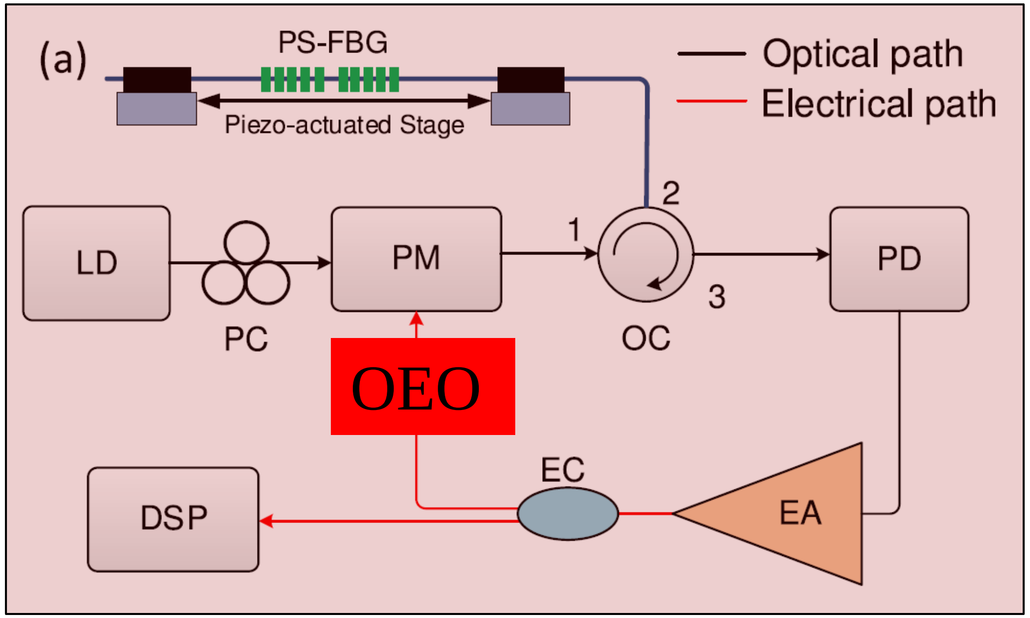

Optical spectrum change → microwave frequency change → Fast-speed and high-resolution sensing

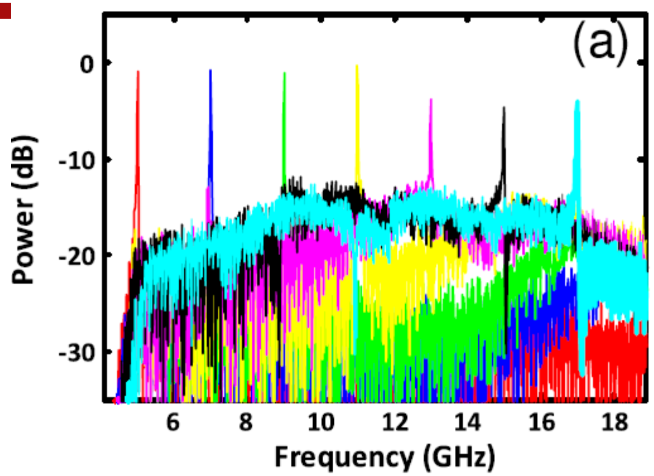

Microwave filter response

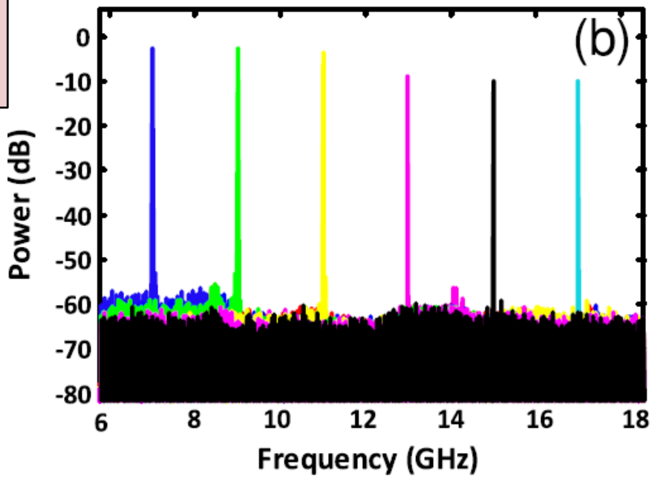

Generated microwave signal

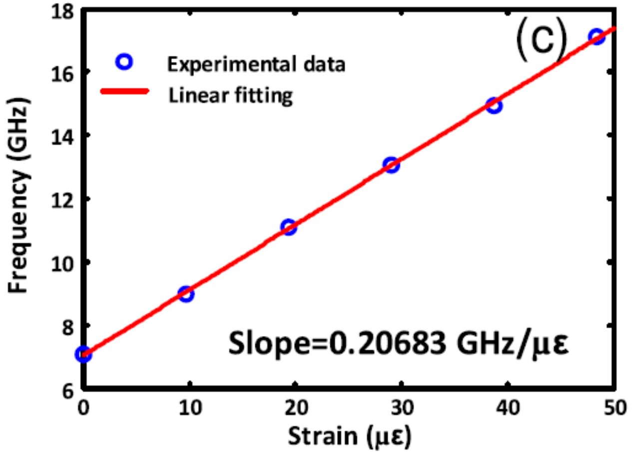

Strain sensing

M. Li, W. Li, J. Yao, and J. Azana, *Proc. OSA Techn. Dig.*. WA, D.C., USA, 2012, Paper BTu2E.3.

Dual-frequency OEO with a PM PS-FBG for transverse load sensing

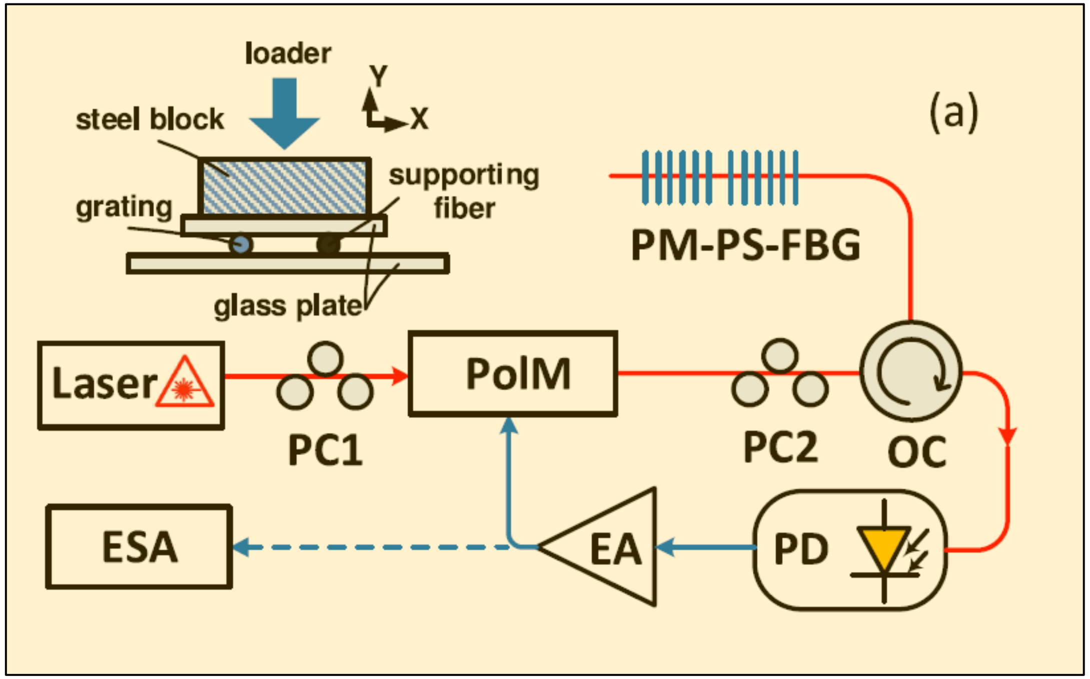

(a) Schematic of the temperature-insensitive **transverse load** sensor based on a dual-frequency OEO employing a polarization-maintaining PS-FBG.

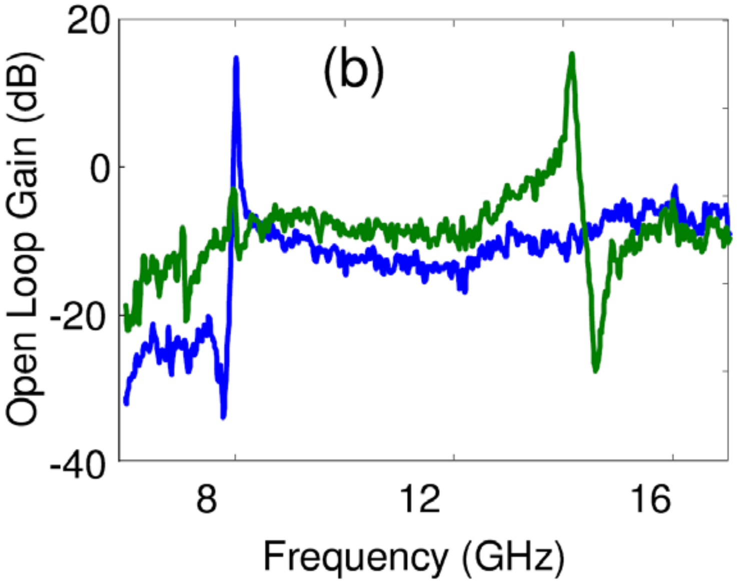

(b) Single passband photonic microwave filter when the incident light is alighted with an angle of 0° or 90° relative to one principal axis (horizontal or vertical) of the PolM.

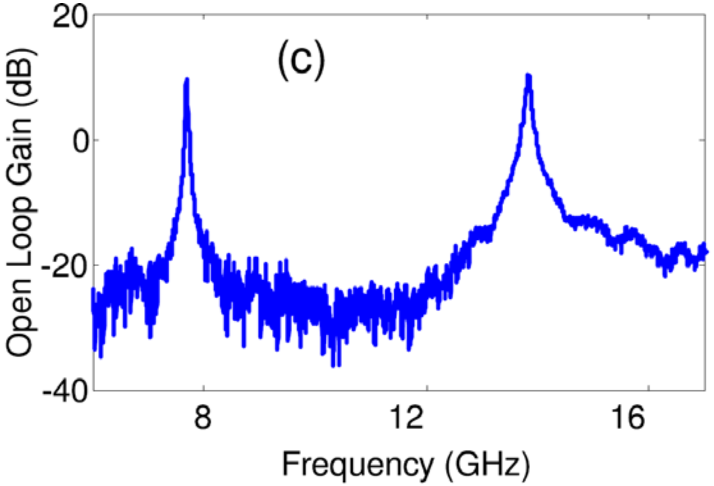

(c) Dual passband photonic microwave filter when the incident light is alighted with an angle of 45° relative to one principal axis of the PolM

F. Kong, W. Li, and J. Yao, *Opt. Lett.*, vol. 38, no. 14, pp. 2611–2613, Jul. 2013.

Dual-frequency OEO with a PM PS-FBG for transverse load sensing

Temperature insensitive

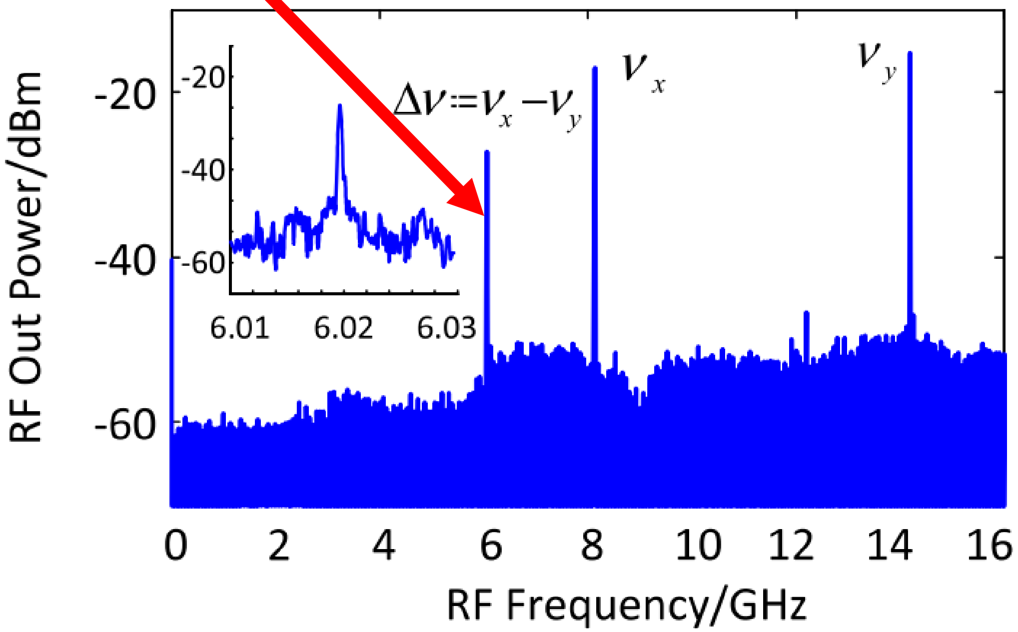

Electrical spectrum of the signal generated by the dual-frequency OEO, with two microwave signals at 8.22 and 14.24 GHz and a beat signal at 6.02 GHz.

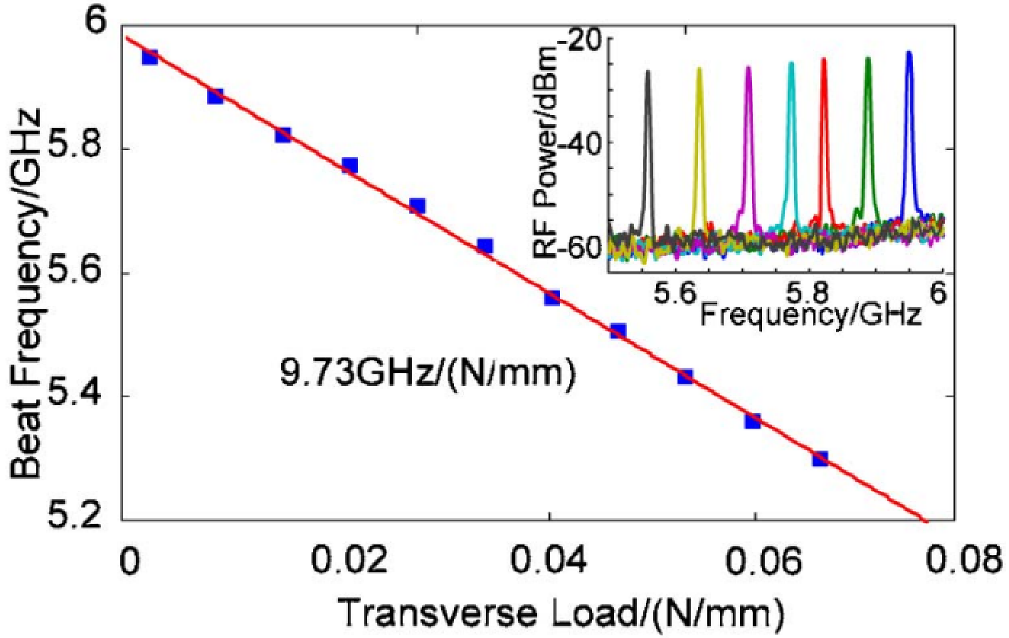

Measured beating frequency as a function of applied transverse load and the electrical spectrum with different load. Inset: the electrical spectrum with different load.

F. Kong, W. Li, and J. Yao, *Opt. Lett.*, vol. 38, no. 14, pp. 2611–2613, Jul. 2013.

Conclusion

1. New MWP systems have been reported for the **generation and processing** of microwave signals (discussed here)

2. Numerous applications such as **wireless communications (RoF)**, and high speed and high-resolution **sensing** (discussed here)

3. Microwave photonics can drive the development of other fields, such as radar, measurements, and instrumentation (not discussed here)

4. **The key challenge: discrete systems → high cost and poor stability→ solution: photonic integration.**

5. Heterogeneous integration is urgently needed to implement systems on chip for low-cost, high-performance microwave photonic systems.

Acknowledgements